Scuola Internazionale Superiore di Studi Avanzati - Trieste

Area of Physics
Ph.D. in Astroparticle Physics

Massive neutrinos and the Large Scale Structure of the Universe

Candidate:

Emanuele Castorina

Supervisor:

Ravi K. Sheth

Emiliano Sefusatti

Thesis submitted in partial fulfillment of the requirements for the degree of Doctor Philosophiae

Academic year 2014/2015

SISSA - Via Bonomea 265 - 34136 TRIESTE - ITALY

Abstract

This thesis deals with the phenomenology of large scale structures in cosmologies with massive neutrinos. Cosmology has the power to constraint the value of neutrino masses down to very high accuracy, but to achieve this target a careful description of the effect neutrinos could induce on cosmological observables is needed.

With the help on numerical N-body simulations that include a massive neutrino component we provide results for clustering beyond the linear level of both cold dark matter and neutrinos, comparing the measurements with analytical predictions derived in higher order perturbative approaches and with existing fitting formulae.

We also discuss the abundance in mass of tracers of the cold dark matter like halos, identifying the right variable, the variance of the cold dark matter field, that describe the counts measured in the simulations. We highlight the systematics effects introduced by a wrong parametrization of the halo mass function, that can bias the inferred cosmological parameters. We present results for the spatial distribution of halos, focusing on the relation with the underlying cold dark matter distribution. To this end we computed the power spectrum of halos in the simulations, finding that the same variable describing the halo mass function provides a consistent picture of spatial clustering of the halos.

The analysis is repeated in redshift space and with higher order correlation functions, the bispectrum in our case, leading to the same conclusions and reinforcing our results.

Foreword

This thesis summarizes part of my research during the PhD, that led to the following publications:

- F. Villaescusa-Navarro, F. Marulli, M. Viel, E. Branchini, E. Castorina, E. Sefusatti, S. Saito, "Cosmology with massive neutrinos I: towards a realistic modeling of the relation between matter, haloes and galaxies", **JCAP 1403 (2014) 011** , [arXiv 1311.0866];

- E. Castorina, E. Sefusatti, R. K. Sheth, F. Villaescusa-Navarro, M. Viel, "Cosmology with massive neutrinos II: on the universality of the halo mass function and bias", **JCAP 1402 (2014) 049**, [arXiv 1311.1212];

- M. Costanzi, F. Villaescusa-Navarro, M. Viel, J, Xia, S. Borgani, E. Castorina, E. Sefusatti, "Cosmology with massive neutrinos III: the halo mass function and an application to galaxy clusters", **JCAP 1312 (2013) 012** , [arXiv 1311.1514];

- E.Castorina, C. Carbone, J. Bel, E. Sefusatti and K. Dolag, "DEMNUni: The clustering of large-scale structures in the presence of massive neutrinos", **JCAP 1507 (2015) 07, 043** , [arxiv 1505.07148].

Contents

Abstract **3**

Foreword **4**

Introduction **10**
Why massive neutrinos? 10
Linear Perturbation theory results 12

The nonlinear regime **21**

1 N-body simulations including massive neutrinos **21**

2 The nonlinear matter power spectrum **26**
2.1 Perturbation Theory 29
2.2 Fitting functions 34

3 Dark matter halos **39**
3.1 The halo mass funtion 41
3.1.1 Universality in the CDM component 41
3.1.2 Cosmological parameters degeneracy 48
3.1.3 Implications for cluster number counts 50
3.2 Halo bias 54
3.2.1 Scale dependent bias 54
3.2.2 Universality in the CDM component 60
3.3 Redshift space distortions 62

4 The matter and halo bispectrum in massive neutrino cosmologies **69**
4.1 The matter bispectrum 70

4.2 The Halo bispectrum 74

5 Conclusions and Outlook **82**

Bibliography **86**

List of Figures

1 Evolution of linear perturbation in the presence of massive neutrinos . . . 13
2 Linear power spectra in massive neutrino cosmologies 15
3 Linear growth rate in massive neutrino cosmologies 16
4 Constraints on neutrino masses I 17
5 Constraints on neutrino masses II 18

1.1 State of the art of N-body simulations including neutrinos as particles . . . 24

2.1 Nonlinear matter power spectra measured in the simulations for $m_\nu = 0.0, 0.3$ eV . . . 27
2.2 Nonlinear matter power spectra measured in the simulations for $m_\nu = 0.3, 0.53$ eV . . . 28
2.3 Comparison between PT predictions for the CDM power spectrum and measurements in the simulations . . . 31
2.4 Comparison between PT predictions for the DM power spectrum and measurements in the simulations . . . 33
2.5 HALOFIT prediction for nonlinear matter power spectra 36
2.6 Cosmological parameters degeneracy in the nonlinear power spectrum . . . 37

3.1 Spherical collapse in the presence of massive neutrinos 42
3.2 Measured halo mass function at $z = 0, 0.5$ 43
3.3 Measured halo mass function at $z = 1, 1.5$ 46
3.4 Universality if the halo mass function 47
3.5 Resolution effects on the halo mass function 48
3.6 Cosmological parameter degeneracies in the halo mass function 49
3.7 Halo mass function for SO halos 50

3.8 Differences in number counts for a Planck-like SZ survey between CDM and DM 52
3.9 Differences in degeneracy directions between cosmological parameters using CDM and DM 54
3.10 Halo bias as a function of scale for halos with $M > 2 \times 10^{13}\, h^{-1}\, M_{\odot}$ 56
3.11 Halo bias as a function of scale for halos with $M > 4 \times 10^{13}\, h^{-1}\, M_{\odot}$ 57
3.12 Degeneracies of cosmological parameters in halo bias 59
3.13 Universality of halo bias 61
3.14 Monopole power spectrum in redshift space measured from simulations 64
3.15 Ratio of the monopole in massive neutrino cosmologies to the same quantity in a ΛCDM Universe 65
3.16 Growth rate as a function of scale measured from the monopole 66
3.17 Comparison of the best fit values for f obtained from the CDM and DM power spectra 67

4.1 Equilateral bispectrum in massive neutrino cosmologies at $z = 1, 0.5$ 71
4.2 Equilateral bispectrum in massive neutrino cosmologies at $z = 1, 2$ 72
4.3 Folded bispectrum in massive neutrino cosmologies 73
4.4 Reduced equilateral bispectrum in massive neutrino cosmologies 74
4.5 χ^2 and best fit parameters at $z = 0$. 75
4.6 χ^2 and best fit parameters at $z = 1$. 76
4.7 Halo bispectrum for equilateral configurations. 77
4.8 Folded bispectrum in massive neutrino cosmologies. 78
4.9 Higher order bias coefficients as a function of peak hight ν . . 79
4.10 Non local bias as a function of linear bias for all cosmologies redshift and halo populations. 80

List of Tables

1.1 Parameters of the H-group of simulations 22
1.2 Parameters of the DEMNUni simulations 23

Introduction

Why massive neutrinos?

In the standard ΛCDM cosmological model the three active neutrinos of the standard model of particle physics are assumed to be massless. Nevertheless, already in 1998 the Super-Kamiokande collaboration presented evidence of neutrino oscillations [1], indicating that at least two neutrinos are massive, and, more recently, new neutrino oscillation experiments seem to exclude a vanishing flavor mixing angle at more than 10 σ (see, *e.g.* [2; 3; 4]). Oscillations experiment are exclusively sensitive to the differences of masses squared and in a standard scenario with three massive eigenstates the best fit values for the mass splitting are [4]

$$\Delta m^2_{12}\ [10^{-5}\ \mathrm{eV}^2] = 7.54^{+0.26}_{-0.22} \qquad |\Delta m^2_{32}|\ [10^{-3}\ \mathrm{eV}^2] = 2.3 \pm 0.06 \qquad (1)$$

The sign of $|\Delta m^2_{32}|$ is extremely difficult to detect with particle physics experiments, although next generation of experiments, like Hyper-Kamiokande[5], could in principle be able to do it. The absolute mass scale is therefore still unknown and this is where cosmology can play a fundamental role.

The Big Bang paradigm predicts the existence of a cosmic neutrino background, see, e.g. [6]. In the very early Universe, cosmic neutrinos contributed to the total radiation energy density, affecting the nucleosynthesis process and therefore the primordial abundance of light elements.

Much later they will become non relativistic and start contributing to the total matter density in the Universe, both at the background and at the perturbation level. The study of the effects of neutrino masses on cosmological observables is of particular relevance for two, distinct, reasons.

First, as we have seen above, the absolute neutrino mass scale remains unknown, and, in this respect, cosmology plays a key role in its determination, being gravity sensitive to the total neutrino mass, $\Sigma\, m_\nu$, rather than to the mass splitting.

Second, an accurate description of massive neutrino effects on LSS is required to avoid systematic errors in the determination of other cosmological parameters, as the dark energy density and equation of state, whose measurements represent one of the main goals of current and future cosmological experiments.

Massive neutrino cosmologies have been extensively studied in the literature (see [6; 7] for a review). In particular the linear perturbation theory in the presence of massive neutrinos is well understood and it is widely used to derive constraints on $\Sigma\, m_\nu$ and other cosmological parameters, from present and future CMB and galaxy surveys observations [8; 9; 10; 11; 12; 13; 14; 15; 16; 17; 18; 19; 20; 21; 22; 23; 24; 25].

However, the increasing precision of cosmological parameter measurements further requires an accurate description of nonlinear corrections, which can be obtained by means of a direct analysis of the output of N-body simulations accounting for a massive neutrino component and then a comparison to analytic tools.

More generally, assessing the (mildly) nonlinear regime of structure formation is a crucial problem in cosmology per sé, even in standard scenarios without massive neutrinos. The nonlinear clustering on dark matter and its relation to the spatial distribution of dark matter halos, and the galaxies which reside in them, are extremely rich and complex processes. Future redshift surveys like Euclid [26] and DESI [27] will be dominated by theoretical systematic errors, coming from our lack of understanding of nonlinear dynamics, in the determination of cosmological parameters. For massive neutrinos the Euclid forecast is $\sigma_{m_\nu} = 20(30)$ meV [26; 28] and it strongly depends on how much we will be able to describe galaxy clustering down to small scales.

This thesis is devoted to the study of the nonlinear evolution of the large scale structure in massive neutrinos cosmologies. After a brief description of well known results in the linear regime in the next section , we start by studying CDM and neutrino clustering on nonlinear scales in Section 2, comparing results from full N-body simulations to Perturbation Theory and fitting formulae. Then we describe properties of discrete tracers such as dark matter halos in massive neutrino cosmologies. We continue with a comparison between analytical predictions and N-body measurements of halo abundances in the presence of massive neutrinos in Section 3.1, presenting some implications from cosmological constraints from galaxy clusters number counts. In Section 3.2 we show result for the spatial distribution of halos and their clustering properties, *i.e.* halo bias. It is straightforward to extend these results to redshift space, as we will see in Section 3.3. Finally we discuss

higher order statistics like the matter and halo bispectrum in Section 4.

Linear Perturbation theory results

Before entering the discussion let us give a brief summary of linear perturbations theory facts in cosmology with massive neutrinos. This will make more clear how we get the constraint on neutrino masses from cosmological probes, some of which are presented at the end of this section.

For excellent reviews of neutrinos in cosmology see [6; 29]. For our purposes, the key elements are as follows. Neutrinos decouple in the early Universe, just before the onset of Big Bang Nucleosynthesis, as ultra-relativistic particles. They then behave as relativistic degrees of freedom, which not only imply they contribute with photons to the total radiation energy density in the Universe but also that their density fluctuations do not grow. Neutrinos become non-relativistic when their mean thermal energy drops below the mass, at a redshift z_{nr} given by

$$1 + z_{nr}(m_\nu) \simeq 1890 \left(\frac{m_\nu}{1\,\mathrm{eV}}\right) , \tag{2}$$

where m_ν is the neutrino mass. Thereafter, the total dark matter (DM) background density is given by

$$\Omega_m = \Omega_c + \Omega_b + \Omega_\nu , \qquad \Omega_\nu = \frac{\sum m_\nu}{93.14h^2\ \mathrm{eV}}. \tag{3}$$

At the perturbation level the impact of massive neutrinos was first clearly explained in 1980 by [30]. Since neutrinos are relativistic particles at decoupling, their equilibrium phase space distribution, in a homogeneous Universe, remains a relativistic Fermi-Dirac distribution independent of the subsequent evolution,

$$f_o(q) = \frac{1}{1 + \exp(q/aT_\nu)} , \tag{4}$$

where $q = ap$ is the comoving momentum and T_ν is the neutrino temperature that drops as the scale factor a. Therefore a priori neutrinos cannot be treated as a (perfect) fluid as we usually do for CDM, and there is no reason to assume anisotropic stresses to be zero. This implies that neutrinos perturbations should be computed by solving the Vlasov equation of the perturbed distribution function

$$f(q, x, \hat{\vec{n}}, t) = f_o(q)[1 + \Psi(q, x, \hat{\vec{n}}, t)] \tag{5}$$

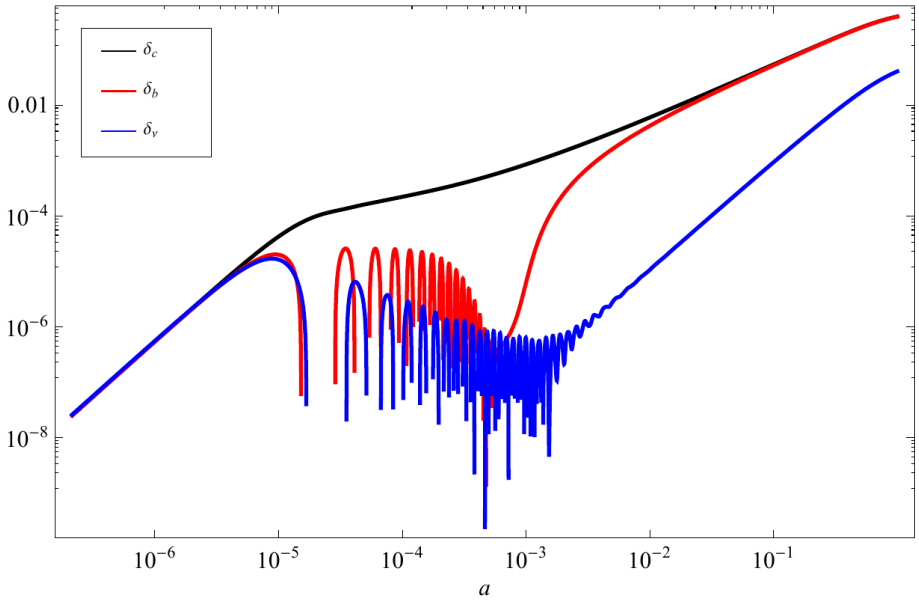

Figure 1: Evolution of a linear perturbation of wavenumber $k = 1\,h^{-1}\,\mathrm{Mpc}$ for CDM(black), baryons(red), and neutrinos(blue).

whose moments represent density, pressure and so on. The Vlasov equation can be expanded in an infinite hierarchy of terms, and then truncated to achieve a given precision. This is the way Boltzmann codes like CAMB[31] or CLASS[32] solve for the evolution of massive neutrinos at the linear level. However one could show that long after the non relativistic transition, and on sufficiently small scales, higher order moments are suppressed with respect to the energy density and a fluid approximation can be employed, *i.e.* only the first two equation of the hierarchy [33; 34]. Then by analogy with sound waves propagation with finite speed of sound we can say that Fermi-Dirac thermal velocities, v_{th}, introduce a typical scale, the free streaming length $\lambda_{\rm FS}$, defined as the distance traveled by a massive neutrinos between two different times. As relativistic particles neutrinos moves almost at the speed of light and the free streaming scale is the Hubble scale, but then, after the non-relativistic transition

$$\lambda_{\rm FS}(m_\nu, z) = a\left(\frac{2\pi}{k_{fs}}\right) \simeq 7.7\frac{H_0(1+z)}{H(z)}\left(\frac{1\,eV}{m_\nu}\right)\ h^{-1}\,\mathrm{Mpc}\,. \qquad (6)$$

Density fluctuations on scales smaller than $\lambda_{\rm FS}$ are washed out, while on

scales much larger neutrinos behave as cold dark matter. In Figure 1 we plot the evolution of linear perturbations on a small scale, $k = 1\,h^{-1}\,\mathrm{Mpc}$, for the three fluids filling our Universe (photons are not shown for simplicity): while CDM perturbations start growing much earlier than others, at horizon entry, baryons initially oscillate in the photon-baryon plasma until decoupling and then catch up very fast with CDM. Neutrinos (in this case $m_\nu = 0.17$ eV) oscillates and are suppressed because of free streaming and after the non-relativistic start to grow but cannot catch up with CDM and baryons.

It is convenient to think of a perturbation δ_m in the total matter field as a weighted sum of the fluctuations $\delta_{cdm}(=\delta_b)$ and δ_ν in the CDM and ν fields:

$$\delta_m \equiv (1-f_\nu)\,\delta_{cdm} + f_\nu\,\delta_\nu\,, \quad \text{where} \quad f_\nu \equiv \Omega_\nu/\Omega_m. \tag{7}$$

and in what follows we will use $P_{mm}(k)$ to denote the power spectrum of the total field, $P_{cc}(k)$ and $P_{\nu\nu}(k)$ the power spectra of the CDM (+ baryons) and ν fields, and $P_{\nu c}(k)$ the cross-power between the two fields. Therefore,

$$P_{mm}(k) = (1-f_\nu)^2\,P_{cc}(k) + f_\nu^2 P_{\nu\nu}(k) + 2f_\nu(1-f_\nu)P_{\nu c}(k). \tag{8}$$

As we already saw, the growth of neutrino fluctuations is governed by their free streaming length $\lambda_{\rm FS}$, below which perturbations are washed out. The free streaming wavenumber has a minimum at $z = z_{nr}$

$$k_{nr} = k_{fs}(z_{nr}) \simeq 0.018\Omega_m^{1/2}\left(\frac{m_\nu}{1\,eV}\right)\,h\,\mathrm{Mpc}^{-1}\,. \tag{9}$$

which is the largest scale can be affected by the presence of neutrino perturbations. This scale is typically larger than the scale at which nonlinear effects manifest themselves at low redshifts. At sufficiently large k, there is no power in the ν field, so $P_{mm} \to (1-f_\nu)^2\,P_{cc}$, thus,

$$P_{mm}(k) = \begin{cases} P_{cc}(k) & \text{if } k < k_{nr} \\ (1-f_\nu)^2\,P_{cc}(k) & \text{if } k \gg k_{nr}\,. \end{cases} \tag{10}$$

that means $P_{cc}(k) \geq P_{mm}(k)$ on all scales, see left panel of Figure 3. These limiting cases suggest that the CDM and matter fields are actually rather similar when $f_\nu \ll 1$ is small. One measure of this is the cross-correlation coefficient

$$r_{cm} \equiv \frac{P_{cm}}{\sqrt{P_{cc}P_{mm}}}. \tag{11}$$

Since

$$P_{cm} = \langle\delta_c\delta_m\rangle = \langle\delta_c((1-f_\nu)\delta_c + f_\nu\delta_\nu)\rangle = (1-f_\nu)P_{cc} + f_\nu P_{c\nu}\,, \tag{12}$$

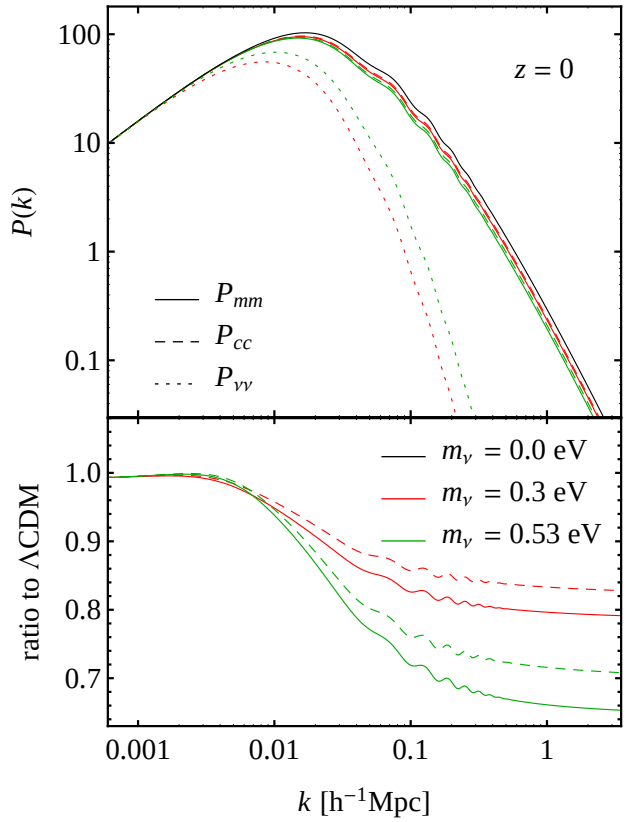

Figure 2: Left panel: linear power spectrum in cosmologies with massive neutrinos at $z = 0$. Continuous lines show the total matter power spectrum, P_{mm}, dashed lines the cdm contribution to it , $Pcc(k)$, while the dotted ones the neutrino auto power spectrum, $P_{\nu\nu}(k)$. Lower panel: ration between $P_{mm}(k)$ (or $P_{cc}(k)$) and the power spectrum in a baseline ΛCDM cosmology. All the models share the same value of Ω_m, n_s and A_s, assuming Planck2013 best fit parameters [35].

and

$$\begin{aligned}\sqrt{P_{cc}\,P_{mm}} &= \sqrt{(1-f_\nu)^2 P_{cc}^2 + f_\nu^2 P_{\nu\nu} P_{cc} + 2 f_\nu (1-f_\nu) P_{c\nu} P_{cc}} \\ &= (1-f_\nu) P_{cc} + f_\nu P_{c\nu} + \mathcal{O}(f_\nu^2) = P_{cm} + \mathcal{O}(f_\nu^2)\,, \end{aligned} \tag{13}$$

differences from $r_{cm} \simeq 1$ only appear at second order in f_ν.

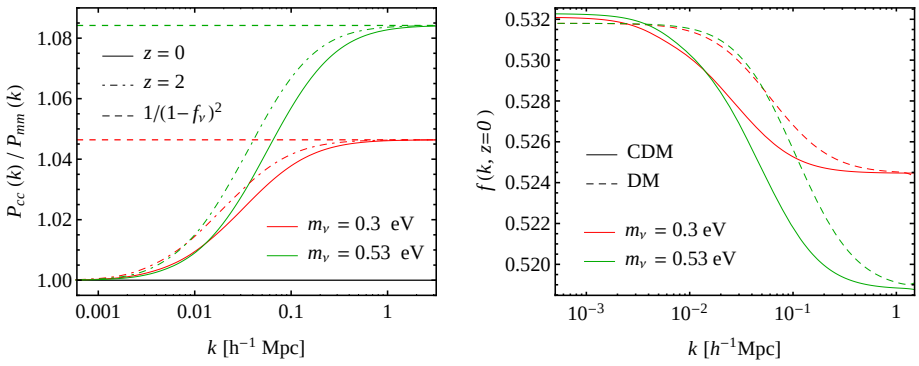

Figure 3: Left panel: Ratio of the CDM and total matter power spectra in a given cosmology that includes massive neutrinos. The asymptotic regime of equation Eq. (10) is reached at very large k. Right panel: growth rate of CDM perturbations at $z = 0$ in cosmologies with massive neutrinos. Scale dependence of f on intermediate is also function of redshift, not only of neutrino masses.

Massive neutrinos also have back-reaction effects on the evolution of CDM perturbations. On the largest scales we saw that neutrinos behave as CDM and therefore nothing changes in the growth of structure. On scales much smaller than the free streaming length, $k \gg k_{nr}$ neutrinos are washed out and we could write for CDM

$$\ddot{\delta}_c + 2H(t)\dot{\delta}_c - \frac{3}{2}H(t)^2(1 - f_\nu)\delta_c = 0 \tag{14}$$

which results from neglecting the neutrino contribution to the Poisson equation. The solution to the above equation reads, during the matter dominated era, [30]

$$\delta_c \propto a^{1-\frac{3}{5}f_\nu} \quad \text{for} \quad k \gg k_{nr}. \tag{15}$$

On intermediate scales, more relevant to current and future observations, CDM perturbation interpolates between the two asymptotic regimes resulting in scale dependent linear growth factor $D(k, a)$. We can put things together and compute the net effect of massive neutrinos on observables like the matter power spectrum. If the total matter density in eq. (7) is fixed, then the total matter power spectrum in a massive neutrino model, $P_{mm}(k; f_\nu)$, is reduced by a constant factor on scales $k \gg k_{nr}$ and for small values of f_ν

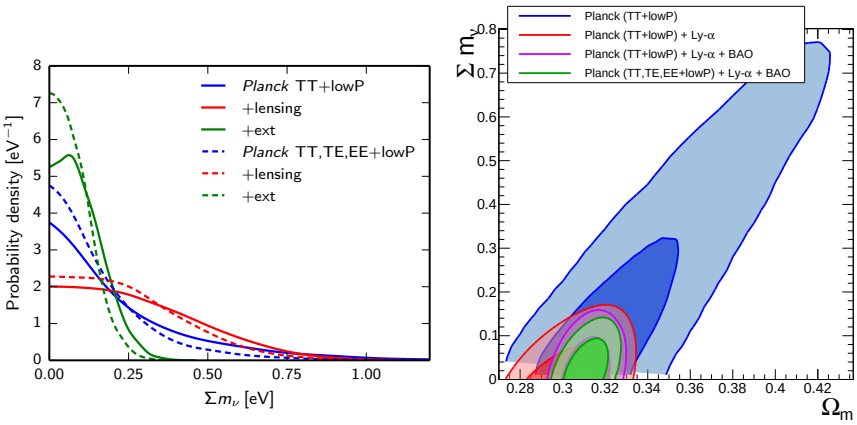

Figure 4: Left panel: posterior distribution for the sum of neutrino masses from of Planck data alone, in blue and red, and Planck combined with other probes, in green. Reproduced from [37]. Right panel: Constraints on neutrino masses from the Ly-α forest data and CMB data. Reproduced from [38].

[36; 6]

$$\frac{P_{mm}(k; f_\nu)}{P_{mm}(k; f_\nu = 0)} \simeq 1 - 8 f_\nu \,, \tag{16}$$

while from Eq. (10) and Eq. (8), it follows that the suppression for the CDM power spectrum, P_{cc}, is given by a factor $\sim (1 - 6 f_\nu)$. The difference in the suppression between the two power spectra is shown in the right panel of Figure 2. In an analysis of a galaxy survey this suppression is exactly what is used to constraints neutrino masses. It is also be important, especially for the discussion of redshift space distortions in Section 3.3, to quantify the effect of massive neutrinos on the linear growth rate defined, for CDM, as

$$f_c(k, a) \equiv \frac{\mathrm{d} \ln D_c(k, a)}{\mathrm{d} \ln a} \,. \tag{17}$$

In the first place, in massive neutrino scenarios, the growth rate becomes scale-dependent, as a natural consequence of the scale-dependent growth function D_c. In particular, the *small-scale* asymptotic suppression expected in linear theory is given by [30]

$$\frac{f_c(k)}{f_{\Lambda\mathrm{CDM}}} \overset{k \gg k_{\mathrm{FS}}}{\longrightarrow} \frac{1}{4} \left(5 - \sqrt{25 - 24\, f_\nu} \right) \simeq 1 - \frac{3}{5} f_\nu \,, \tag{18}$$

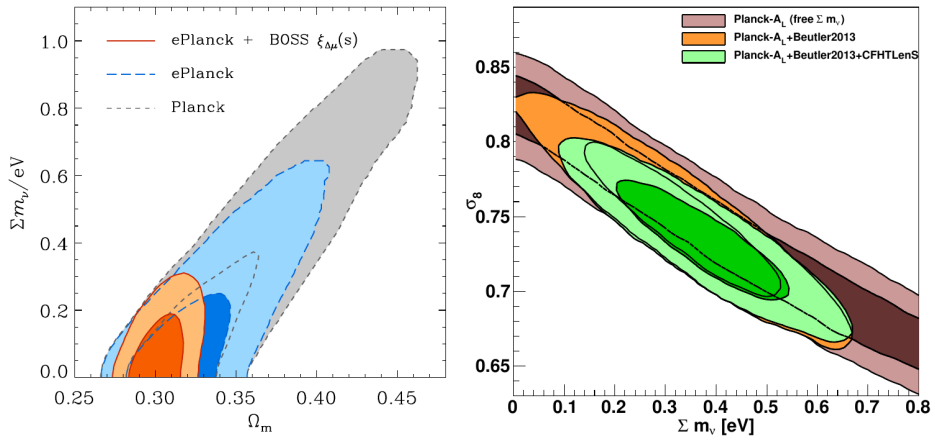

Figure 5: Constraints on neutrino masses from analyses of galaxy clustering in BOSS DR11[39]. On the left, taken from [40], results in real space using clustering wedges, and on the right results form multipoles in Fourier space [23].

and corresponds to a 2.4% effect for a $\Sigma\, m_\nu$= 0.53 eV model. However, for the same model, the suppression is below the percent level on large scales, $k \lesssim 0.05\, h\,\mathrm{Mpc}^{-1}$. In the case of the total matter growth rate, $f_m(k)$, the suppression, again for the $\Sigma\, m_\nu$= 0.53 eV, reaches the 1% level at slightly smaller scales, $k \simeq 0.05\, h\,\mathrm{Mpc}^{-1}$ (linear theory predictions for both the ratio $f_c/f_{\Lambda\mathrm{CDM}}$ and $f_m/f_{\Lambda\mathrm{CDM}}$ are shown as dashed curves in Figure 3). It is also important to notice that on intermediate scales the scale dependence induced on f_c is also function of redshift, non just of neutrino masses.

Finally we recap some constraints on neutrino masses from large scale structures datasets. CMB anisotropies measured from the Planck Satellite, including CMB gravitational lensing, combined with other probes of the expansion rate of the Universe yields $\sum m_\nu < 0.234$ eV (95%) [37], corresponding to the blue line of the left panel of Figure 4. Even if at the time of photon decoupling neutrinos were still relativistic, nevertheless CMB is sensitive to neutrino masses through lensing, Integrated Sachs-Wolf effect and Silk damping.

The most stringent bound on neutrino masses comes from combination of CMB data and Ly-α forest power spectrum [38], $\sum m_\nu < 0.12$ eV (95%), shown in the right panel of Figure 4. Ly-α forest is so powerful in constraining neutrino masses since it probes small scales where, as we have seen, massive

neutrinos effects are larger.

Analyses of the full shape of the galaxy power spectrum or of the two-point correlation function also put constrains on the value of neutrino masses. However lack of understanding of nonlinear physics responsible for the clustering pattern we observe in the galaxy distribution make these kind on analyses more difficult. As an example Figure 5 shows constraints on neutrino masses from the CMASS sample of BOSS DR11, in the left panel using measurement in real space[40], and on the right using the same data but in Fourier space[23]. There is some tension, at more the $1-\sigma$ level, between the two, mainly coming from different assumptions in the theoretical modeling. In particular the analysis in [23] stands alone, with the controversial exception of galaxy clusters [41; 42], and points towards larger value of neutrino masses, $\sum m_\nu = 0.34 \pm 0.15$ eV.

The nonlinear regime

Chapter 1

N-body simulations including massive neutrinos

There are two main ways of implementing massive neutrinos in standard N-body simulations. One is the so called grid-method[43; 44], in which neutrinos only contribute to the long distance force through the particle mesh (PM) method, providing a fast implementation of the matter evolution in neutrino cosmologies, but with the limitation that it does not properly capture the non-linear neutrino regime. Moreover the use of the grid method is, thus, only justified on regimes where the non-linear neutrino effects are negligible (at $z > 2$ and on large linear scales [45; 44; 46])

The other method includes neutrinos in the N-body as particles [44; 45], and it is the one we employ in this work. The simulations have been performed using the tree particle mesh-smoothed particle hydrodynamics (TreePM-SPH) code GADGET-3, an improved version of the code described in [47], specifically modified in [44], to account for the presence of massive neutrinos. This version of GADGET-3follows the evolution of CDM and neutrino particles, treating them as two distinct sets of collisionless particles. In this implementation, neutrinos differ from CDM only because at the starting redshift of the simulation they receive an extra thermal velocity component obtained by random sampling the neutrino Fermi-Dirac linear momentum distribution. To properly sample the distribution a (large) minimum number of neutrino particles is required, $N_\nu > 512^3$. The initial conditions of the N-body simulations have been generated at z = 99, using the Zeldovich approximation for both the CDM and the neutrino particles. The same random phases as for the cold dark matter are used to ensure adiabatic initial conditions. The transfer functions have been obtained through CAMB

H-group	$\sum m_\nu$[eV]	Ω_c	f_ν	$\sigma_{8,mm}$	$\sigma_{8,cc}$	$m_p^c[\,h^{-1}\,M_\odot]$
Set A						
H0	0.0	0.2208	0.000	0.832	0.832	5.60×10^{11}
H3	0.3	0.2142	0.024	0.752	0.768	5.46×10^{11}
H6	0.6	0.2076	0.048	0.675	0.701	5.33×10^{11}
Set B						
H0s8	0.0	0.2208	0.000	0.675	0.675	5.60×10^{11}
H0s8-CDM	0.0	0.2208	0.000	0.701	0.701	5.60×10^{11}
H6s8	0.6	0.2076	0.048	0.832	0.864	5.33×10^{11}

Table 1.1: Summary of cosmological parameters and derived quantities for the six models assumed for our N-body simulations. The values $\Omega_b = 0.05$, $\Omega_m = 0.2708$, $h = 0.7$, $n_s = 1$ are shared by all models.

and we have incorporated the baryon effects (for instance the BAO wiggles in the $P(k)$) into the CDM particles by using a transfer function that is a weighted average of the transfer functions of the CDM and the baryons

$$T_{cb}(k) = \frac{\Omega_c\, T_c(k) + \Omega_b\, T_b(k)}{\Omega_c + \Omega_b} \tag{1.1}$$

Given the large amount of memory required by the simulations, baryon physics is not included. Nevertheless we expect baryonic effects to be mostly insensitive to neutrinos being massless (CDM) or massive, and therefore not relevant when we compare the effect of massive neutrinos on LSS measurements to the same quantities measured in a standard cosmological model. In addition we expect also that any additional effect produced by the interplay of neutrinos with baryon physics should be of higher order. This is supported also from[48] which shows that the neutrino induced suppression in the total matter power spectrum is very much the same also when neutrinos are considered in the presence of baryons. We will make use of two different group of simulations, the H-group presented in [49; 50; 51] and the DEMNuni simulation suite of [52].

The first group includes simulations for three different value of masses: $\sum m_\nu = 0$, 0.3, 0.6 eV; from now on, we will use m_ν to mean $\sum m_\nu$. Inside the H-group a first set of simulations (Set A) shares the following cosmological parameters: $\Omega_b = 0.05$, $\Omega_\Lambda = 0.7292$, $h = 0.7$, $n_s = 1$ and $A_s = 2.43 \times 10^{-9}$,

DEMNUni	$\sum m_\nu$[eV]	Ω_{cdm}	f_ν	$\sigma_{8,mm}$	$\sigma_{8,cc}$	$m_p^c[\,h^{-1}\,M_\odot]$
S1	0.00	0.2700	0.000	0.846	0.846	8.27×10^{10}
S2	0.17	0.2659	0.013	0.803	0.813	8.16×10^{10}
S3	0.30	0.2628	0.022	0.770	0.786	8.08×10^{10}
S4	0.53	0.2573	0.040	0.717	0.740	7.94×10^{10}

Table 1.2: Summary of cosmological parameters and derived quantities for the four models assumed for the DEMNUni simulations. The values of σ_8 have been computed at $z = 0$, and $\Omega_b = 0.05$, $\Omega_m = 0.32$, $h = 0.67$, $n_s = 0.96$ are shared by all the models.

with zero curvature. The total matter density is also fixed to $\Omega_m = \Omega_b + \Omega_c + \Omega_\nu = 0.2708$, such that the cold dark matter density changes as Ω_ν varies. In addition, the shared value for the amplitude of initial fluctuations A_s results in different values for the amplitude of cold and total matter perturbations at late times, parametrized, for instance, respectively by $\sigma_{8,cc}$ and $\sigma_{8,mm}$.

A second set of three simulations (Set B) explores possible degeneracies of the initial amplitude A_s with the value of m_ν, still keeping Ω_b, Ω_m, h and $n_s = 1$ at the same values. In Set B, tow simulations describe two massless neutrinos cosmologies where we changed the initial amplitude A_s to match the σ_8 of the DM component and CDM component of the $m_\nu = 0.6$ model in Set A. The third one has $m_\nu = 0.6$ eV but matches $\sigma_{8,cc}$ to the massless neutrino model in Set A. Table 1.2 summarizes the different sets of parameters of the H-group.

For each model we performed eight realizations with different random seeds of a cubic box of linear size 1000 h^{-1} Mpc with 512^3 CDM particles and 512^3 neutrino particles, so that for each model we reach a combined effective volume of $8\,h^{-3}\,\mathrm{Gpc}^3$. Auto and cross power spectra of the different species (CDM, DM, neutrinos) are computed at $z = 2$, 1, 0.5 and 0, where halo catalogs are also produced.

The second group of simulations have been presented in [52]. The DEMNUni simulations have been conceived for the testing of different probes, including galaxy surveys, CMB lensing, and their cross-correlations, in the presence of massive neutrinos. To this aim, this set of simulations is characterised by a volume big enough to include the very large-scale perturbation modes, and, at the same time, by a good mass resolution to investigate small-scales nonlinearity and neutrino free streaming. Moreover,

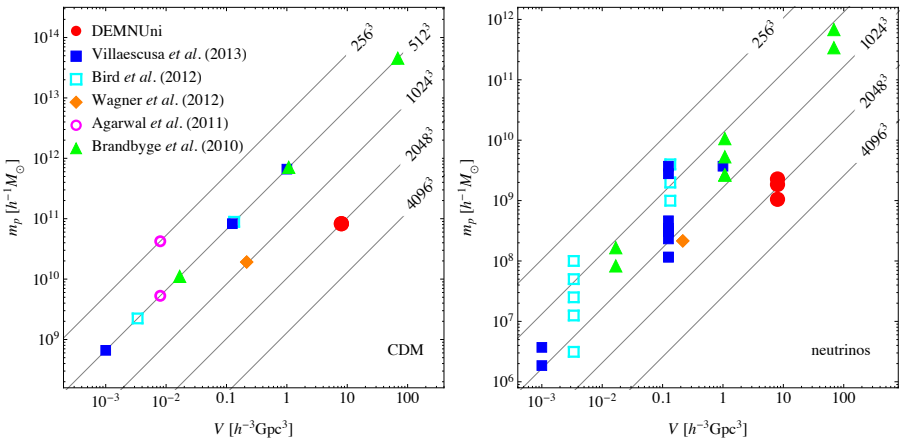

Figure 1.1: Left panel: comparison between the DEMNUni runs and previous, recent simulations of massive neutrino cosmologies in terms of CDM and neutrino particle mass resolution against simulation volume. Grey diagonal lines indicate the number of CDM particles. Right panel: same as left one but for neutrino particle mass resolution. Multiple points for the same set of simulations reflect the different values of neutrino masses used (for simplicity we always assume $\Omega_m = 0.32$ and $f_\nu = 0.02$ to compute neutrinos particle masses)

for the accurate reconstruction of the light-cone back to the starting redshift of the simulations, it has been used an output-time spacing small enough that possible systematic errors, due to the interpolation between neighbouring redshifts along the line of sight, result to be negligible.

We have produced a total of four different DEMNUni simulations, choosing the cosmological parameters according to the *Planck* 2013 results [35], namely a flat ΛCDM model generalised to a $\nu\Lambda$CDM , *i.e.* a massive neutrino model, by varying only the sum of the neutrino masses over the values $\Sigma\, m_\nu = 0$, 0.17, 0.3, 0.53 eV (and consequently the corresponding values of Ω_ν and Ω_c, while keeping fixed Ω_m and the amplitude of primordial curvature perturbations A_s). Each DEMNUni simulation is characterised by a comoving volume of $8\,h^{-3}\,\mathrm{Gpc}^3$, filled with 2048^3 dark matter particles and, when present, 2048^3 neutrino particles. Table 1.2 provides a summary of the cosmological parameters that characterise the different runs. It shows as well the derived quantities $\sigma_{8,mm}$ and $\sigma_{8,cc}$ corresponding to the r.m.s. of perturbations on spheres of $8\,h^{-1}\,\mathrm{Mpc}$, computed respectively for the total

and CDM matter components at $z = 0$, and the CDM and neutrino mass particle resolutions, which vary according to the value of Ω_c and Ω_ν.

The state of the art of N-body simulations including massive neutrinos as particles is shown in Figure 1.1 in terms of mass resolution for the CDM particles and simulation volume . The two sets of simulation used in this works corresponds to the blue squares, the H-group, and the red disks, the DEMNUni suite. With respect to previous simulations, the DEMNUni suite represents an improvement of about an order of magnitude in terms of particle number (only [45] considered a larger box, but with considerably smaller mass resolution).

Chapter 2

The nonlinear matter power spectrum

As shown in the beginning of this thesis, the shape of the linear power spectrum is quite sensitive to the value of neutrino masses. This dependence becomes even stronger in the mildly and fully nonlinear regimes [45; 48]. Taking advantage of the large DEMNUni simulations volume, in this section we aim at testing the accuracy of current analytical predictions for the nonlinear matter power spectrum, P_{mm}, in the presence of massive neutrinos. To this end, we measure individually the different components to P_{mm} in Eq. (8), from very large scales, $k \sim 0.003\,h\,\mathrm{Mpc}^{-1}$, down to fully nonlinear scales, $k \sim 3\,h\,\mathrm{Mpc}^{-1}$, and compare these measurements with PT predictions, in the mildly nonlinear regime, and fitting functions as HALOFIT [53; 54], in the fully nonlinear regime[1]. The goal here is to understand if possible departures from the linear regime of neutrino perturbations have to be taken into account for precision cosmology at the % level.

Before proceeding to the comparison with the nonlinear, analytical predictions, however, we take a look at each component and its relative contribution to the nonlinear P_{mm} measured from the simulations. Figures 2.1 and 2.2 show the CDM auto power spectrum, $(1-f_\nu)^2\,P_{cc}$ (*dashed curves*), the neutrino auto power spectrum, $f_\nu^2\,P_{\nu\nu}$ (*dotted curves*), and the cross CDM-neutrino power spectrum, $2\,f_\nu\,(1-f_\nu)\,P_{c\nu}$ (*dot-dashed*), as extracted from the simulations (*thick curves*), and the corresponding linear predictions (*thin curves*). Each plot corresponds to a different value of the neutrino mass in

[1] While the mass resolution of the DEMNUni simulations would allow to look at much smaller scales, of the order of $k \sim 10\,h\,\mathrm{Mpc}^{-1}$, we do not investigate this regime since it is dominated by baryon physics [55; 56; 57; 58; 59].

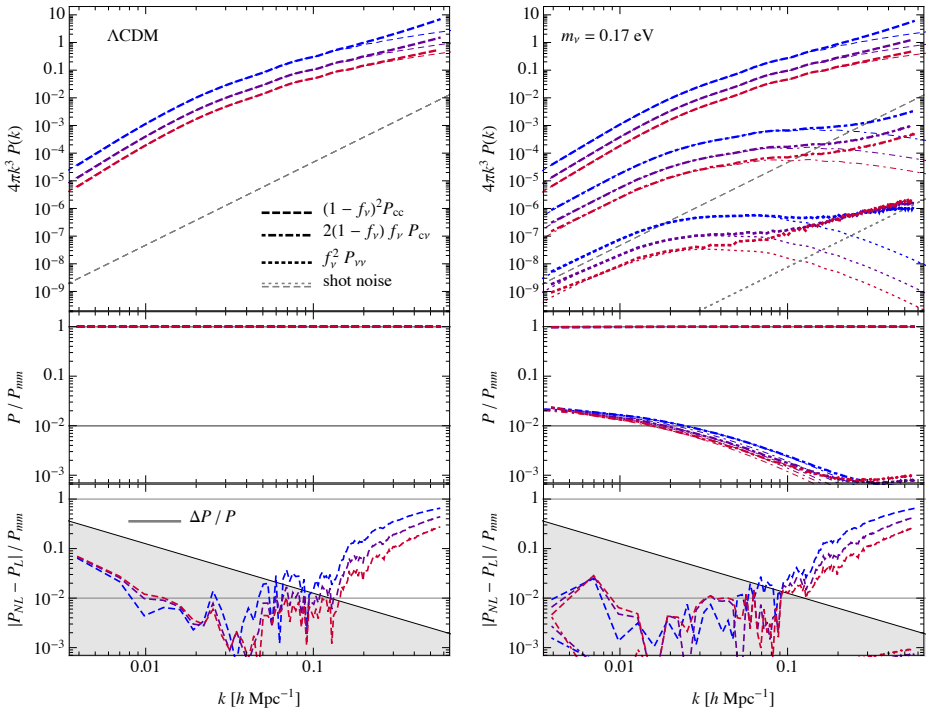

Figure 2.1: Comparison between the different contributions to the nonlinear matter power spectrum, $(1-f_\nu)^2\,P_{cc}$ (*dashed curves*), $f_\nu^2\,P_{\nu\nu}$ (*dotted*) and $2\,f_\nu\,(1-f_\nu)\,P_{c\nu}$ (*dot-dashed*), as described in the text. All the measurements at redshifts $z = 0$, 1, 2 are shown with shades varying, respectively, from blue to red. Thin coloured curves correspond to the respective linear predictions. Dashed and dotted grey lines on the top panels show the shot-noise contributions to the CDM and neutrinos power spectra. The shaded area in the bottom panel shows values below the 1-σ, relative, Gaussian uncertainty on $\Delta P(k)/P(k) = 1/\sqrt{2\pi k^2/k_f^2}$, k_f being the fundamental frequency of the simulation box.

the simulations. Within each plot, the top panel shows the adimensional power spectrum, $4\,\pi\,k^3\,P(k)$, the middle panel the ratio of each contribution to P_{mm}, in the nonlinear and linear cases, and the bottom panel shows the ratio $(P_{NL} - P_L)/P_{mm}$, *i.e.* the difference between each measured nonlinear component, P_{NL}, in Eq. (8), and the corresponding linear prediction, P_L, compared to the nonlinear P_{mm}. All the measurements at redshifts

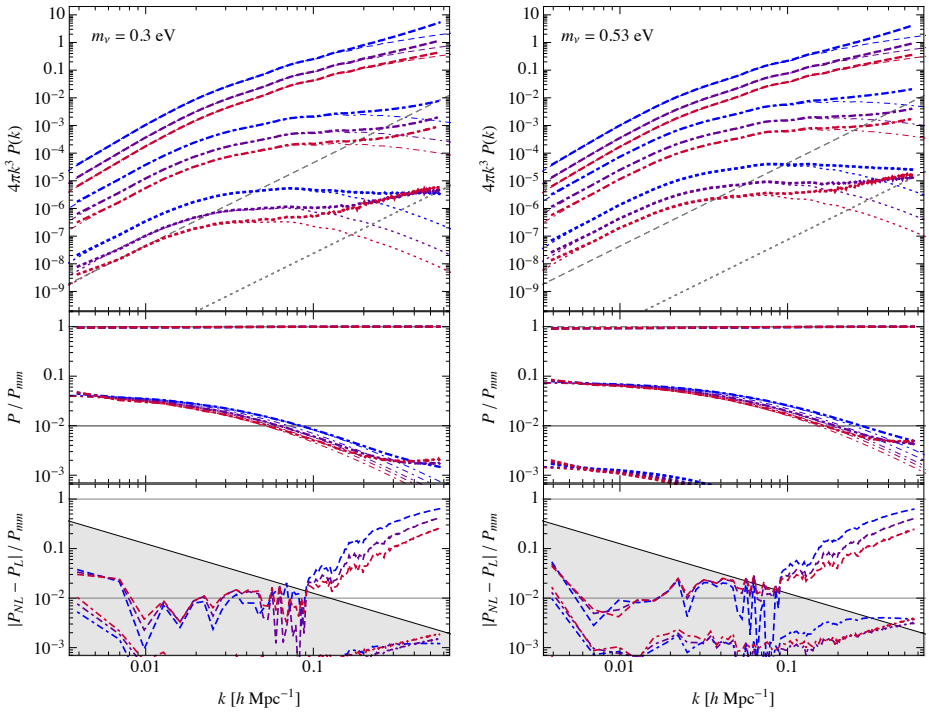

Figure 2.2: Same as figure 2.1, but for $\Sigma\, m_\nu$= 0.3, 0.53 eV.

$z = 0$, 1, 2 are shown with different shades varying from blue to red. Dashed and dotted grey lines on the top panels show the shot-noise contributions to the CDM and neutrinos power spectra, respectively. The shaded area in the bottom panel show the region below the 1-σ, Gaussian uncertainty on $P(k)$, given by $\Delta^2 P(k) = P^2(k)/(2\pi k^2/k_f^2)$, k_f being the fundamental frequency of the simulation box (the shot-noise contribution to the variance is ignored for simplicity).

In the linear regime, $k \lesssim 0.1\, h\,\mathrm{Mpc}^{-1}$, most of the power comes from the CDM component, with the cross power spectrum term accounting roughly for a 10% of the total P_{mm}, and the neutrinos being already negligible (see middle panels of Figures 2.1 and 2.2). On nonlinear scales, from the lower panels we notice that most of the nonlinear contribution to P_{mm} is still given by P_{cc}, which is the only component significantly deviating from the linear prediction, while the other two terms remain linear, and, therefore, less and

less important as we move to smaller scales[2]. It should be kept in mind that each contribution in Figures 2.1 and 2.2 is multiplied by the proper power of f_ν or $(1 - f_\nu)$, with $f_\nu \simeq \mathcal{O}(2 - 4\%)$. We therefore conclude that, on the scales probed by the DEMNUni simulations, and considering the present constraints on the sum of neutrino masses, *the total nonlinear matter power spectrum, in massive neutrino cosmologies, can be described at the 1% level by accounting for the nonlinear evolution of CDM perturbations alone, while adopting the linear prediction for the other components.* This result will be useful for analytical predictions of the nonlinear P_{mm} discussed in the next sections.

2.1 Perturbation Theory

The large volume of the DEMNUni simulations also gives us the possibility to measure the matter power spectrum in neutrino cosmologies at the 1% accuracy level, on a very large range of scales, allowing a test of PT predictions at the accuracy level required by current and futures galaxy surveys.

Several works in the literature have discussed the effects of massive neutrinos in cosmological perturbation theory beyond the linear level [61; 62; 63; 64; 65; 33; 12; 66; 67; 68]. In these descriptions, the neutrino component is treated, similarly to the CDM one, as a single perfect fluid, fully characterised in terms of its density and velocity divergence (see, however, [69; 70] for a multiple-flow approach to the evolution of neutrino perturbations). The main difference with respect to the ΛCDM case is represented by an effective sound speed modifying the Euler equation for the neutrino component, and accounting for the neutrino velocity distribution. The first consequence, at the linear level, is a scale-dependent linear growth factor, $D(k, z)$, for both the CDM and neutrino components. However, the perfect-fluid approximation fails to provide an accuracy for the neutrino power spectrum below the 10% level [33]. Nonetheless, as shown in section 2, since the neutrino contribution to the total matter power spectrum is order of magnitudes smaller than the CDM one, such discrepancies on the neutrino component alone do not affect significantly the CDM and total matter power spectra. Therefore, we will

[2]Let us notice that measurements of the neutrino auto power spectrum and neutrino-cold matter cross power spectrum shown in both Figures 2.1 and 2.2, present a spurious contribution at small scales *not* to be confused with a residual shot noise component. Such contribution, which scales roughly (but not exactly) as $1/k$, is due to the neutrino velocity distribution and it does not grow with time, so that at low redshift is overtaken by the expected neutrino power spectrum. A detailed discussion of numerical issues associated with the set-up of the initial conditions will be discussed in a forthcoming work [60].

assume the two-fluid approximation for all the comparisons of analytical versus numerical results in this section.

In addition, even if in the mildly nonlinear regime the effective sound speed affects as well the mode-coupling at all the orders of the perturbative expansion, we will follow the same approach adopted by [63]. They have shown that limiting the neutrino-induced scale-dependence to the linear growth factor alone (and, therefore, the use of standard EdS- like kernels in the perturbative expansion) proves to be a quite good approximation to the full one-Loop PT solution for the nonlinear CDM field, on scales where one-loop PT is expected to be accurate.

Finally, we will make the additional approximation, already proposed in [61], of describing the neutrino perturbations by means of their linear solution. While this is not *per se* a good assumption [67; 66], it does provide the correct neutrino contribution to the total matter power spectrum on the (large) scales where such contribution is relevant.

As a starting point for future, more accurate comparisons, we will consider, therefore, the following perturbative prediction for the total matter power spectrum

$$P_{mm}^{PT}(k) = (1 - f_\nu)^2 \, P_{cc}^{PT}(k) + 2 \, (1 - f_\nu) \, f_\nu \, P_{c\nu}^{L}(k) + f_\nu^2 \, P_{\nu\nu}^{L}(k) \, . \qquad (2.1)$$

Here, the contribution $P_{cc}^{PT}(k, z)$ represents the nonlinear power spectrum predicted in perturbation theory along the lines of [63], *i.e.* it is computed in terms of its linear counterpart, $P_{cc}^{L}(k, z)$, which provides the correct *linear* scale-dependence of the growth factor, but assumes the standard EdS nonlinear kernels in the perturbative expansion. Differently from previous works, however, we do not only consider standard, one-loop corrections to P_{cc}^{L}, but we take into account also standard PT two-loop corrections, as well as the "regularised" predictions based on the multi-point propagator expansion of [71], computed using the RegPT code of [72]. However the RegPT code does not account for the evolution of the scale-dependent linear growth factor, in general, and in particular in massive neutrino models; therefore the linear $P(k)$ and σ_8 at $z = 0$ are not sufficient to produce the correct outputs at redshifts $z > 0$. To overcome this difficulty, we do not let the code evolve the $P(k, z = 0)$ using the hard-coded ΛCDM growth factor, but instead we provide directly as input the linear $P(k, z > 0)$ from CAMB (which therefore correctly includes the scale-dependent evolution of the linear growth factor), and cheat the code by pretending that the computation is done at $z = 0$, so that it is not required to evolve $P(k)$ with the wrong hard-coded growth factor.

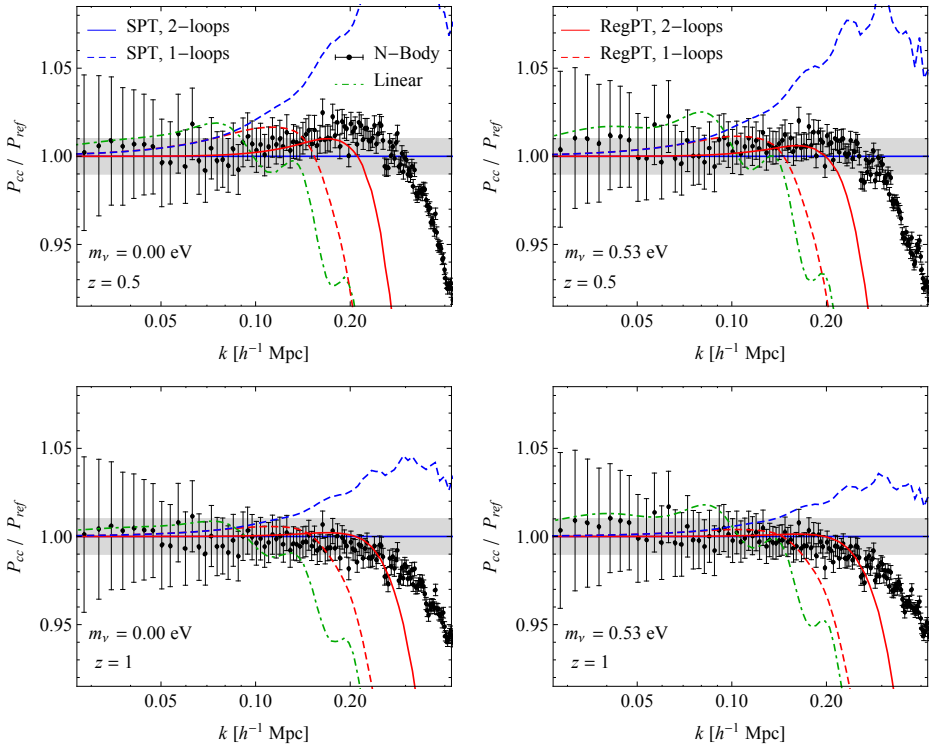

Figure 2.3: Perturbation Theory predictions for the cold matter power spectrum $P_{cc}(k)$. Each panel shows the measurements from the N-body simulations, divided by the reference power spectrum given by the two-loop, standard PT results (*black points with error-bars*). Also shown are the corresponding ratios for the linear (*green, dotted*), one-loop, standard PT (*blue, thin, dashed curve*), multi-point propagator expansion at one- (*red, thick, dashed*) and two-loops (*red, thick, continuous*) ass obtained from the REGPT code of [72].

While this is not the most rigorous approach, it represents a practical application, to massive neutrino scenarios, of available tools developed within the ΛCDM framework. As we will see, the gain in accuracy achieved by recent resummation schemes, applied here to the CDM component alone, might compensate for the crude approximations that this approach implies. Clearly we are only considering predictions for the CDM and total matter power spectra, as these statistics are the relevant ones for galaxy clustering and weak lensing observations.

In Figure 2.3 we show the perturbative results against the measurements at $z = 0.5$, 1, and for $\Sigma\, m_\nu = 0$, 0.53 eV. Error bars are the theoretical expectation for a Gaussian field, that is

$$\Delta P^2(k) = \frac{1}{2\pi\, k^2\, k_f} \left[P(k) + \frac{1}{(2\,\pi)^3\, \bar{n}} \right]^2 , \tag{2.2}$$

where $k_f \equiv 2\pi/L$ is the fundamental frequency of the simulation box, L being its linear size, and $\bar{n}$ is the particle number density accounting for the shot-noise component[3].

Let us first notice that, in the ΛCDM case (left panels in Figure 2.3), the two-loops standard PT does not provide a good fit to the data at low redshifts [74; 75], while it reproduces fairly well the simulation measurements at $z \geq 1$. Analytic predictions are 1% accurate at $z = 1$, up to a maximum wave-number $k_{max} \simeq 0.3\, h\, \mathrm{Mpc}^{-1}$ [4].

Turning our attention to the CDM power spectrum in massive neutrino cosmologies (right panels in Figure 2.3), at all z's we find approximately the same accuracy of to the ΛCDM case.

Given a prediction for the CDM power spectrum accurate at the 1% level up to a given k_{max}, we check if the perturbative approach of Eq. (2.1) reproduces, with the same level of accuracy, the total matter power spectrum measured from the simulations. The results are illustrated in Figure 2.4, which shows that, indeed, the linear treatment of the $P_{c\nu}$ and P_ν contributions to the total P_{mm} proves to be a very good approximation. The difference in the accuracy of the predictions between the $\Sigma\, m_\nu = 0.3$ eV (*left panels*) and the $\Sigma\, m_\nu = 0.53$ eV (*right panels*) cases is again mainly due to the different values of f_ν and, therefore, to the different effect of neutrino free streaming on dark matter perturbations, according to the total neutrino mass: for a given value of Ω_m, a larger value of $\Sigma\, m_\nu$ not only increases the relative amount of neutrino perturbations that are washed out below the free streaming scale, λ_{FS}, consequently reducing the contribution of P_ν and $P_{c\nu}$ to the total P_{mm}, but also decreases the factor $(1 - f_\nu)^2$ in front of P_{cc} in Eq. (2.1), where the nonlinear evolution of P_{cc} is in turn suppressed, with respect to the massless case, by the action of the total gravitational potential sourced both by CDM and massive neutrinos. Apart from inducing a scale-dependence of the linear growth factors for CDM and total matter, the main direct product

[3] The relatively small scatter of data points with respect to the error bars is due to the specific seed chosen for the random number generator used for the set-up of the initial conditions [73].

[4] It is worth noticing that the agreement may also depend on the simulation mass resolution; we expect that much higher resolutions lead to more power at small scales [76].

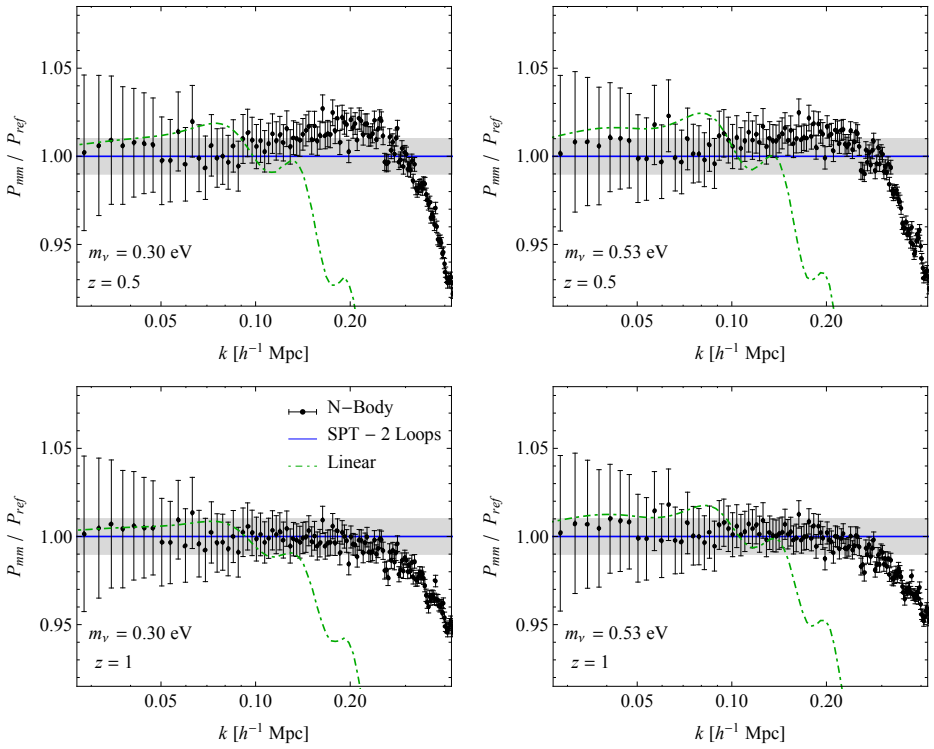

Figure 2.4: Same as Figure 2.3 but for the total matter power spectrum with $\Sigma\, m_\nu$= 0.3 eV (*left panels*) and 0.53 eV (*right panels*). Theoretical predictions have been obtained using Eq. (2.1), *i.e.* computing nonlinear correction for CDM only.

of this physical mechanism is represented by a lower amplitude of linear perturbations at $z = 0$, where $\sigma_{8,cc} = 0.786$, 0.740, and $\sigma_{8,mm} = 0.770$, 0.717, for $\Sigma\, m_\nu$= 0.3, 0.53 eV, respectively. We will show in §2.2 that, on scales much smaller than the so-called turn-over scale, beyond the mildly nonlinear regime, $k > 0.2\ h\,\mathrm{Mpc}^{-1}$, where the growth factor scale-dependence induced by neutrino free streaming approaches its asymptotic value depending only on f_ν (see Eq. (18) in §3.3), the effect of massive neutrinos on P_{cc} and P_{mm} mostly reduces to a mere rescaling of the power spectra in the massless case, according to the values of $\sigma_{8,cc}$ and $\sigma_{8,mm}$.

Recently the BOSS collaboration released new constraints on neutrino masses based on measurements of the galaxy power spectrum multipoles

in redshift space [23] at the mean redshift $z = 0.57$. They assumed the theoretical modellling of the data and hence the constraint of $f\sigma_8$ to be robust against variation of the cosmology, justifying this claim in massive neutrino cosmologies with the use of RegPT on the total P_{mm}. The outcome of such a calculation, in principle even less theoretically justified than our crude assumptions, is very similar to our results obtained via Eq. (2.1); we have checked that any difference between the two approaches stays below the 1% level at the scales relevant for current observations.

A test somehow similar to the one presented here is shown in [77], where the authors compare different PT predictions, including the Time-RG method of [78; 64], to simulations of CDM particles, modifying only the background evolution and the initial conditions to account for free streaming massive neutrinos. They show that PT predictions are in agreement with the measurements of CDM power spectra, extracted from their CMD simulations, at the % level, over a similar range of scales as tested in this work. However they assume a scale-independent growth rate to rescale back the late time ($z = 0$) CDM power spectrum, $P_{cc}(k)$, to the initial redshift of the simulations. By doing so, the linear dynamics cannot be correctly recovered at any z other than $z = 0$.

Finally, the crucial results of this section rely on the discussion of section 2 and the measurements shown in Figures 2.1 and 2.2, that is the contributions from the two terms, other than P_{cc}, entering Eq. (2.1), and in particular from the cross power spectrum $P_{c\nu}$, always remain negligible compared to P_{cc} on nonlinear scales, at least for the level of accuracy requested for PT to be useful.

2.2 Fitting functions

Given the limitations of the perturbative approaches, it is sometimes convenient and/or sufficient to resort to fitting functions for the nonlinear matter power spectrum. In this section we see how the approximation of linear evolution for neutrino perturbation can be applied as well to the HALOFIT prescription [53].

The HALOFIT formula, originally based on stable clustering considerations [79; 80], provides a mapping between the linear power spectrum and the nonlinear one, which in turn depends on few cosmological parameters, *e.g.*, Ω_m, and several free parameters determined by comparisons against measurements from N-body simulations. A new, more accurate, version of the fitting formula has been recently presented by [54]. The revised formula

is expected to be accurate at the 5% level for $k < 1\,h\,\mathrm{Mpc}^{-1}$ and $z \leq 10$, while it degrades to the 10% level for $k < 10\,h\,\mathrm{Mpc}^{-1}$ and $z \leq 3$.

In the context of massive neutrinos cosmologies, Ref. [48] provided corrections (controlled by a few, additional parameters) to the original HALOFIT formula, in order to account for neutrinos effects on the nonlinear *total* matter power spectrum[5]. However, as shown in Figures 2.1 and 2.2, nonlinear corrections to the cross power spectrum between CDM and neutrinos are below the percent level, therefore we wonder if, similarly to Eq. (2.1), a fitting formula for the total matter power spectrum, $P_{mm}(k)$, could be given in terms of the linear predictions, $P^L_{c\nu}(k)$ and $P^L_{\nu\nu}(k)$, and the HALOFIT fitting formula applied directly to the linear CDM power spectrum, $P^{HF}_{cc}(k)$, that is

$$P^{HF}_{mm}(k) \equiv (1-f_\nu)^2\,P^{HF}_{cc}(k) + 2\,f_\nu\,(1-f_\nu)\,P^L_{c\nu}(k) + f_\nu^2\;P^L_{\nu\nu}(k)\,. \qquad (2.3)$$

Here $P^{HF}_{cc}(k) \equiv \mathcal{F}_{HF}[P^L_{cc}(k)]$, where the HALOFIT mapping, $\mathcal{F}_{HF}$, between linear and nonlinear power spectra does not account for additional corrections due to massive neutrino physics.

In the left column of Figure 2.5 we show the ratio of the measured CDM power spectrum, $P_{cc}(k)$, to the prediction, $P^{HF}_{cc}(k)$. Each row corresponds to a distinct value of $\Sigma\,m_\nu$, while each panel shows the value of this ratio at redshifts $z = 0$, 0.5, 1, 1.5, 2, with colour shades ranging from blue to red. The shaded areas denote the regions beyond the accuracy claimed for the revised formula of [54]. The left panels of Figure 2.5 show, indeed, not only that $P^{HF}_{cc}(k)$ provides the expected accuracy, but that it works equally well for all the considered values of the total neutrino mass. This is essential to justify our assumption of applying the HALOFIT mapping to the CDM component alone. Here, we stress again that the version of HALOFIT employed for $\mathcal{F}_{HF}[P^L_{cc}(k)]$ does not include any effect due to massive neutrinos on the CDM clustering, since here we use the HALOFIT version developed by [54] in the ΛCDM framework. This result is similar to that obtained in §2.1 for perturbation theory, and it is a crucial step before checking the validity of the assumptions made in Eq. (2.3).

The right column of Figure 2.5 presents the ratio of the measured total matter power spectrum, $P_{mm}(k)$, to the prediction $P^{HF}_{mm}(k)$ of Eq. (2.3). In addition, dashed curves show the inverse ratio of $P^{HF}_{mm}(k)$ to the specific HALOFIT extension to massive neutrino cosmologies of [48], denoted as $P^{HF-\nu}_{mm}(k)$. We notice that the simple prescription of Eq. (2.3), while avoiding

[5]The massive neutrino corrections of [48] have been implemented, along the revised version of [54], in the most recent versions of the `camb` [31] and `class` [81] codes.

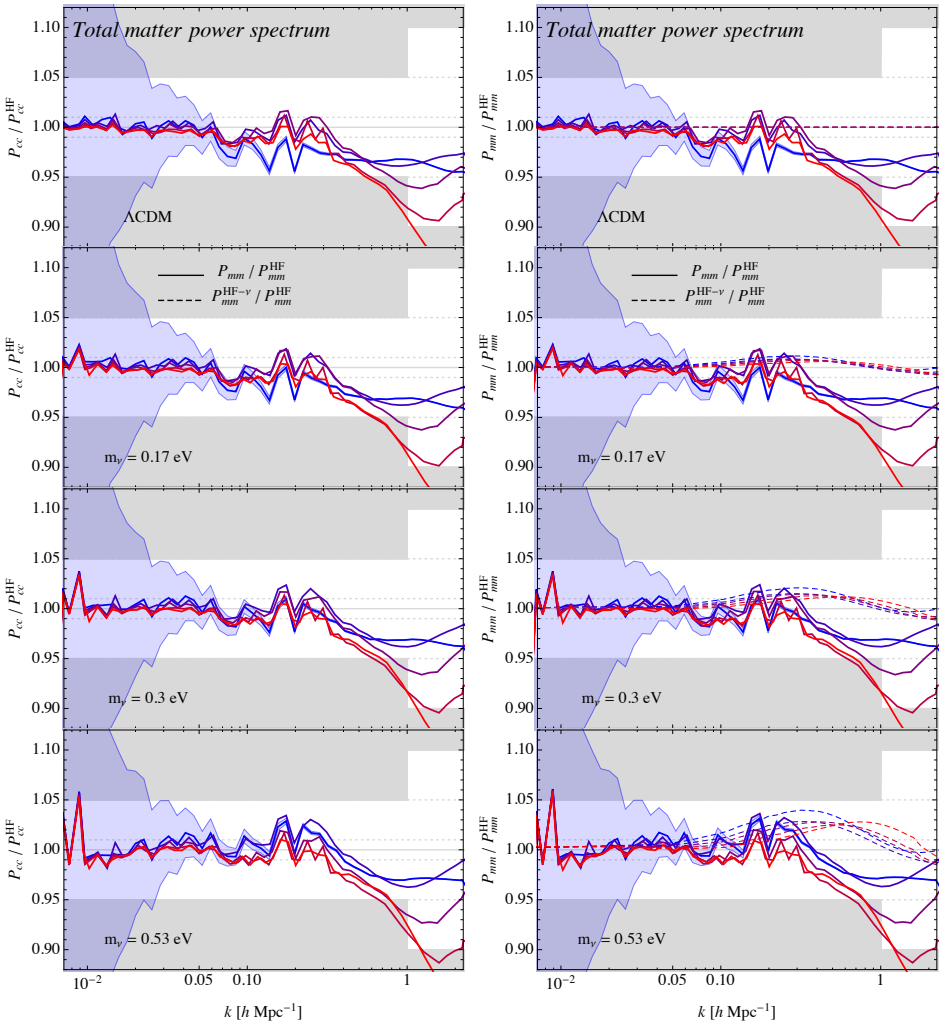

Figure 2.5: *Left column*: ratio of the measured CDM nonlinear power spectrum, P_{cc}, to the HALOFIT prediction $P_{cc,HF}$ from [54], with no additional parameters to account for neutrino effects. Each panel correspond to one value of $\Sigma\, m_\nu$, with different colours denoting different redshifts: $z = 0$, 0.5, 1, 1.5, 2, blue to red. Shaded areas denote the regions beyond the accuracy expected for the formula. *Right column*: ratio of the measured total matter nonlinear power spectrum, P_{mm}, to the prediction, P^{HF}_{mm}, of Eq. (2.3).

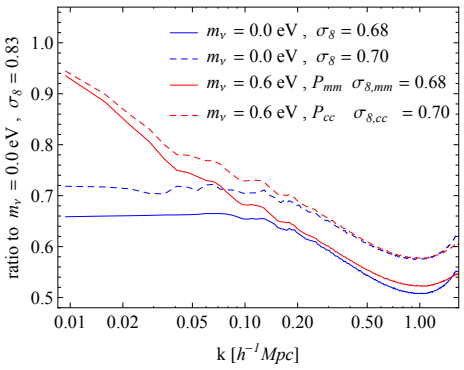

Figure 2.6: Comparison between the nonlinear power spectra measured in two ΛCDM models (*blue curves*) with $\sigma_8 = 0.68$ (*continuous*) and $\sigma_8 = 0.70$ (*dashed*) against the same quantity measured in massive neutrinos models (*red curves*) with $\sigma_{8,mm} = 0.68$ (*continuous*) and $\sigma_{8,cc} = 0.70$ (*dashed*). All the quantities are shown as ratios to the power spectrum for a ΛCDM model with $\sigma_8 = 0.83$ to compare the *shape* of the suppression resulting from either a lower overall normalisation or neutrino effects. Measurements for this figure only are from the simulations of [49].

introducing additional parameters to the fitting formula of [54], remains well within the expected HALOFIT accuracy. On the other hand, the discrepancies between the prediction of Eq. (2.3) and the $P_{mm}^{HF-\nu}(k)$ fit of [48] are within 4%, with the latter *ad-hoc* fit not improving particularly over the former.

Here we would like to make some final considerations. The results of this section rely on the fact that, in the first place, in the absence of strong baryon physics, on scales much beyond the mildly nonlinear regime, $k > 0.2\ h\,\mathrm{Mpc}^{-1}$, where the linear growth factor scale-dependence induced by neutrino free streaming approaches its asymptotic value, the extent of the nonlinear evolution of the power spectrum can be accounted for via the amplitude of the linear power spectrum, *regardless* of the physical mechanism responsible for the amplitude itself. In other terms, on nonlinear scales, we expect a similar behaviour for the nonlinear matter power spectrum evolved from a linear power spectrum suppressed by massive neutrino free streaming, as from a different linear power spectrum with a lower, primordial normalisation. This assertion can be easily tested with N-body simulations and the results are shown in Figure 2.6, which makes use, however, of measurements from the simulations described in [49; 82]. The plot shows ratios, with respect to the matter power spectrum in a given ΛCDM cosmology with $\sigma_8 = 0.83$, of

the matter power spectrum in other ΛCDM cosmologies (with different σ_8 normalisations), and of the CDM and total matter power spectra in massive neutrino cosmologies, where either the value of $\sigma_{8,cc}$ or $\sigma_{8,mm}$ are matched to the ΛCDM ones. We observe that on nonlinear scales, $0.2 < k < 1\ h\,\mathrm{Mpc}^{-1}$, a ΛCDM model with a given σ_8 is nearly indistinguishable from a massive neutrino model with the same value for $\sigma_{8,cc}$. A lower agreement is found when the match is done in terms of $\sigma_{8,mm}$, since the relevant nonlinear evolution is indeed given by CDM perturbations. This result represents the well known degeneracy between $\Sigma\, m_\nu$ and σ_8 at small scales, and implies that the enhanced, nonlinear suppression of the matter power spectrum on nonlinear scales can be obtained tuning the normalisation of the linear one, without resorting to peculiar effects of massive neutrinos. Nonetheless, here we stress that, such kind of degeneracy can be broken when observing the power spectra on a much larger range of scales, $0.01 < k < 5\ h\,\mathrm{Mpc}^{-1}$, or at different redshifts, by means of future large sky galaxy surveys as, *e.g.*, Euclid.

Chapter 3

Dark matter halos

The abundance by mass of galaxy clusters, and of the dark matter halos which surround them, is a major tool for cosmological parameter estimation (see [83] for a review). Large catalogs are now available from optical [84], X-ray [85; 86] and Sunyaev-Zel'Dovich (SZ) observations [87; 88; 41]. Previous work has shown that, in neutrino-less ΛCDM models, the halo mass function over a wide range of redshifts and background cosmologies can be scaled to an almost universal form [89; 90]. This universality is particularly useful, as it vastly simplifies analyses of observed datasets. However, it has been known for some time that this sort of universality should only be an approximation [90; 91], and departures from universality of about the expected level have indeed been detected in recent simulations [92; 93]. Here we study the issue of universality, and departures from it, in the context of neutrino cosmologies. While these are interesting in their own right, this study is motivated in part by the tension reported by the Planck collaboration between their temperature and cluster counts measurements [41; 94].

The shape of the (halo) galaxy power spectrum and correlation function are also sensitive to the underlying cosmology, and can be used to put strong constraints on cosmological parameters [95; 96]. In particular, such observables are able to provide upper bounds to the sum of neutrino masses, [8; 9; 10; 11; 12; 14; 15; 16; 19; 17; 23; 38]. In the Halo Model of large scale structure [97] these are a consequence of the fact that the spatial clustering of dark matter halos is biased with respect to that of the total mass, and the details of how this bias depends on halo mass depend on the background cosmological model. Therefore, a related goal of this work is to provide an analysis of halo bias in neutrino cosmologies.

Halos in each simulation, both in the H-group and the in DEMNUni's,

are identified by running the Friends-of-Friends (FoF) algorithm [98] on the CDM particles only, with linking length set to $b = 0.2$ times the mean CDM-particle distance. The FoF halo masses are corrected for the statistical noise arising from particle discreteness following [99], by setting $M_{halo} = N_{corr}\, m_p^c$, m_p^c being the cold dark matter particle mass and

$$N_{corr} = N_p\,(1 - N_p^{-0.6}), \tag{3.1}$$

where N_p is the original number of particles linked together by the FoF algorithm. For the minimum number of particles per halo considered in this paper, $N_p = 32$, this correction can be larger than 15%. Since eq. (3.1) is a correction to N_p only, halos of the same mass in different cosmologies undergo different corrections because m_p^c is different in the different runs (because Ω_c increases when Ω_ν decreases). Halo power spectra and cross halo-matter power spectra are computed applying different cuts in mass. The shot-noise contribution to the halo power spectra at $z = 2$ is large, so we only present results for $z = 1$, 0.5 and 0.

One might have worried that if neutrinos affect halo profiles, then eq. (3.1) should be slightly modified in neutrino cosmologies. Simulations have indeed shown that halos in neutrino cosmologies are less concentrated than their counterparts in standard ΛCDM models, because their formation time is delayed due to the suppression of the power spectrum induced by neutrinos [46; 45]. However this effect is rather small and it can be safely neglected.

Another possible choice would be to run the FoF algorithm on all the particles in the box. This test is discussed in detail in [49]. The halo power spectra (for the two mass thresholds defined above), differ by less than 0.5%, in good agreement with the expectation that CDM particles contribute the most to the mass of halo and hence to its center of mass. However some discrepancies are present in the halo mass function, especially at low masses, produced by spurious assignment of neutrinos to halos. For small halo masses, in fact, neutrinos are not bound, they free-stream due to their large velocities, but the FoF finder wrongly assigns them to halos. This contamination is more important at low neutrino number densities like those considered in this paper. A proper procedure which excludes unbound neutrino particles would therefore lead to differences in the halo power spectrum that are expected to be even smaller than those found in our simple test. For high-mass halos the contribution of both bound and unbound neutrinos to the total mass is small, typically less than 0.5%. In the following we will always consider FoF CDM-only halos, but see [49] for further details and tests.

3.1 The halo mass funtion

3.1.1 Universality in the CDM component

At any redshift z the comoving number density of halos per unit mass, $n(M)$, can be written in the following form

$$n(M) = \frac{\rho}{M} f(\sigma, z) \frac{d \ln \sigma^{-1}}{dM} , \tag{3.2}$$

where

$$\sigma^2(M, z) = \int d^3k \, P(k, z) \, W_R^2(k) \tag{3.3}$$

is the r.m.s. of the linear density field smoothed on a scale R with a filter function $W(kR)$, ρ is the comoving background density. The relation between the smoothing scale R and the halo mass M is dictated by the choice of the filter function, being given by

$$M \equiv \rho \int d^3x \, W(x, R) . \tag{3.4}$$

In this context, we will define the mass function to be universal when $f(\sigma, z) = f(\sigma)$, i.e. the function $f(\sigma)$ does not depend on redshift. This shows that the quantity which is expected to be nearly universal is not $n(M)$ itself but

$$\nu \, f(\nu) \equiv \frac{M^2}{\rho} \, n(M) \, \frac{d \ln M}{d \ln \nu}, \tag{3.5}$$

where $\nu \equiv \delta_{cr}/\sigma$, for some constant δ_{cr} which we will discuss shortly. (It is unfortunate that this scaling variable is called ν when it has, of course, nothing to do with neutrinos! We trust this will not lead to confusion.) Operationally, one measures this quantity by first transforming M to $\ln \nu$, and then binning the counts in ν upon giving each halo a weight which equals M/ρ.

Without previous knowledge of the effects that a non-vanishing neutrino mass could have on the process of halo formation it is not obvious what to use in eq. (3.2) for the quantities ρ, M and σ, since they can be defined either in terms of all dark matter species or in terms of the cold one alone. All we will justify later, we identify halos in simulations by using the CDM component only. In this case, one would define the relation between CDM halo mass and the scale of a TopHat filter by

$$M = \frac{4\pi}{3} \, \rho_{cdm} \, R^3 . \tag{3.6}$$

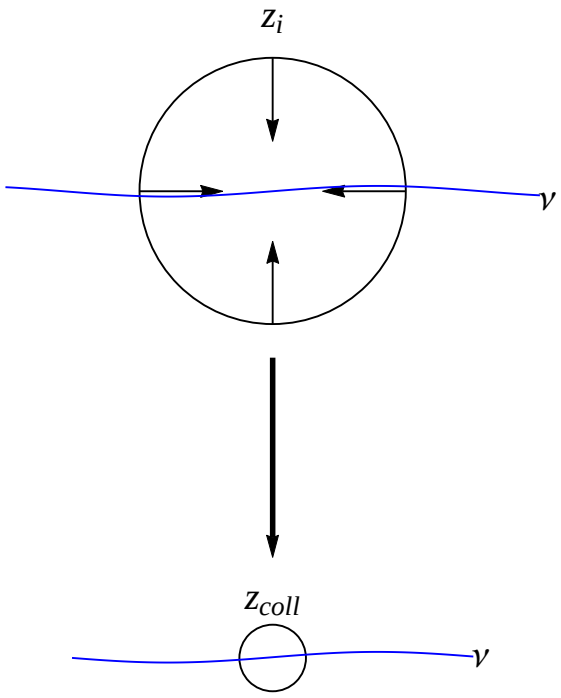

Figure 3.1: Pictorial view of spherical collapse in massive neutrino cosmologies. At the initial time, z_i neutrino perturbations are so shallow on the scale of the initial patch that are irrelevant for the subsequent evolution.

Then, since the M in eq. (3.2) is really M_{cdm}, the ρ in eq. (3.2) should be replaced by ρ_{cdm}, i.e. the *cold* dark matter density. This choice is consistent with previous work [45; 100; 46], where it is shown that the halo counts in $f_\nu \neq 0$ simulations are in better agreement with known (i.e. $f_\nu = 0$ based) fitting formulae if ρ_{cdm} is used.

The last piece of information we need is the appropriate quantity to use for σ in eq. (3.2). It is tempting to assume that the relevant quantity is σ_{cc}, which should be computed by setting $P = P_{cc}$ in eq.(3.3). We believe this is well-motivated for the following reason. In the spherical collapse model, and assuming general relativity, the evolution of a spherical region is controlled by the amount of mass inside its initial volume. For a Gaussian random field, as the linear density field δ, a natural choice to describe the system is its variance smoothed on the scale R associated to the initial region, $\sigma(R)$. Due to the

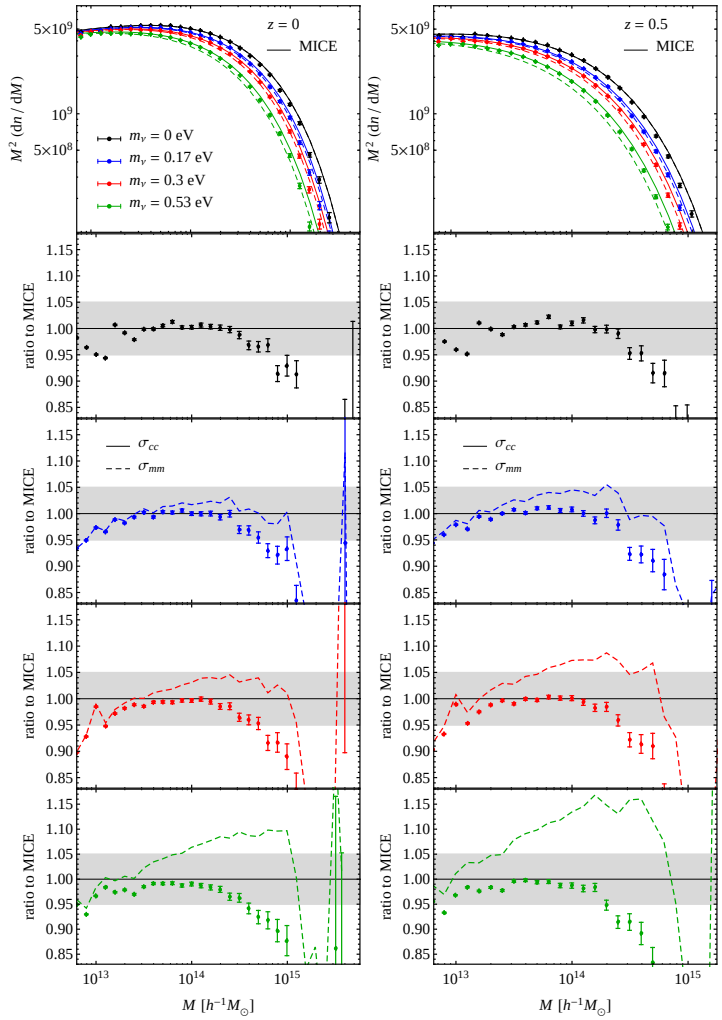

Figure 3.2: Halo mass function for the four DEMNUni models at redshift $z = 0$ (*left panel*) and $z = 0.5$ (*right panel*). Top panels show the quantity $M^2\, n(M)$ as a function of mass, together with the predictions of the MICE fitting formula [93] using $\sigma = \sigma_{mm}$ (*dotted curves*) and $\sigma = \sigma_{cc}$ (*dashed curves*). Black, blue and red and green data points correspond respectively to the $m_\nu = 0$, 0.17,0.3 and 0.53 eV results. Lower panels show the residuals of measurements with respect to the MICE formula with $\sigma = \sigma_{cc}$.

tiny value of neutrino masses, the scale R, usually a few Megaparsecs, is much smaller than the free streaming length of massive neutrinos $\lambda_{\rm FS}$, typically tens of Megaparsec, and therefore neutrino perturbations are vanishingly small inside the collapsing region. This implies that $\sigma(R)$ should be computed using the CDM plus baryon perturbations only, *i.e.* treating the CDM as though it alone is clustering in an effective background cosmology which depends on the large scale value of ρ_ν. A similar argument applies to the critical overdensity required for collapse at a given redshift, δ_{cr}, that depends on neutrino masses only through their effect on the background evolution [101]. Moreover, studies of spherical halo collapse suggest that what really matters for halo formation is the ratio δ_{cr}/σ, where δ_{cr} is the density which linear theory predicts is associated with nonlinear halo collapse [89; 102; 90]. When $f_\nu = 0$ then $\delta_{cr} \approx 1.686$ is only a very weak function of (Ω, Λ) (e.g. [103]), so one might expect the dependence of δ_{cr} on $\Omega_{eff}(f_\nu)$ and $\Lambda_{eff}(f_\nu)$, and hence on f_ν itself to be negligible. [101; 104; 105] have confirmed that the effects of massive neutrinos on δ_{cr} are less than 1% for the range of f_ν we will consider. solving numerically for the collapse of a Top-Hat perturbation in a massive neutrino cosmology. That is to say, in these massive neutrino models, the physically relevant quantity δ_{cr}/σ is really δ_{cr}/σ_{cc}, and since δ_{cr} is almost independent of m_ν, the scaling variable is actually just σ_{cc}. In Figure 3.1 we sketch how a spherical perturbation evolves in massive neutrino cosmologies, with neutrinos playing a negligible role.

Note that $\sigma_{cc} \geq \sigma_{mm}$ always (see Figure 2) implying that for a given cosmology, using σ_{cc} in the computation of the mass function leads to more halos than using σ_{mm}

Nevertheless we emphasize that if neutrino perturbations had played a role in the collapse of regions, as happens for warm DM or clustering quintessence, then we would not have been allowed to simply replace σ with σ_{cc}. In these other cases, a more complicated analysis (following methods outlined in [106]) would be needed. Note that a model which uses σ_{cc} predicts more halos than one with σ_{mm}, since (after the non-relativistic transition of neutrinos) $\sigma_{cc} \geq \sigma_{mm}$ for all relevant smoothing scales (see eq. 10).

The uppermost panels of Figure 3.2 show $M^2\, n(M)$ as a function of halo mass M in the four DEMNuni cosmologies (black, blue, red and green symbols); the left and right columns show results at $z = 0$ and $z = 0.5$. In each panel, the symbols show the measurements and errorbars represent Poisson noise. These are compared with the fitting formula which describes the MICE simulations:

$$f(\sigma, z) = A(z) \left[\sigma^{-a(z)} + b\right]\, e^{-c(z)/\sigma^2}\,, \tag{3.7}$$

where the parameters $A(z)$, $a(z)$, $b(z)$ and $c(z)$ depend on redshift (we use the values from [93]).

For the cosmologies with massive neutrinos, we do this in two ways, by setting $\sigma = \sigma_{mm}$ (dotted curves) or σ_{cc} (dashed curves)[1]. I.e., the dotted and dashed curves represent the assumptions that the relevant sigma is the rms fluctuation in total density field or the CDM component respectively. For the $m_\nu = 0$ eV case, where $P_{cc} \equiv P_{mm}$, we only show a dashed curve. The lower panels of Figure 3.2 show the residuals with respect to the σ_{cc}-based curve, separately for the three cosmologies of Set A, second to fourth row.

We notice, in the first place, a small (less than 5%) discrepancy between our ΛCDM, $m_\nu = 0$ eV simulations and the MICE fit over the whole relevant mass range. As this discrepancy is about the same at higher redshifts, we conclude that our simulations show z-dependent departures from universality that are close to those observed in the MICE analysis, see also Figure 3.3. We will return to this shortly. Agreement with the MICE predictions is not, in any event, the focus our attention. More interesting, is that the difference with respect to the MICE fits remain roughly the same for all values of m_ν when σ_{cc} is used, whereas they grow significantly when σ_{mm} is used instead (dotted curves).

To better highlight the difference between the two descriptions, it is convenient to compare measurements of the differential mass function directly as a function of the variable $\nu \equiv \delta_{cr}/\sigma$, for which the mass function is given by eq.(3.5). Such a comparison is made in Figure 3.4 which presents the same measurements of Figure 3.2, this time in terms of $\nu f(\nu)$. In particular, each panel shows the ratio of $\nu f(\nu)$ from MICE to the one of the four simulations with different neutrino masses at a given redshift ($z = 0$, left panel, and 1, right panel). Also shown is the prediction from the MICE fit of [93], which explicitly depends on redshift, as a dashed black curve. Left column shows the results as a function of $\nu = \delta_{cr}/\sigma_{cc}(M)$, i.e. in terms of the r.m.s. of the cold dark matter, while in the right column we set $\nu = \delta_{cr}/\sigma_{mm}(M)$. It is evident that the description in terms of σ_{mm} results in large departures from universality as m_ν is varied. In contrast, using σ_{cc} yields results which are

[1]To partially remove finite-volume effects, we set the lower cut-off in the integral of eq. (3.3) to the fundamental frequency of the box, $k_F = 2\pi/(2,000\,h^{-1}\,\mathrm{Mpc})$. Another possible correction for the finite size of the simulation box could be to measure the linear power spectrum from the box itself once the initial displacements were generated instead of using Boltzmann codes (see, e.g. [107; 108]). This method has the advantage of removing cosmic variance and volume effects, but it gives a different σ-M relation for each box that one has then to average over. For practical reasons we assume the linear power spectra to be given by the `CAMB` predictions for each model and we always assume the mass-scale relation as in eq. (3.6).

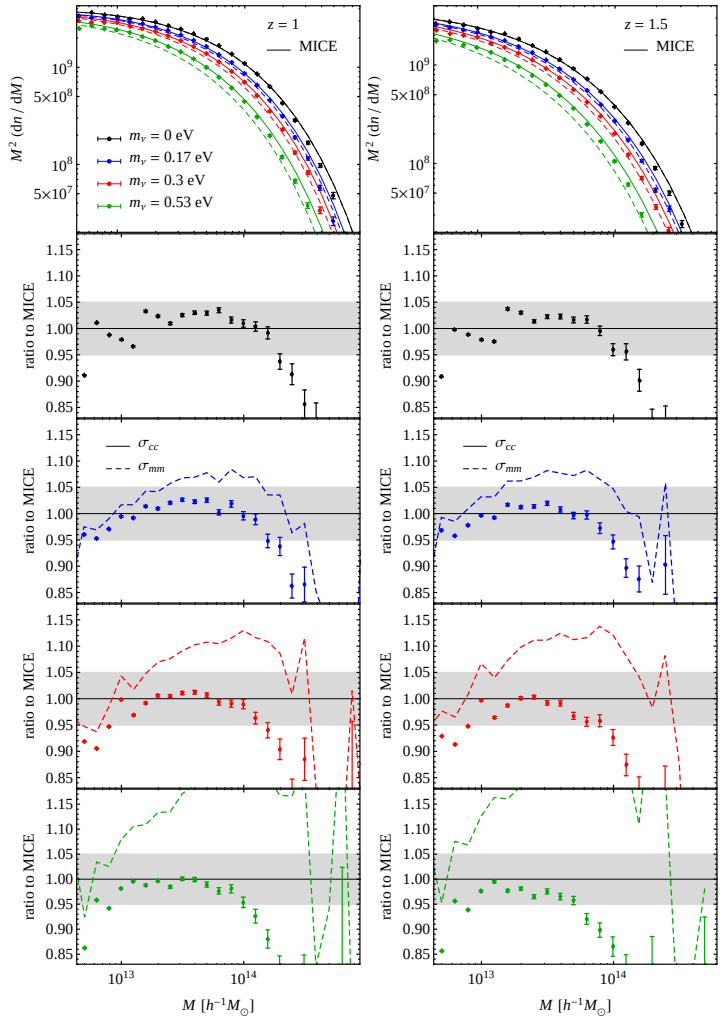

Figure 3.3: Same as Figure 3.2 but at $z = 1, 1.5$.

much more universal.

We can also use halo mass function expressed in terms of ν to compare the two groups of simulation used in this work, making possible to show how the DEMNUni suite represents a huge improvement in both volume and resolution with respect to previous simulations that included a massive neutrino component. In Figure 3.5 we plot halo abundances as a function of the peak height ν from DEMNUni simulations together with the mea-

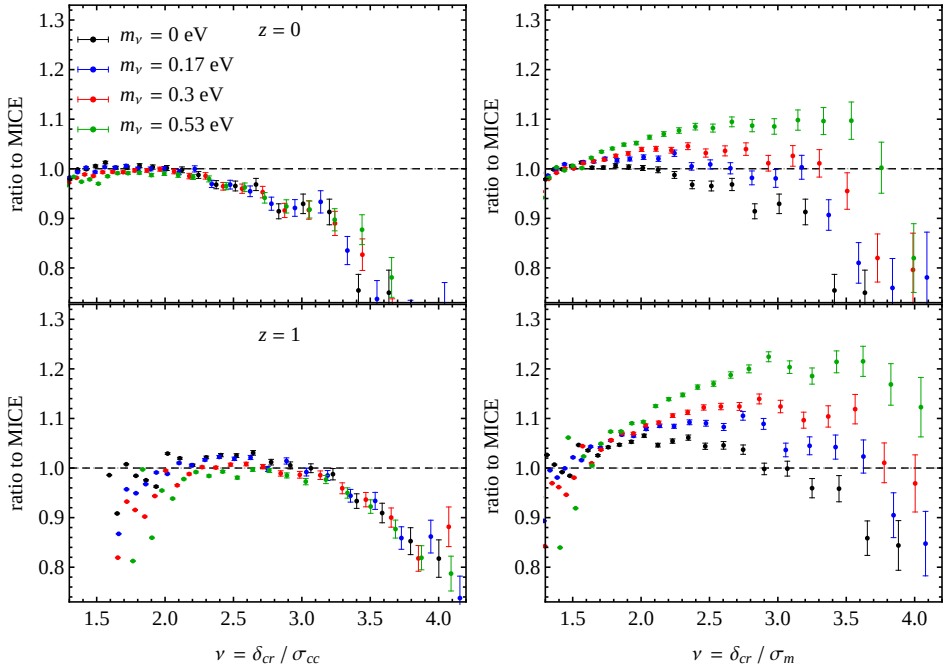

Figure 3.4: Ratio of the measured $\nu\, f(\nu)$ to the MICE formula. Left panels use $\nu = \delta_{cr}/\sigma_{cc}$ while right panels use $\nu = \delta_{cr}/\sigma_{mm}$. Different panels, top to bottom, show the different redshifts $z = 0$ and 1 with all neutrino masses (distinguished by color) shown together.

surements in the H-group. Especially at small values of ν we see that the large number of particles used in the DEMNUni suite allow us to properly resolve low mass halos which instead are affected by resolution effects in the H-group. Assuming universality with respect to cosmology, at $z = 0$ measurements in the DEMNUni at $m_\nu = 0.0$, 0.53 eV align within the errorbars at $\nu \simeq 2$, which corresponds to $M \simeq 1.9 \times 10^{14}\, h^{-1}\, M_\odot$, while in the H-group for the halos in the $m_\nu = 0.0$, 0.6 simulations this happens at $M \simeq 4.3 \times 10^{14}\, h^{-1}\, M_\odot$. At $z = 1$ in DEMNUni we are not affected by resolution at $M \geq 1.0 \times 10^{14}\, h^{-1}\, M_\odot$ and at $M \geq 2.4 \times 10^{14}\, h^{-1}\, M_\odot$ in the H-group. However the H-group is very useful to study degeneracy in cosmological parameters, and halo bias given the large number of realizations available for each model.

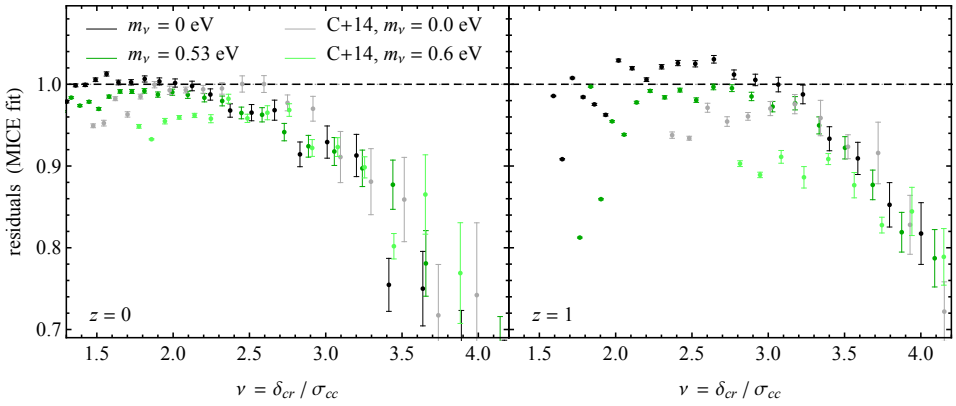

Figure 3.5: Comparison between the halo mass function measured in the DEMNUni suite and in previous work. Left panel shows in black and green measurements in the DEMNUni suite at $z = 0$ for the ΛCDM model and the $\sum m_\nu = 0.6$ eV, while grey and light green points with errorbars are taken from [50]. Right panel presents the same quantities but at $z = 1$.

3.1.2 Cosmological parameters degeneracy

We now look in more detail at the degeneracy between m_ν and σ_8, the variance of matter fluctuations on a scale of $R = 8\,h^{-1}\,\mathrm{Mpc}$. One might expect that the effect of neutrino masses on the halo mass function can be re-absorbed by a suitable change of $\sigma_{8,cc}$ in a standard ΛCDM Universe, in which case the only way to break the degeneracy being measurements at different redshifts, exploiting the differences in the linear growth factors. To explore this we use the H-group of simulation, in particular set B. This allows us to compare an $m_\nu = 0.6$ eV model (H6s8) with a massless neutrino model of set A (H0) that has the same value of $\sigma_{8,mm} = 0.83$. In addition, we can compare two massless neutrino models (H0s8 and H0s8-CDM) to the $m_\nu = 0.6$ eV model of set A (H6), matching the values of both $\sigma_{8,mm}$ and $\sigma_{8,cc}$ of the latter.

As we have seen, CDM halos are primarily sensitive to the relation between neutrino masses and the σ_8 of the CDM species only. Therefore had we normalized the power spectrum of a ΛCDM Universe with the same $\sigma_{8,mm}(z = 0)$ of the correspondent neutrino cosmology, at fixed Ω_m we would have obtained different halo counts even at $z = 0$, with larger discrepancies at higher redshifts. This is shown in figure 3.6. Here, left panels present

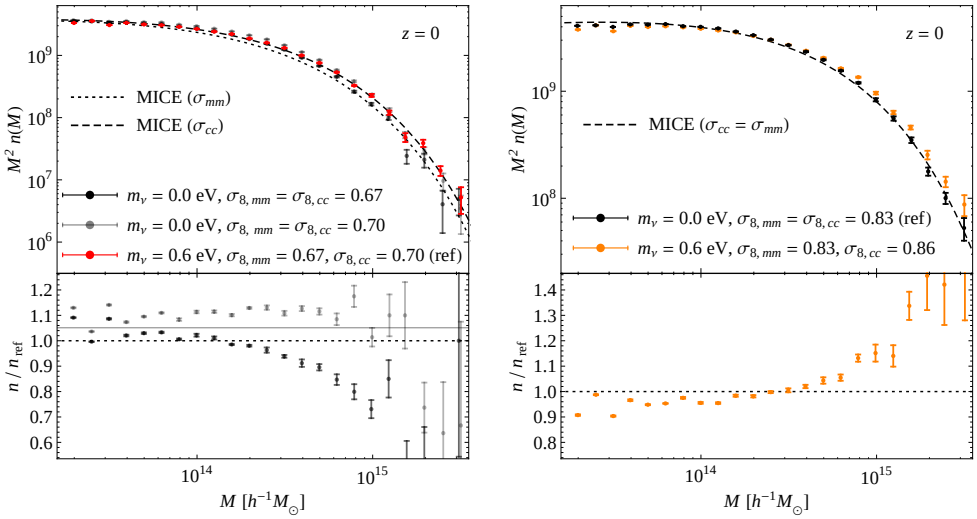

Figure 3.6: Degeneracy between m_ν and $\sigma_{8,mm}$, $\sigma_{8,cc}$: comparison of the mass functions as a function of the mass M and at $z = 0$ from $m_\nu = 0.0$ eV and $m_\nu = 0.6$ eV models, sharing the same value of $\sigma_{8,cc}$ or $\sigma_{8,mm}$. Left panels: comparison between model H6 (red data points) and models H0s8 (grey) and H0s8-CDM (light gray). The lower panel shows the ratio of H0s8 and H0s8-CDM to H6, with the black horizontal line showing the ratio Ω_c(H0s8-CDM)/Ω_c(H6). Right panels: comparison between model H0 (black data points) and model H6s8 (orange). The lower panel shows the ratio of H6s8 to H0.

measurements of the halo mass function at $z = 0$ as a function of mass for the models H6 in red, H0s8 in gray, and H0s8-CDM in light gray, where as expected from previous considerations the H6 cosmology has more objects than the H0s8 model. The difference with increasing M increase as the ratio $\sigma_{cc}(R)/\sigma_{mm}(R)$ grows. The H0s8-CDM model lies much closer to the H6 model: the ratio of the two is almost constant and its difference from unity is mainly due to the different background density appearing on the r.h.s. of eq. (3.2), shown as a continuous horizontal line in the residuals plot. The same arguments hold for the right panel of Figure 3.6, where we compare the H0 run to H6s8, which has $m_\nu = 0.6$ eV and σ_8 matched to be the same as that of H0 at $z = 0$. Again the halo counts differ substantially in the two simulations: H6s8 has more halos because its CDM field has more power on all relevant scales than does the H0 run.

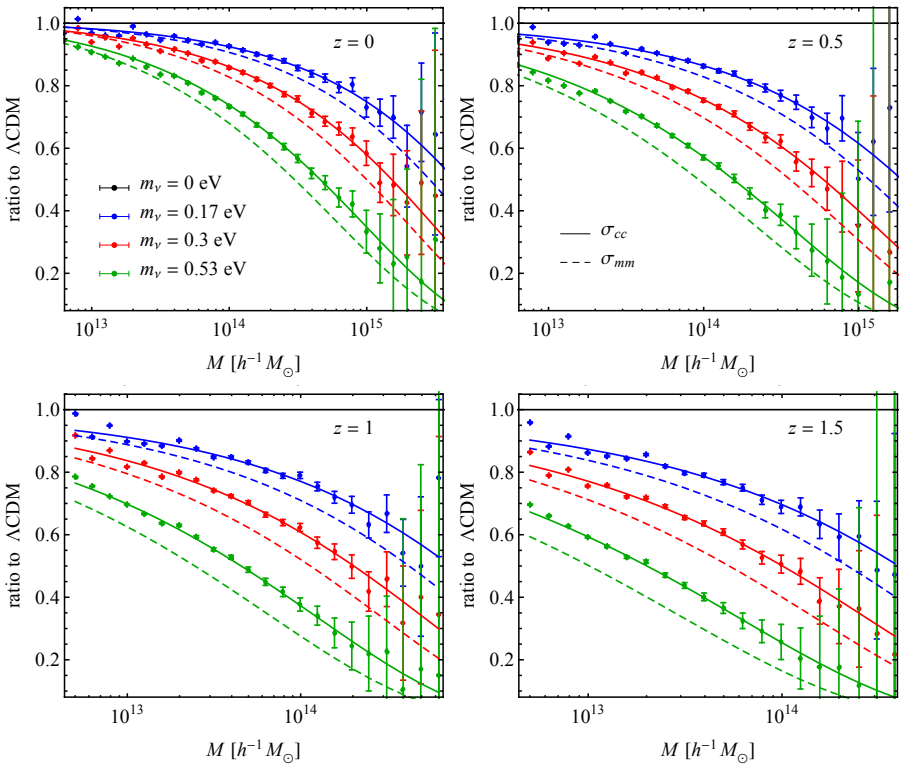

Figure 3.7: Ratio of halo abundances for spherically defined halos in massive neutrino cosmologies to abundances in a standard cosmological model. Theoretical predictions, using σ_{cc} (*continuous curves*) and using σ_{mm} (*dashed curves*), have been obtained using the formula of [92].

3.1.3 Implications for cluster number counts

Results presented in the previous section have important implications for cosmological parameters inference from galaxy clusters observations. In most of previous cosmological analyses [87; 88; 41; 94] the total matter fluctuations, i.e. $\sigma = \sigma_{mm}$, have been used for the prediction of the mass function, leading to possible systematic errors in the derived constraints. The difference is not limited to the expected number of galaxy clusters, which are more numerous if one uses the cold dark matter matter spectrum, but, most importantly, it affects the universality of the halo mass function with respect to cosmology. A key assumption in cosmological analyses is that the shape of the mass

function is insensitive to changes in the background cosmology when the total matter power spectrum is used, while we have shown that this is not the case for massive neutrino models. For cosmological analyses this effect is even more relevant than the relative difference in the same cosmology of the expected number counts from the two prescriptions for the power spectrum.

Observations of galaxy clusters with X-rays and Sunyaev-Zel'dovich measurements are usually calibrated onto spherically defined objects. This means that for this kind of observable FoF halos are not well suited. We therefore repeated the analysis for Spherical Overdensity (SO) halos, identifying halos with SUBFIND[109; 110] as spherical regions with a mean matter density equal to two hundred times the background density. The measurements, shown as ratios to the ΛCDM case, are presented in Figure 3.7, where now we use the Tinker *et al.* fitting formula as a reference for SO halos [92]. Also in this case we observe that the Tinker *et al.* fit, developed in the ΛCDM framework, provides a good fit to simulations with a massive neutrino component when $\bar{\rho} = \bar{\rho}_c$ and $\sigma = \sigma_{cc}$ are used instead of their total dark matter counterparts.

We know would like to be a bit more quantitative, trying to quantify how a different prescription for the HMF can affect the constraints on cosmological parameters provided by cluster number counts by changing the number of clusters predicted for a given cosmology and survey[111].

The number of cluster expected to be detected within a survey with sky coverage $\Delta\Omega$ in a redshift bin $[z_i, z_{i+1}]$ can be expressed as:

$$N_i = \int_{z_i}^{z_{i+1}} \mathrm{d}z \int_{\Delta\Omega} \mathrm{d}\Omega \frac{\mathrm{d}V}{\mathrm{d}z\mathrm{d}\Omega} \int_0^\infty dM\, X(M, z, \Omega)\, n(M, z)\,, \tag{3.8}$$

where $\mathrm{d}V/\mathrm{d}z\mathrm{d}\Omega$ is the comoving volume element per unit redshift and solid angle, $X(M, z, \Omega)$ is the survey completeness and $n(M, z)$ is the halo mass function. In what follows we adopt the Tinker functional from for the mass function defined in eq. (3.7) with the best-fit parameters for the overdensity $\Delta = 200$ as provided by [92].

The completeness function depends on the strategy and specifics of the survey. For the purpose of this work we can simply express this function as

$$X(M, z, \Omega) = \int_{M_{\mathrm{lim}}(z)}^\infty \mathrm{d}M^{\mathrm{ob}} p(M^{\mathrm{ob}} \| M)\,, \tag{3.9}$$

where the lower limit in the mass integral, $M_{\mathrm{lim}}(z)$, represent the minimum value of the observed mass for a cluster to be included in the survey, and it is determined by the survey selection function and the fiducial signal-to-noise level adopted.

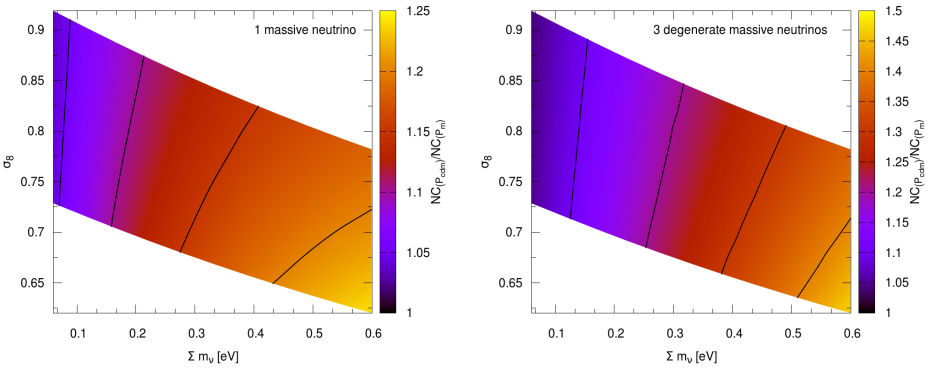

Figure 3.8: Ratio of the number counts obtained using the CDM over the matter prescription for different combinations of $(\sum m_\nu - \sigma_8)$ values (*colour-coded*) and different neutrino mass splitting: one massive neutrino (*left* panel) and three degenerate massive neutrinos (*right* panel). For a given cosmology, the cold dark matter prescription predicts a larger number of clusters, especially for high neutrino mass and cosmology with three massive neutrinos. Black curves trace lines of constant value of the ratio; from the left: $1.05, 1.10, 1.15, 1.20$ *left* panel; $1.1, 1.2, 1.3, 1.4$ *right* panel.

The function $p(M^{ob}\|M)$ gives the probability that a clusters of true mass M has a measured mass given by M^{ob} and takes into account the uncertainties that a scaling relation introduces in the knowledge of the cluster mass. Under the assumption of a lognormal-distributed intrinsic scatter around the nominal scaling relation with variance $\sigma^2_{\ln M}$, the probability of assigning to a cluster of true mass M an observed mass M^{ob} can be written as [112]:

$$p(M^{\rm ob}\|M) \;=\; \frac{1}{M^{\rm ob}\sqrt{\left(2\pi\sigma^2_{\ln M}\right)}}\exp\left[-\frac{(\ln M^{\rm ob} - B_{\rm M} - \ln M)^2}{2\sigma^2_{\ln M}}\right], \quad (3.10)$$

where the parameter $B_{\rm M}$ represents the fractional value of the systematic bias in the mass estimate.

We can use Eq. (3.8) to study the implications of different prescriptions for the HMF prediction in the predicted number of observed galaxy clusters. By replacing $P_{\rm m}(k,z)$ with $P_{\rm cdm}(k,z)$ one neglects the suppression of the total DM density fluctuations on scales smaller than their free-streaming

length, the scale below which neutrinos cannot cluster due to their high thermal velocity.

In Fig. 3.8 we show the ratio of the cluster counts predicted using the $P_{\rm cdm}(k,z)$ prescription over the one predicted using $P_{\rm m}(k,z)$ (colour coded) for different combinations of $(\sum m_\nu - \sigma_8)$ values and for two neutrino mass split schemes: a single massive neutrino (left panel) and three degenerate massive neutrinos (right panel). The plots have been obtained varying $\sum m_\nu$ and A_s and keeping fixed Ω_m, Ω_b, τ, H_0 and n_s to the Planck13 mean value ([35]; Table 2, *Planck*+WP). We computed the number counts integrating eq. (3.8) between $0.0 < z < 1.0$ with a sky coverage $\Delta\Omega = 27.000$ deg^2 and using the limiting mass $M_{\rm lim}(z)$[2] provided by the Planck Collaboration (dashed black line in Fig. 3 of [41]). Moreover, since we are simply interested in quantify the relative effect of using an improved HMF calibration we assumed no uncertainties in the estimation of the true mass ($M = M^{\rm ob}$) and we set $B_{\rm M} = 0$ and $\sigma^2_{\ln M} \to 0$ in eq. (3.10).

Assuming one massive neutrino, changing the matter power spectrum to the cold dark matter one in the HMF prediction increases the expected number of clusters by $\sim 5\%$ in the minimal normal hierarchy scenario ($\sum m_\nu = 0.06$eV), reaching differences of $\sim 20\%$ for masses of $\sum m_\nu \sim 0.4$eV. Considering instead three degenerate massive neutrinos, the CDM prescription gives even a larger correction to the cluster counts: the split of the total neutrino mass between three species causes the free-streaming length to increase, therefore widening the range in which $P_{\rm m}(k,z)$ is suppressed with respect to $P_{\rm cdm}(k,z)$. As a result, the difference in cluster counts computed with the two prescriptions reaches $\sim 30\%$ for neutrino mass of the order of $\sum m_\nu = 0.4$eV. For a given cosmology the magnitude of the ratio slightly depends also on the specifics of the survey: a lower $M_{\rm lim}(z)$ would entail a larger difference between the expected number of clusters computed with the two different calibrations.

The difference in the predictions in turn affects the degeneracy between cosmological parameters. An example of this effect is shown in figure 3.9, in the $(\sum m_\nu - A_s)$ plane (left panel) and the corresponding $(\sum m_\nu - \sigma_8)$ plane (right panel). The curves correspond to constant number counts obtained using $P_{\rm m}(k,z)$ (black) or $P_{\rm cdm}(k,z)$ (red) in the halo mass function definition, following the same procedure of figure 3.8 to compute the expected number of clusters. Solid and dashed curves are for models with one massive neutrino

[2]Following the recipe given in [113], the limiting mass has been converted to $M_{\rm lim,200}(z)$ – the limiting mass within a radius encompassing an overdensity equal to 200 times the mean density of the Universe – consistently with the chosen halo mass function.

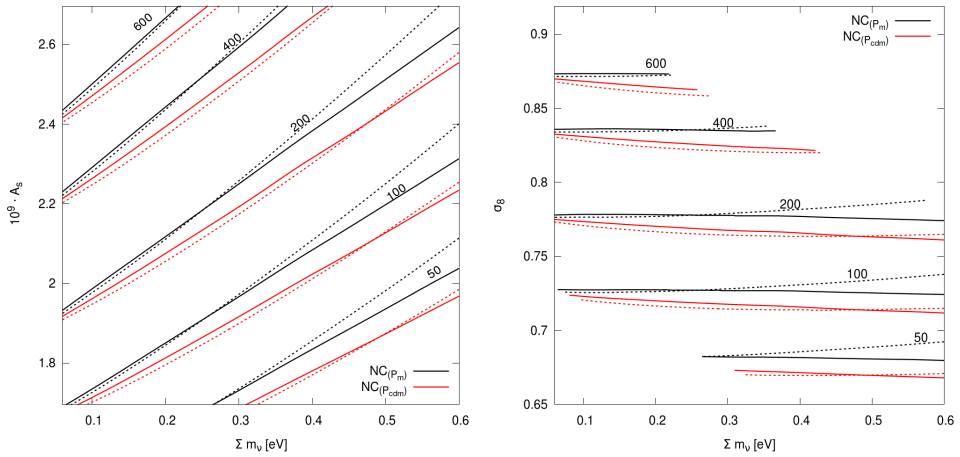

Figure 3.9: Curves of constant number counts ($N = 600$, 200, 100 and 50, top to bottom) in the plane $\sum m_\nu - 10^9 \cdot A_s$ (*left panel*) and in the plane $\sum m_\nu$ - σ_8 (*right panel*), for the two prescriptions for the halo mass function, matter (*black*) and cold dark matter (*red*) and for two neutrino mass splitting schemes, single massive neutrino (*solid lines*) and three degenerate massive neutrinos (*dashed lines*). The different slope of the balck and red curves shows the different degeneracy direction between parameters in the prescriptions.

and three degenerate massive neutrinos, respectively. The different slope of the curves indicates a different degeneracy direction between parameters. Consistently with the results shown in figure 3.8 the change in the slope is more pronounced in the case of three massive neutrinos.

3.2 Halo bias

3.2.1 Scale dependent bias

In ΛCDM models with massless neutrinos the relation between halo overdensity δ_h and the matter overdensity δ_m on very large scales is expected to be linear and deterministic, i.e. (see, e.g. [114; 115; 116])

$$\delta_h(x) = b\,\delta_m(x)\,, \tag{3.11}$$

with a constant bias parameter b, resulting in the simple expression for the halo power spectrum given by $P_{hh}(k) = b^2\,P_{mm}(k)$. Additional nonlinear but local corrections in the equation above induce a scale-dependence in the

relation between halo and matter power spectra and are however necessary to describe higher-order correlations, as we will se in Chapter 4.

In a cosmology with massive neutrinos defining halo bias in terms of the total or cold matter density field is, in principle, a matter of convenience. Nevertheless given the scale-dependent difference between P_{mm} and P_{cc} we can expect an additional scale-dependence in P_{hm} or P_{hc}, relevant at relatively large-scales, resulting simply from a "wrong" choice. In other words, if bias is constant on large-scales in one case, it cannot be so in the other. We will show that – not surprisingly after the results of the previous section – formulating the problem is in terms of the cold dark matter field is the right thing to do.

To proceed, we define auto- and cross- bias factors with respect to the CDM-field:

$$b_c^{(hh)} \equiv \sqrt{\frac{P_{hh}(k)}{P_{cc}(k)}}\,, \tag{3.12}$$

$$b_c^{(hc)} \equiv \frac{P_{hc}(k)}{P_{cc}(k)}\,, \tag{3.13}$$

as well as the analogous quantities

$$b_m^{(hh)} \equiv \sqrt{\frac{P_{hh}(k)}{P_{mm}(k)}}\,, \tag{3.14}$$

$$b_m^{(hm)} \equiv \frac{P_{hm}(k)}{P_{mm}(k)}\,, \tag{3.15}$$

for the bias with respect to P_{mm}. Previous work in neutrino-less cosmologies has shown that the bias factors from the cross-correlations tend to be a few percent larger than those from auto-correlations [117; 118].

For each of the simulation sets in Table 1.2 we measured these bias factors for two halo populations: one has $M > 2\times10^{13}\,h^{-1}\,M_\odot$ and the other $M > 4\times10^{13}\,h^{-1}\,M_\odot$, irrespective of redshift and cosmological parameters.

We focus first on a comparison between the different halo bias definitions described above, b_m and b_c. Figure 3.10 shows the bias, as a function of scale, determined for halos with $M > 2\times10^{13}\,h^{-1}\,M_\odot$ while figure 3.11 shows the same measurements for halo populations determined by $M > 4\times10^{13}\,h^{-1}\,M_\odot$. Left column shows $b_c^{(hh)}(k)$ (symbols with connecting continuous curves) and $b_m^{(hh)}(k)$ (symbols with dashed curves) defined respectively in eqs. (3.12) and (3.14) for the three models of Set A. The right column shows $b_c^{(hc)}(k)$ (symbols with connecting continuous curves) and $b_m^{(hm)}(k)$ (symbols with

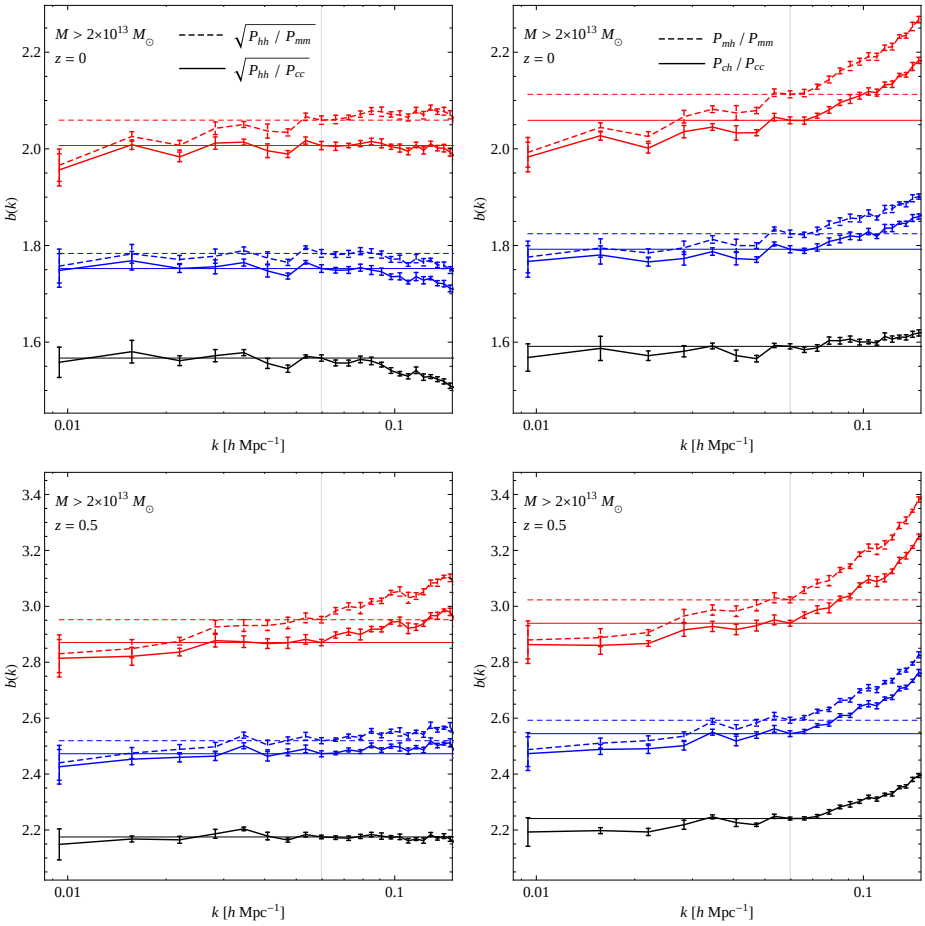

Figure 3.10: Halo bias as a function of scale determined from the simulation Set A for halos with $M > 2 \times 10^{13}\, h^{-1}\, M_\odot$. Left panels show the measurements of linear bias $b_c^{(hh)}$ (*continuous curves*) and $b_m^{(hh)}$ (*dashed curves*) from the halo power spectrum $P_{hh}(k)$. Right panels show $b_c^{(hc)}$ (*continuous curves*) and $b_m^{(hm)}$ (*dashed curves*) respectively from the P_{hc} and P_{hm} cross-power spectra. Top left panels correspond to $z = 0$, bottom panels to $z = 0.5$. The continuous and dotted horizontal lines show the constant bias values determined from measurements of b_c and b_m, respectively, at $k = 0.07\, h\,\mathrm{Mpc}^{-1}$, shown in turn as a vertical gray line in all panels. Error bars show the uncertainty on mean over the eight realizations.

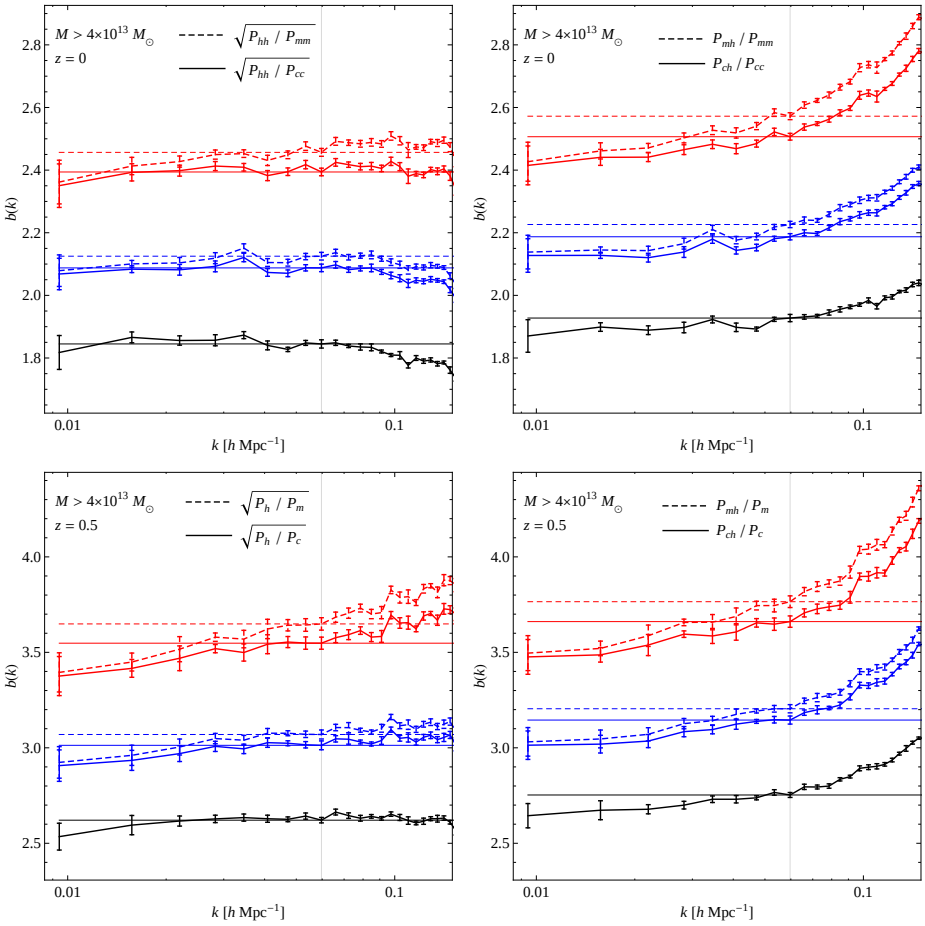

Figure 3.11: Same as previous figure 3.10 but for halos with $M > 4 \times 10^{13}\, h^{-1}\, M_\odot$.

dashed curves) defined in eqs. (3.13) and (3.15) in terms of cross-power spectra. Top row shows the results at $z = 0$, bottom row at $z = 0.5$. To guide the eye, the continuous and dashed horizontal lines show the values of $b_c(k)$ and $b_m(k)$ at $k = 0.07\, h\,\mathrm{Mpc}^{-1}$ (shown as a vertical line): below this value of k, the bias is observed to be constant for most measurements. This value also defines the bias values we use for the study of bias as a function of ν later in figure 3.13.

The fixed mass threshold clearly results in different bias values for the

three models. This is a consequence of the fact that the same mass threshold corresponds to quite different number counts for the different models [90]. The figure also illustrates the different scale-dependence of the two bias definitions. The departure from a constant value is more evident for the bias defined w.r.t. P_{mm}. This is consistent with eq. (3.12) and with the analysis of $n(M)$ presented in section 3.1, reinforcing our understanding of observables in massive neutrino cosmologies in terms of the CDM distribution. However, a noticeable k-dependence is also present for the b_c measurements, increasing with the value of the bias itself. This might be due to nonlinear effects that we ignore in our comparison and are the subject of ongoing work.

Although the auto- and cross- values differ slightly, both b_c and b_m converge to the same values on the largest scales (smallest k values) probed by the simulations, reflecting the fact that for $k \lesssim k_{nr}$ the DM and CDM linear power spectra are the same. For $k > k_{nr}$ but still in the linear regime, both b_m^{hh} and b_m^{hm} exhibit scale dependence, but have the same asymptotic behavior, given that

$$b_m^{(hh)} \equiv \sqrt{\frac{P_{hh}}{P_{mm}}} = b_c^{(hh)} \sqrt{\frac{P_{cc}}{P_{mm}}} \xrightarrow{k \gg k_{nr}} b_c^{(hh)}(1 - f_\nu)\,, \tag{3.16}$$

and

$$b_m^{(hm)} \equiv \frac{P_{hm}}{P_{mm}} = b_c^{(hc)} \frac{P_{cm}}{P_{cc}} \xrightarrow{k \gg k_{nr}} b_c^{(hc)}(1 - f_\nu)\,. \tag{3.17}$$

At $k = 0.07\,h\,\mathrm{Mpc}^{-1}$, the $b_m^{(hh)}$ coefficients are 5% larger than the corresponding $b_c^{(hh)}$ values for $m_\nu = 0.6$ eV.

It is interesting to compare now the bias values in models with and without massive neutrinos that have the same value of σ_8. The left panel of figure 3.12 compares the results for the lowest mass threshold at $z = 0$ of the model with $m_\nu = 0.6$ eV (H6, red data points), already shown in figure 3.11, with those of the two massless neutrino models from simulation Set B, matching in turn the value of $\sigma_{8,mm}$ (H0s8, black data points) and $\sigma_{8,cc}$ (H0s8-CDM, gray data points), the latter taken as reference model.

At fixed mass threshold objects in the H0s8 runs are more clustered than in the H6 and H0s8-CDM runs, as expected from measurements of the mass function (see figure 3.6). Despite these marginal differences, however, it is important to notice that the three models are characterized by a bias $b_c(k)$ with the same dependence on scale. This is particularly evident in terms of their relative differences, shown in the lower panels, which are identical for both $b_c^{(hh)}$ and $b_c^{(hc)}$. One could argue that the agreement between the bias measured in such different models could be further improved by appropriately

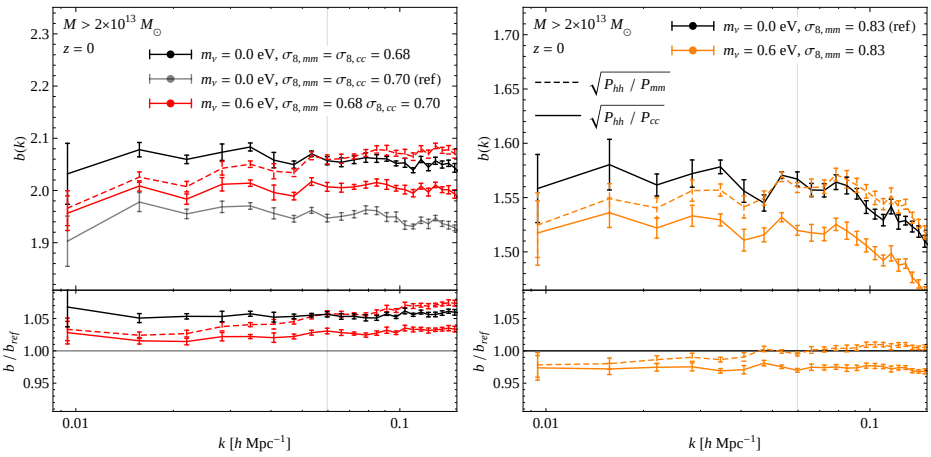

Figure 3.12: Degeneracy m_ν-σ_8: halo bias at $z = 0$ determined from the simulation set B. Left panel: comparison of the H6 model (in red) to the H0s8 (dark gray) and H0s8-CDM (light gray) models. As before continuous lines correspond to bias with respect to the cold dark matter power spectrum, while dashed lines to bias with respect to the total matter power spectrum. Right panel: comparison of the H0 model(in black) to the H6s8 model (in yellow), the two sharing the same value of $\sigma_{8,mm}$. In both panels we considered only halos with $M > 2 \times 10^{13}\, h^{-1}\, M_\odot$.

rescaling the spectral index of the linear power spectrum of the model H0s8-CDM to match the one of H6 at the scale where $\sigma_{cc} = \delta_{cr}$. Doing so would not fix the additional scale-dependence of $b_m(k)$.

Similar conclusions can be drawn from the right panel of figure 3.12 where we show, instead, a comparison of the H0 model to the H6s8 model, sharing the same value of $\sigma_{8,mm}$.

In recent analyses which constrain neutrino masses using galaxy clustering in large redshift surveys bias is treated as a free parameter over which to marginalize (see, e.g. [17; 19; 23]). The standard practice defines the bias with respect to the total matter power spectrum, and assumes that b_m is scale-independent up to some k_{max}. Our analysis shows that bias coefficients defined in this way are, in fact, scale-dependent, even at linear scales. Therefore, to avoid systematics inaccuracies, future analysis of galaxy surveys data must account for this.

Of course study of linear bias ia only the first step towards modeling the

halo and galaxy power spectrum down to small scales. As we have seen in Figure 3.10 nonlinearities in the bias kick on large scale and must be taken into account in a realistic analysis. For extension to nonlinear bias model in cosmologies with and without massive neutrinos we refer the reader to [119; 120; 121].

3.2.2 Universality in the CDM component

The final part of this section is devoted to study the universality of bias, measured at a fixed scale k and described as a function of the variable $\nu = \delta_{cr}/\sigma$ as the mass threshold, the redshift and cosmological models are varied. If $\nu f(\nu)$ is universal, then

$$b = 1 - \frac{1}{\delta_{cr}} \frac{d \ln f(\nu)}{d \ln \nu} , \tag{3.18}$$

is also a universal function of ν. However, our measurements correspond to

$$\bar{b}(> M_{min}) = \frac{\int_{M_{min}} b(M)\, n(M)\, dM}{\int_{M_{min}} n(M)\, dM} , \tag{3.19}$$

with $M_{min} = 2 \times 10^{13}\, h^{-1}\, M_\odot$ and $4 \times 10^{13}\, h^{-1}\, M_\odot$; in terms of the scaling variable, this reads

$$\bar{b}(> \nu_{min}) = \frac{\int_{\nu_{min}} b(\nu)\, [f(\nu)/M(\nu)]\, d\nu}{\int_{\nu_{min}} [f(\nu)/M(\nu)]\, d\nu} , \tag{3.20}$$

where $\nu_{min} = \delta_{cr}/\sigma(M_{min})$ and where the presence of the factor $1/M$ in the integrand does not allow $\bar{b}$ to be a function of ν_{min} alone. In principle, this introduces an explicit dependence on cosmology, even if $\nu f(\nu)$ and $b(\nu)$ themselves are universal.

Figure 3.13 shows the measurements of the linear bias *at* $k = 0.06\, h\,\mathrm{Mpc}^{-1}$ from both the halo power spectrum (left panels) and halo-matter cross-power spectrum (right panels) at three different redshifts ($z = 0$, 0.5 and 1), for two mass thresholds ($M > 2$ and $4 \times 10^{13}\, h^{-1}\, M_\odot$) and for all the neutrino cosmologies (Set A and B), as a function of the value of $\nu = \delta_{cr}/\sigma_{cc}$. The measured values are compared, in the upper panels, to the prediction for the standard ST mass function and bias (dotted curves) computed from eq. (3.19) for the massless neutrino cosmology at redshift zero. Due to the small residual scale-dependence, a different choice of the value of k leads to the same results, with more noise at large scales.

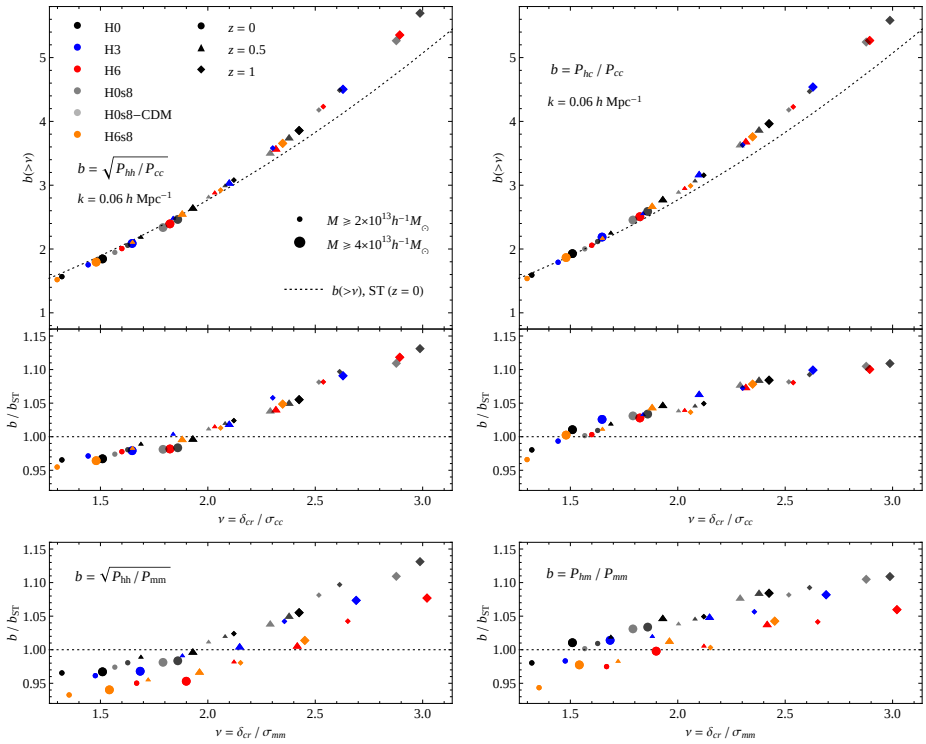

Figure 3.13: Measurements of the linear bias coefficient as a function of the value of $\nu = \delta_{cr}/\sigma$ corresponding to the mass threshold from the halo power spectrum (*left panels*) and halo-matter cross-power spectrum (*right panels*) at three different redshifts ($z = 0$, 0.5, 1), for two mass thresholds ($M > 2$ and $4 \times 10^{13}\, h^{-1}\, M_{\odot}$) and for all the cosmologies under consideration. Theoretical predictions for the linear bias from the standard ST mass function evaluated for the H0 model at $z = 0$ are shown by the dotted curve. The middle panel shows the residuals w.r.t. the ST prediction. Top and middle panels assume halos to be biased w.r.t. the cold DM perturbations and therefore assume $\nu = \delta_{cr}/\sigma_{cc}$. The bottom panels shows the residuals w.r.t. ST assuming instead halos to be biased w.r.t. the total matter perturbations and $\nu = \delta_{cr}/\sigma_{mm}$.

We notice that the dependence of such predictions on cosmology and redshift are very small. Indeed, this fact can be appreciated from the data points themselves: all results from different masses, redshifts and cosmologies are aligned as one would expect for a function of ν alone. Small departures

from such overall behavior can be seen in the middle panels, showing the residuals w.r.t. the ST predictions. Notice that we do expect some departure from universality both from the mass function results as from the definition of $\bar{b}(> M)$ itself. These effects are, nevertheless, much smaller than those obtained defining bias from the total matter power spectrum and plotting the results as a function of $\nu = \delta_{cr}/\sigma_{mm}$, as shown in the lower panels of figure 3.13, separated for clarity. Here, we show only the ratio w.r.t. the ST prediction, the latter coinciding with the one used in the middle panels to allow a direct comparison.

We have seen that, if we adopt as a definition for the peak height $\nu = \delta_{cr}/\sigma_{cc}$, linear bias is to a very good approximation a universal function with respect to redshift even if the halo mass function is not, in agreement with previous findings [122]. This can be understood from the Peak-Background Split argument [115; 90], where bias coefficients are defined as a logarithmic derivative of the dimensionless mass function $f(\nu)$, eq. (3.18). Linear bias is, to a large extent, a universal function, since most significant departures from universality w.r.t. redshift in the mass function come as changes in the amplitude, independently of the halo mass.

3.3 Redshift space distortions

The biasing between the galaxy and matter distributions is not the only effect to be taken into account for a correct estimate of the matter power spectrum from galaxy redshift observations. In a real survey, the proper motions of galaxies with respect to the homogeneous expansion of the Universe affect the determination of their distance along the line-of-sight (see, *e.g.* [123; 124; 125; 126]). However, on sufficiently large scales these redshift space distortions provide information on the peculiar velocity field of matter perturbations, in particular on the growth rate of the density field. As a result, they are extensively used to constrain cosmological parameters and test deviation from standard gravity [127; 128; 129; 130]. In preparation for future large spectroscopic surveys, the effect of neutrino masses on RSD modelling needs to be carefully investigated to avoid fake signatures of modified gravity for instance. In the following we present a preliminary assessment of the scale-dependence of the growth rate induced by the free streaming length of neutrinos, and its measurement from the DEMNUni simulations.

In the standard cosmological model, and in the large-scale limit where linear theory applies, the distortion induced by peculiar velocities on the

density contrast δ_m can be written in Fourier space as [123]

$$\delta_{m,s}(\vec{k}) = (1 + f\mu^2)\,\delta_m(k)\,, \tag{3.21}$$

where $\mu = \vec{k} \cdot \hat{z}/k$ is the angle between the line-of-sight and the wave vector $\vec{k}$, while $f(a)$ is the linear growth rate, defined as the logarithmic derivative of the linear growth factor $D(a)$, that is

$$f(a) \equiv \frac{d\ln D(a)}{d\ln a}\,. \tag{3.22}$$

A similar expression holds for linearly biased tracers which follow the matter flow (*i.e.* with no velocity bias[3]). For instance, the halo overdensity in redshift space, $\delta_{h,s}$, can be written as

$$\delta_{h,s}(\vec{k}) = (b + f\mu^2)\delta_m \equiv (1 + \beta\mu^2)\,b\,\delta_m(k)\,, \tag{3.23}$$

where b is the linear scale-independent bias, and we define $\beta \equiv f/b$. It follows that the halo power spectrum in redshift space can be written as the product of a polynomial in μ times the halo power spectrum in real space. Since the halo power spectrum in real space depends only on the modulus of the wave vector, the angular dependence induced by RSD is entirely encoded in the pre-factor of Eq. (3.23). As a result, the redshift-space halo power spectrum can be decomposed in multipoles using just the first three even Legendre polynomials $L_\ell(\mu)$

$$P_{hh,s}(\vec{k}) = (1 + \beta\mu^2)^2\,P_{hh}(k) = \sum_{l=0,2,4} P_{hh,\ell}\,L_\ell(\mu)\,. \tag{3.24}$$

The monopole, quadrupole and hexadecapole coefficients read

$$P_{hh,0}(k) = \left(1 + \frac{2}{3}\beta + \frac{1}{5}\beta^2\right) P_{hh}(k) \tag{3.25}$$

$$P_{hh,2}(k) = \left(\frac{4}{3}\beta + \frac{4}{7}\beta^2\right) P_{hh}(k) \tag{3.26}$$

$$P_{hh,4}(k) = \frac{8}{35}\beta^2 P_{hh}(k), \tag{3.27}$$

where the RSD parameter β determines the relative amplitude of the multipoles. In a ΛCDM cosmology, β is predicted to be scale-independent on

[3]Note that the assumption of no velocity bias is better justified for halos w.r.t. the cold matter perturbations rather than w.r.t. the total matter ones.

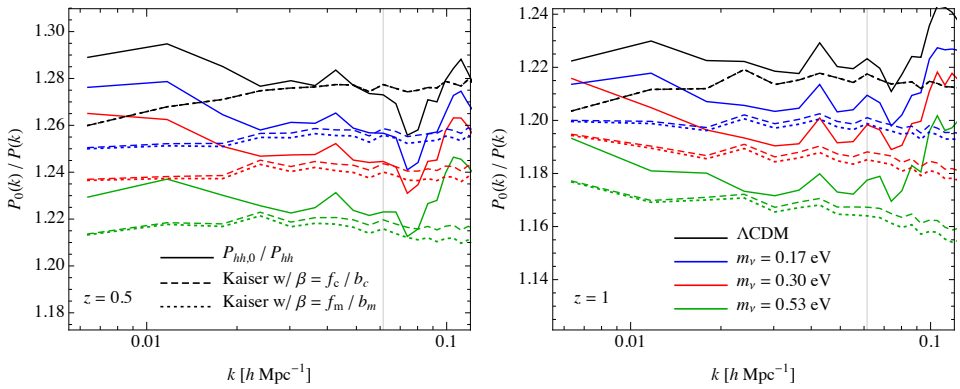

Figure 3.14: Comparison of the ratio between the monopole of the redshift-space halo power spectrum to the real-space halo power spectrum, $P_{hh,0}(k)/P_{hh}(k)$ (*continuous curves*) against the value predicted by the Kaiser formula, Eq. (3.25), as a function of $\beta = f_c/b_c$ (*dashed curves*) or $\beta = f_m/b_m$ (*dotted curves*). $f_c(k)$ and $f_m(k)$ correspond to the linear theory growth rate respectively of cold and total matter perturbations, while the b_c and b_m are the *measured* values of the halo bias according to the two definitions of Eqs. (3.12) and (3.14). Notice that we *do not* use best fit values for the bias parameters, but we use instead the measured $b(k)$ as a function of scale.

large scales, as a direct consequence of the scale-independence of both linear bias and growth rate. On the other hand, both quantities might be scale-dependent when massive neutrinos are present.

First, as we saw in sec , Figure 3, growth of linear perturbations become scale dependent. At fixed linear bias this effect tend to suppress, at most a few %, the Kaiser factor β w.r.t. a standard cosmology. In the second place, if we defined the halo bias w.r.t. the total matter field, according to Eq. (3.14), we would add to the quantity β an additional source of scale-dependence. Let us notice here that, a choice of what linear bias is, b_c or b_m, comes with a choice also for $f = f_c$ of $f = f_m$.

In all the cases, we expect the Kaiser factor β to exhibit a scale-dependence, which, by choosing $\beta = f_c/b_c$, will result only from the growth rate $f_c(k)$. In the other case, $\beta = f_m/b_m$, a partial compensation occurs between the linear bias, which increases with the wave-number, and the growth factor that actually decreases with k. In Figure 3.14 we show the ratio of the monopole of the redshift-space halo power spectrum, $P_{hh,0}(k)$, to

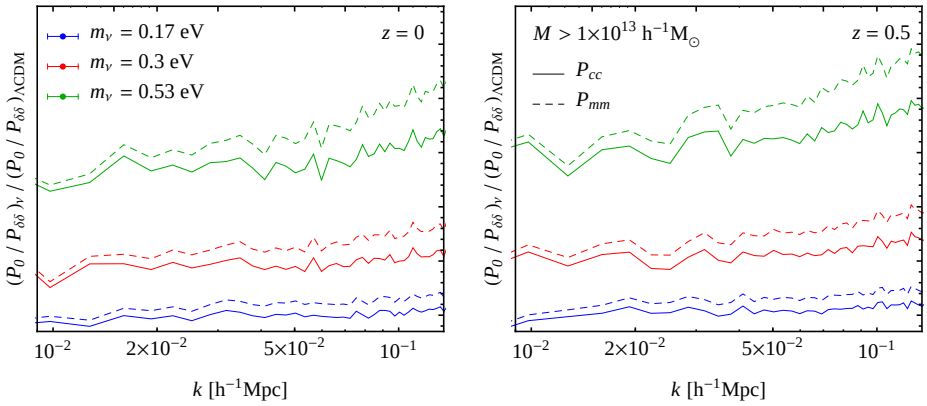

Figure 3.15: Ratio of the halo monopole power spectrum to the nonlinear $P(k)$ as measured in a massive neutrino cosmology, then divided by the same ratio in the ΛCDM simulation. Only halos with mass $M > 1 \times 10^{13}\, h^{-1}\, M_\odot$ have been considered. The two possible choices of non-linear power spectra in a neutrino cosmology have both been considered, P_{cc} (*continuous lines*) and P_{mm} (*dashed lines*).

the halo power spectrum in real space, $P_{hh}(k)$, for the models listed in Table 1.2, and we compare the measurements from the DEMNUni simulations to the corresponding predictions provided by the Kaiser formula written both in terms of $\beta = f_c/b_c$ and $\beta = f_m/b_m$. In such predictions we *do not* use best fit values for the bias parameters, but we use instead the *measured* $b(k)$ where the scale-dependence is affected by cosmic variance. While the noisy measurements do not allow to clearly determine the scale-independence of such a quantity, we notice that $\beta = f_c/b_c$ does provide a slightly better prediction than $\beta = f_m/b_m$, as compared to simulations.

To partially remove cosmic variancee in Figure 3.15 we show the ratio of the halo monopole to the measured (C)DM power spectrum in massive neutrino cosmologies, divided by the corresponding quantity computed in a ΛCDM simulation. In this case it's clear the extra scale dependence in the DM case (dashed lines) coming from an different choice for linear bias. Similar conclusions hold for the other multipoles, but cosmic variance is very large making difficult a clear comparison with the Kaiser formula.

As a further test, in Figure 3.16 we consider directly the growth rate f obtained from measurements of the monopole of the redshift-space halo power spectrum, $P_{hh,0}(k)$, and the real-space halo and cold matter power spectra,

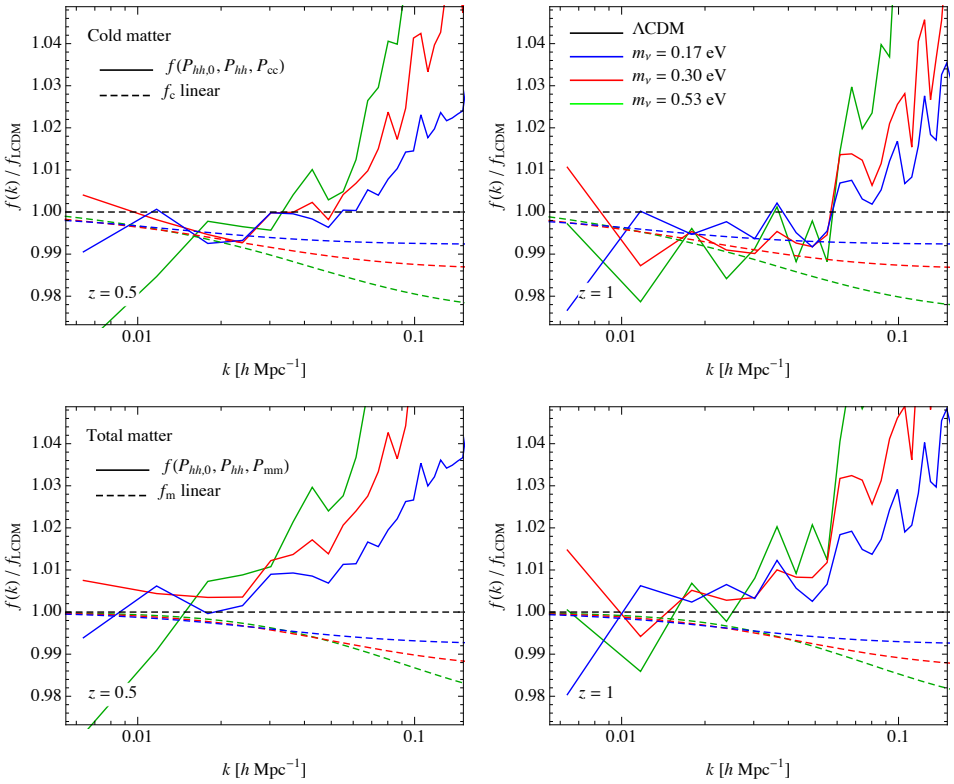

Figure 3.16: *Top panels*: Linear growth rate obtained from measurements of the redshift-space (monopole) and real-space halo power spectrum according to Eq. (3.25) and from measurements of the linear halo bias $b(k) = \sqrt{P_{hh}(k)/P_{cc}(k)}$ at redshifts $z = 0.5$ (*left*) and $z = 1$ (*right*). Dashed curves denote the linear theory (scale-dependent) predictions for cold matter perturbations, $f_c(k)$. All the quantities are shown in terms of their ratio to the corresponding ΛCDM values. *Bottom panels*: Same as in the top panels, but assuming the linear halo bias defined in terms of total matter perturbations. In this case, the comparison is made to the linear theory prediction for the total matter growth rate, $f_m(k)$.

$P_{hh}(k)$ and $P_{cc}(k)$ respectively, under the assumption that the Kaiser formula provides a good description of RSD at large scales. Assuming $\beta = f/b_c$, from

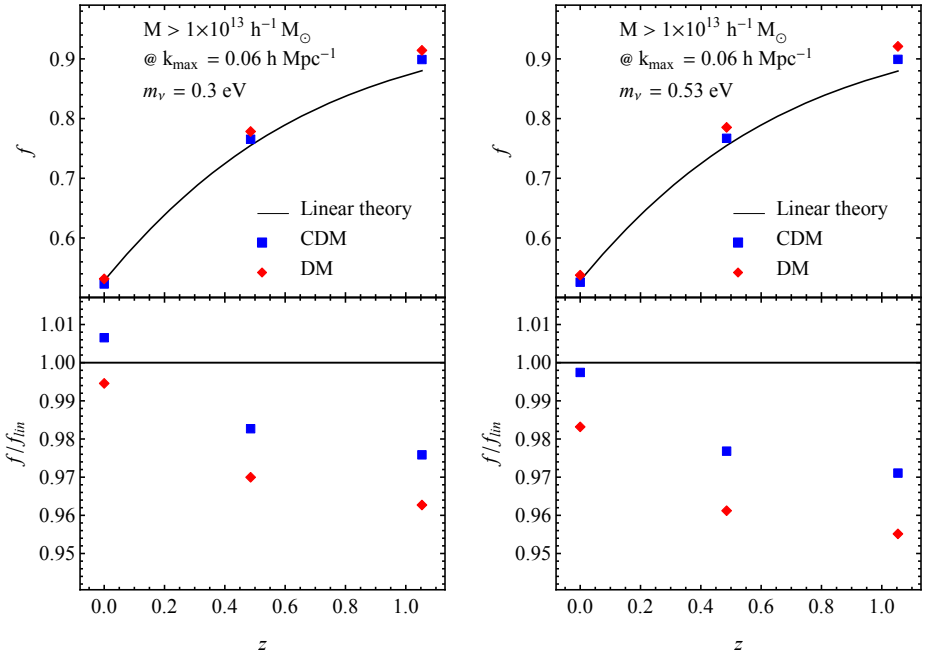

Figure 3.17: Best fit value for f obtained from measurements of P^0_{hh}/P_{NL}, assuming the Kaiser formula and linear scale independent linear bias. The true values corresponding to the cosmology of the simulations are the black points, while red and blue points assume constant halo bias with respect to CDM and DM respectively.

Eq. (3.25) we have

$$f(k) = \sqrt{\frac{P_{hh}(k)}{P_{cc}(k)}}\,\frac{1}{3}\left[\sqrt{45\,\frac{P_{hh,0}(k)}{P_{hh}(k)} - 20} - 5\right], \tag{3.28}$$

while assuming $\beta = f/b_m$ we obtain a similar expression where P_{mm} replaces P_{cc}. In order to further reduce cosmic variance, we show the recovered value of f as ratio to the ΛCDM case. These measurements, as a function of k, can then be directly compared with linear theory predictions for $f_c(k)$ and $f_m(k)$.

The top panels of Figure 3.17 show f obtained from Eq. (3.28) under the cold matter hypothesis compared to the predictions for $f_c(k)$ at redshift $z = 0.5$, 1. We notice that, in the higher redshift case in particular, despite

the noise, the measurements are consistent with the linear predictions at large scales when f is obtained from the measured P_{cc}. A greater discrepancy instead is observed when f is obtained from the measured total matter $P_{mm}(k)$, as compared to the predictions for $f_m(k)$ in the bottom panels. It is evident that, in addition to the high level of noise, nonlinearities are highly significant already on these scales and do not allow any conclusive statement. Yet if such discrepancy will be confirmed by future investigations, we could expect that using b_m as a definition for bias in the Kaiser formula could lead to a systematic error on the determination of the growth rate at the level of 1-2%, see Figure 3.17. For this purpose we took the best fit value for linear bias b from measurements of the halo auto power spectrum P_{hh} assuming scale independence and then we find the best fit value for $f(z)$ at a given k_{max}. Figure 3.17 clearly shows that an incorrect assumption on the bias leads to as systematic effect on the recovered value of the growth rate, the effect being the 2% for $m_\nu = 0.53$ eV.

Clearly this represents a very preliminary and admittedly simplistic test of possible systematic effects in the determination of the growth rate $f(k)$ in the context of massive neutrinos cosmologies. If the description of halo clustering in terms of cold matter perturbation does indeed represents the correct approach, this test can serve as a confirmation that the DEMNUni simulations reproduce linear theory predictions for the growth rate including, to a certain extent, its scale-dependence. We reserve for future work a more detailed analysis of RSD effects on the matter density field as well as on realistic mock galaxy distributions, in massive neutrino scenarios. Of particular interest would be any description of nonlinearity that could extend theoretical predictions to smaller scales.

Chapter 4

The matter and halo bispectrum in massive neutrino cosmologies

The late time 3-dimensional distributions of dark matter in a N-body simulations or the distribution of galaxies in a redshift surveys forms a highly non-Gaussian field. In the absence of Primordial Non-Gaussianity, nonlinear gravitational instabilities are the main sources of non-Gaussian density perturbations. This means that two-point statistics are not enough to fully characterize the density or galaxy field, and additional information on structure formation and cosmological parameters is encoded in higher order correlation functions (HOCF). The first non vanishing HOCF in Fourier space is the the three point function of the density field, also knows as the bispectrum $B(\vec{k}_1, \vec{k}_2, \vec{k}_3)$, defined as

$$\langle \delta(\vec{k}_1)\delta(\vec{k}_2)\delta(\vec{k}_3)\rangle \equiv (2\pi)^3 \delta_D(\vec{k}_1 + \vec{k}_2 + \vec{k}_3) B(\vec{k}_1, \vec{k}_2) \tag{4.1}$$

The wavenumbers in the above equation cannot take arbitrary values, they are forced by the Dirac delta to form a triangular configuration, but statistical isotropy implies that the bispectrum does not depend on the orientation of the triangle. Again for a review of the bispectrum and HOCF see [114]. At the level of the density field, since the bispectrum, and HOCF in general, are by definition nonlinear quantities, their measurements represent an important tool to check the validity of perturbation theory beyond linear order. If a model works for the power spectrum in the mildly nonlinear regime, it has to work as well for the bispectrum. The same is true for RSD beyond the Kaiser approximation. Several attempts have been performed

in this direction, an incomplete list of reference would at least include [131; 132; 133; 134; 135; 136; 137; 138; 139; 140].

On the other hand, as we have seen in Section 3.2, knowing how discrete objects such as halos and galaxies trace the underlying dark matter distribution is one of the major challenge in extracting cosmological parameters. This bias relation is nonlinear and it affects both the halo power spectrum and halo bispectrum. It is therefore possible to use the shape dependence of the bispectrum to partially break the degeneracy between linear and non-linear bias, allowing for better constraints on cosmological parameters [141; 142; 143; 144; 145; 118; 146; 138; 147]. Moreover given the extra dependence on the angle between wavenumbers the bispectrum contains cosmological information which is not present at all in the power specrturm[143]. For a Fisher-Matrix calculation of the benefits of combining power spectrum and bispectrum in the next generation of galaxy surveys, see [148]

In real data the bispectrum of galaxies have been already measured in different redshift surveys [149; 147; 150; 151]. One of the main difficulties here is the computation of the Covariance Matrix for the bispectrum measurements, which is related to the definition of a nearly optimal estimator for the bispectrum that we still lack [152; 144]. However with some approximations the authors in [153] have been able, for the first time, to constraint the growth rate f and σ_8 separately by combining measurements of the bispectrum and the powee spectrum in the BOSS DR11 CMASS sample.

In this Section we present preliminary results for the matter and halo bispectrum in cosmologies with massive neutrinos, comparing with PT preditictions for the matter field, and fitting the halo bispectrum using both a local and non local bias model.

4.1 The matter bispectrum

If the bispectrum in ΛCDM cosmologies has not received all the attention it deserves, in cosmologies with massive neutrinos there is not a single study of HOCFs with the only notable exception of the recent paper by [66] discussing the matter and neutrino bispectrum. In the spirit of the analysis of the power spectrum in Section 2, we will present the first measurements of the density bispectrum in different cosmologies and at different redshifts, trying to isolate massive neutrinos effects, and only afterwards we will compare with PT predictions. For simplicity, and given the arguments in Section 2, we assume the neutrino bispectrum is negligible and our analysis focus on

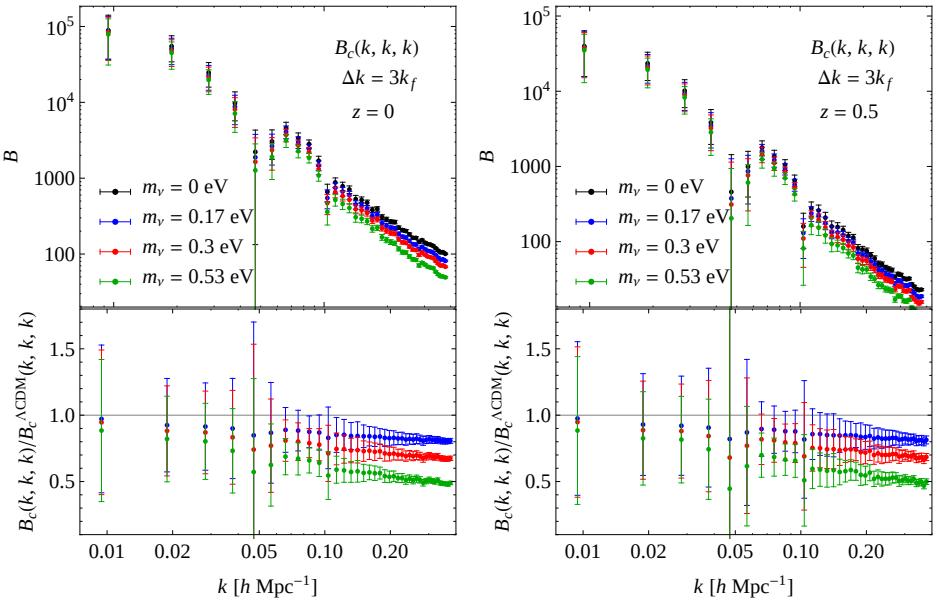

Figure 4.1: Top panel: CDM bispectrum for equilateral configuration, at $z = 0$ left panel and at $z = 0.5$. in cosmologies with and without massive neutrinos. Bottom panel: ratio of the equilateral bispectrum in presence of massive neutrinos to the same quantity in a ΛCDM Universe

the CDM bispectrum only. Given the large volume of the DEMNUni suite we have measured the bispectrum in this simulation set only.

Figure 4.1 presents the measurements of the bispectrum for equilateral configuration, *i.e.* $k_1 = k_2 = k_3$, as a function of the wave number k for the four different cosmologies of the DEMNUni suite at $z = 0, 0.5$. While on the large scales there is no significant effect of massive neutrinos on $B(k, k, k)$, as we move to smaller scales we see a suppression of power due to the lower σ_8 in cosmologies with massive neutrinos and hence lower nonlinearities. From the lower panels we see that the suppression is around the 15% for $m_\nu = 0.17$ eV at $z = 0$ and it is roughly constant across redshift. Figure 4.2 presents the measurements at $z = 1, 2$,

In the absence of primordial non-Gaussianities there is no particular reason to plot one bispectrum configuration rather than others, but visualization of all configurations hide the effects of massive neutrinos, so we decided to show only another configuration, a triangle with $k_1 = 2k_2$. To

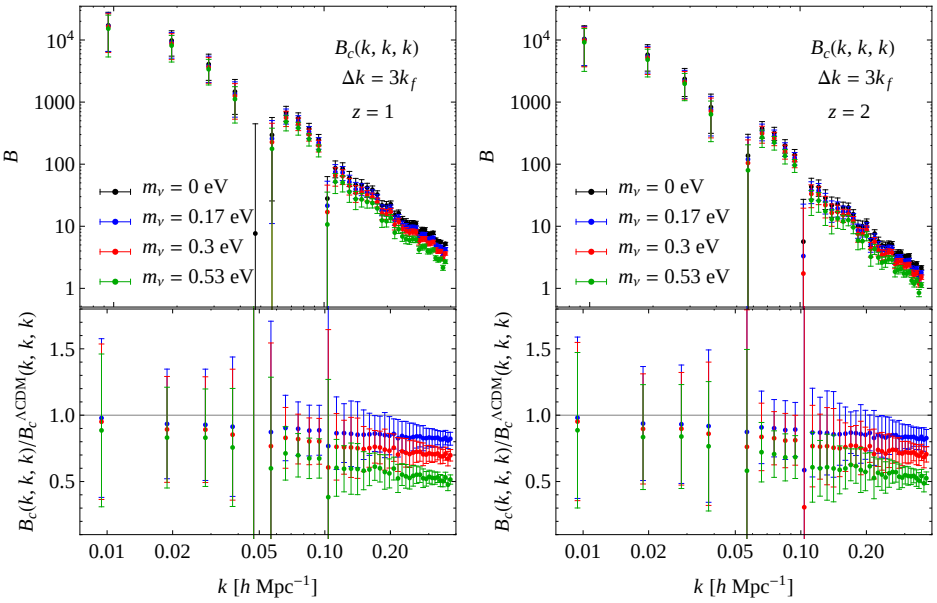

Figure 4.2: Same as Figure 4.1 but at $z = 1, 2$.

avoid redundancies in the presentation, at this stage we also compare with PT predictions for the CDM bispectrum.

Following the argument of Section 2.1 we will assume that any perturbation scheme can be straightforwardly applied to massive neutrino cosmologies without any further modification, provided the right linear power spectrum is used. This means that at tree level in standard perturbation theory the PT CDM bispectrum reads [114]

$$B_c(\vec{k}_1, \vec{k}_2) = 2\mathcal{F}_2(\vec{k}_1, \vec{k}_2)P(k_1)P(k_2) + \text{cyc} \tag{4.2}$$

where

$$\mathcal{F}_2(\vec{k}_1, \vec{k}_2) = \frac{5}{7} + \frac{1}{2}\frac{\vec{k}_1 \cdot \vec{k}_2}{k_1 k_2}\left(\frac{k_1}{k_2} + \frac{k_2}{k_1}\right) + \frac{2}{7}\frac{(\vec{k}_1 \cdot \vec{k}_2)^2}{k_1^2 k_2^2} \tag{4.3}$$

is the standard second-order kernel that arises in PT.

Figure 4.3 shows measurements at $z = 0.5, 1$ of the bispectrum for a particular configuration with $k_1 = 2k_2$ and $k_1 = 0.075\,h^{-1}\,\mathrm{Mpc}$. Differently from the previous case we see that the bispectrum is massive neutrino cosmologies is suppressed on all scales. The continuous lines that tries

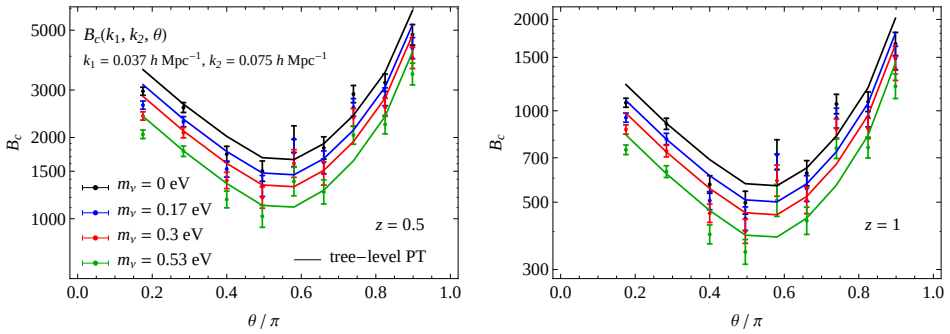

Figure 4.3: bispectrum for a folded configuration with $k_1 = 2k_2$ and $k_1 = 0.075\,h^{-1}$ Mpc in presence of massive neutrinos to the same quantity in a ΛCDM univers, at $z = 0$ (left) and $z = 1$ (right).

to go through the measurements are tree level prediction from Eq. (4.2). The agreement is as good as it gets with these data but once again we emphasize that PT works in massive neutrino cosmologies as well as in ΛCDM cosmologies and this is encouraging if one wants to push PT or other frameworks to higher orders.

Another way to visualize the effect of massive neutrinos on the bispectrum is to compute the reduced bispectrum Q defined as follows

$$Q(\vec{k}_1, \vec{k}_2) = \frac{B(\vec{k}_1, \vec{k}_2)}{P(k_1)P(k_2) + P(k_1)P(k_3) + P(k_2)P(k_3)} \tag{4.4}$$

so that it is independent of the initial amplitude of the linear fluctuations and should isolate effects which are inherently nonlinear. Notice that at tree level in PT the reduced bispectrum is also independent of redshift.

In Figure 4.4 we show the reduced bispectrum for equilateral configurations at $z = 0,05$ in massive neutrino cosmologies divided by the analogous quantity in a standard scenario. We still notice a suppression of Q as neutrino masses increases even if we remove the effect of the power spectrum. However tree-leve PT predicts the same value of the reduced bispectrum for all cosmologies, in this particular configuration, and therefore any deviations in the measurements require higher order corrections in PT.

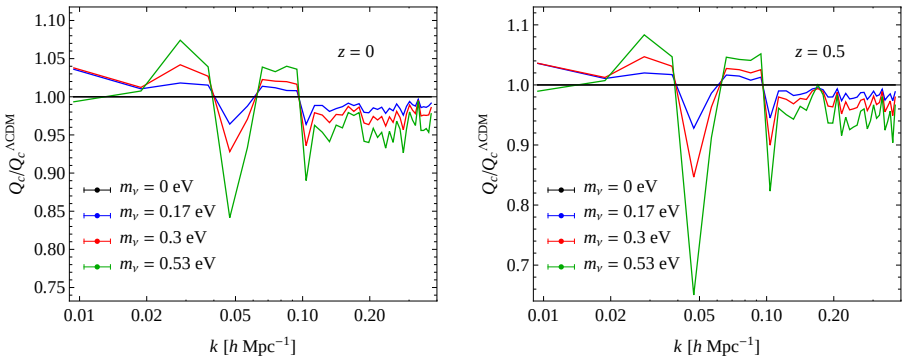

Figure 4.4: Ratio of the reduced bispectrum for equilateral configurations in presence of massive neutrinos to the same quantity in a ΛCDM univers, at $z = 0$ (left) and $z = 0.5$ (right).

4.2 The Halo bispectrum

For halos the picture is only slightly different. At leading order the halo bispectrum reads

$$B_{hhh}(\vec{k}_1, \vec{k}_2) = b_1^3 B_c(\vec{k}_1, \vec{k}_2) + b_1^2 b_2 (P_{cc}(k_1) P_{cc}(k_2) + \text{cyc}) \tag{4.5}$$

where B_c is the tree level CDM bispectrum defined in the previous section and b_1, b_2 are first and second order bias coefficients. For the halo reduced bispectrum instead we have, on large scales [116]

$$Q_{hhh}(\vec{k}_1, \vec{k}_2) = \frac{1}{b_1} Q_c(\vec{k}_1, \vec{k}_2) + \frac{b_2}{b_1^2} \tag{4.6}$$

which explicitily shows how information on the halo bispectrum can help reducing degeneracies between bias coefficients, since b_2 does not change the actual shape of Q.

However it is well know that fitting the power spectrum and the bispectrum using the model in Eq. (4.5) yields different values of linear bias b_1 [133; 143; 138]. That poses a serious problem for the use of the galaxy bispectrum in comological parameter analysis and it indicates that our theoretical model of the halo bispectrum lacks understanding in the bias prescription. The solution came in [120; 121] where the authors shown that even if one starts with a local bias expansion, non local contributions to the bias arise

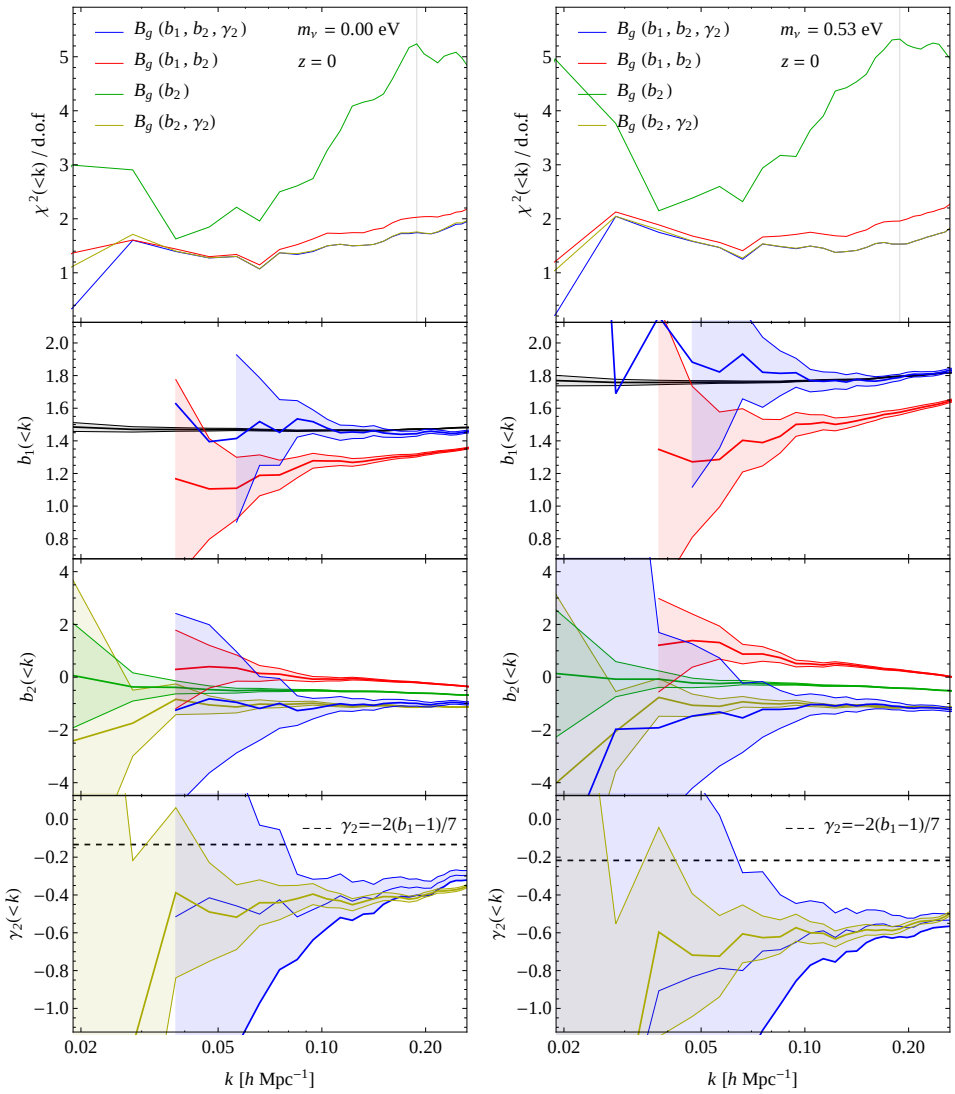

Figure 4.5: Top panel: χ^2 per d.o.f as a function of k for all halos of mass $M > 10^{13} M_\odot$ at $z = 0$. On the left the ΛCDM case, on the right $m_\nu = 0.53$ eV. Lower panels show the best fit bias parameters in different models.

due to correlation of the density field with the large scale tidal field. At the lowest order, introducing this new terms means for the halo bispectrum that

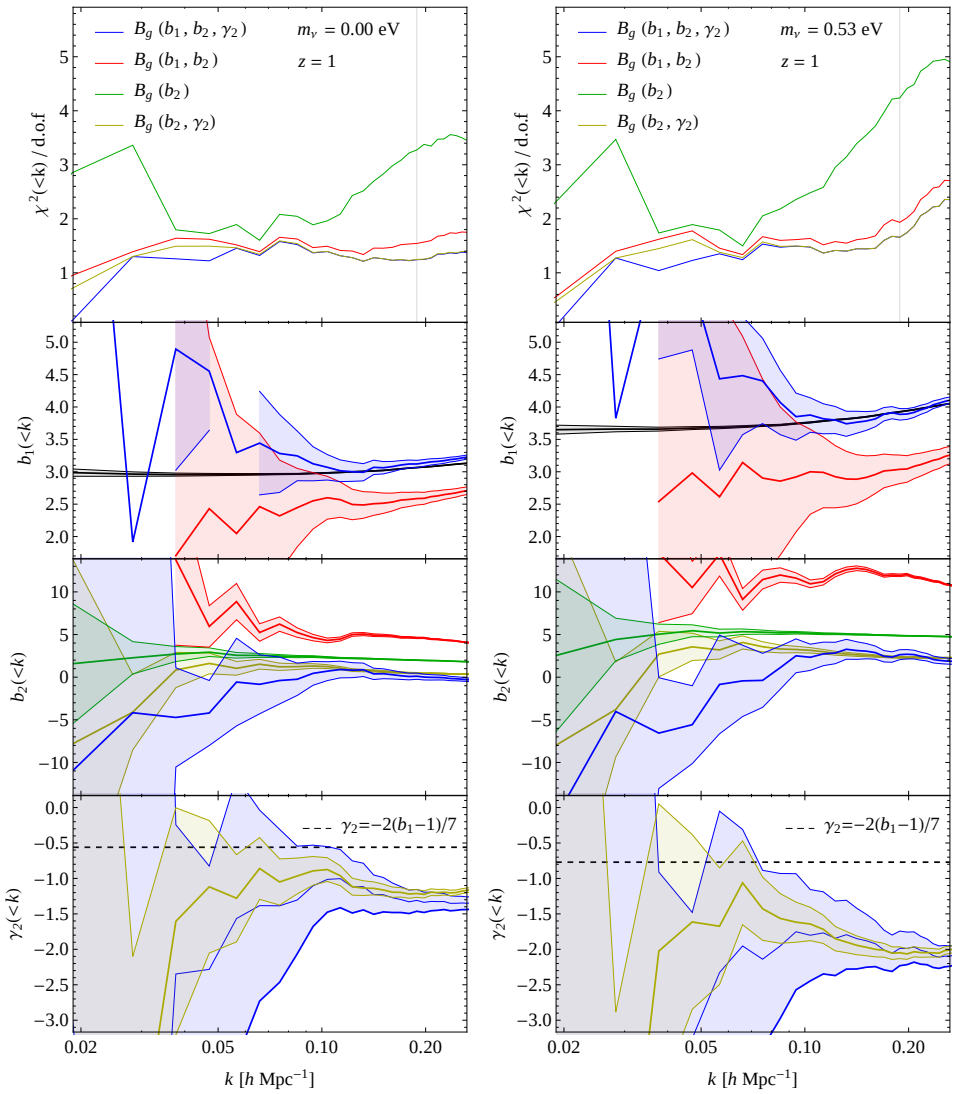

Figure 4.6: Same as Figure 4.5 at $z = 1$.

$$B_{hhh}(\vec{k}_1, \vec{k}_2) = b_1^3 B_c(\vec{k}_1, \vec{k}_2) + b_1^2[b_2 P_c(k_1)P_c(k_2) + 2\gamma_2(\mu_{12}^2 - 1)P_c(k_1)P_c(k_2) + \text{cyc}] \tag{4.7}$$

where μ_{12} is the cosine of the angle between $\vec{k}_1$ and $\vec{k}_2$. The new coefficient

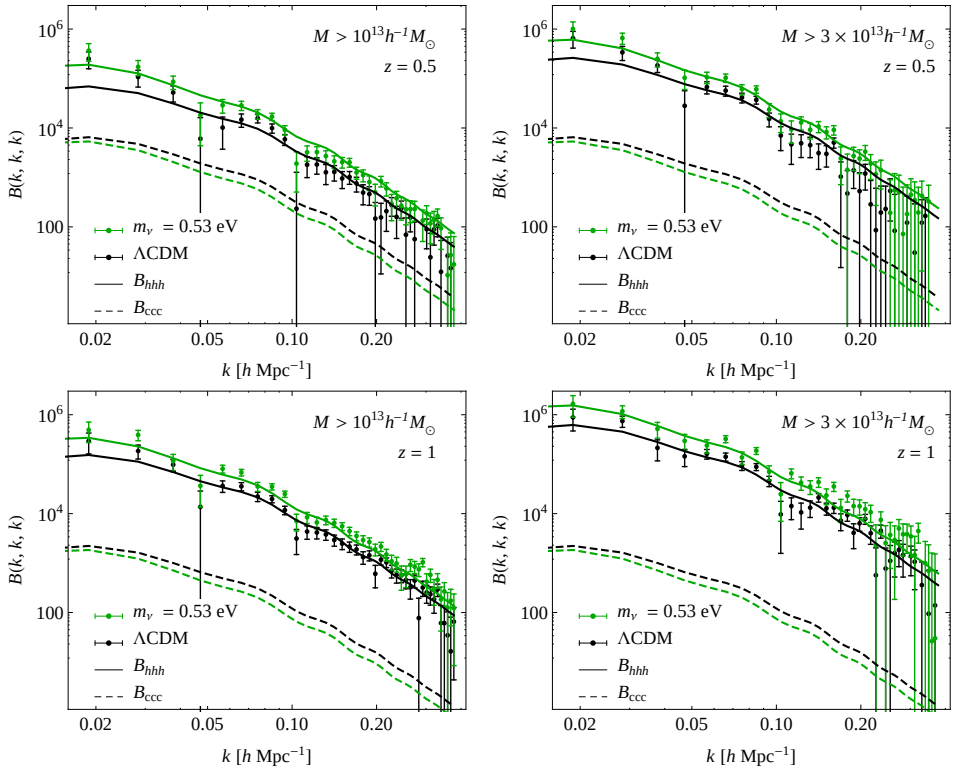

Figure 4.7: Comparison between the halo bispectrum and a non local bias model at $z = 0.5$ for halos with $M > 10^{13}M_\odot$ (left) and $M > 3 \times 10^{13}M_\odot$. The bottom panels present the measurements at $z = 1$.

γ_2, since it is generated perturbatively, can be predicted and it is equal, under some assumptions, to $-2(b_1 - 2)/7$. If now one fits for the three free bias parameters in Eq. (4.7) and compares the best fit value of linear bias with the one obtained from the power spectrum, one finds that the two are compatible. This is shown in Figure 4.5 for $m_\nu = 0, 0.53$ eV at $z = 0$ for all the halos with mass larger that $10^{13}M_\odot$. All triangular configurations have been included in the analysis, although only a few triangles are shown.

The top panel shows the χ^2 per degree of freedom in several different models for the halo bispectrum as a function of the maximum wavenumber included in the fit. In blue the case where we fit for b_1, b_2 and γ_2 as in Eq. (4.7), in red for the local model of Eq. (4.5), and in green and yellow the same models but with linear bias fitted from the power spectrum. In the

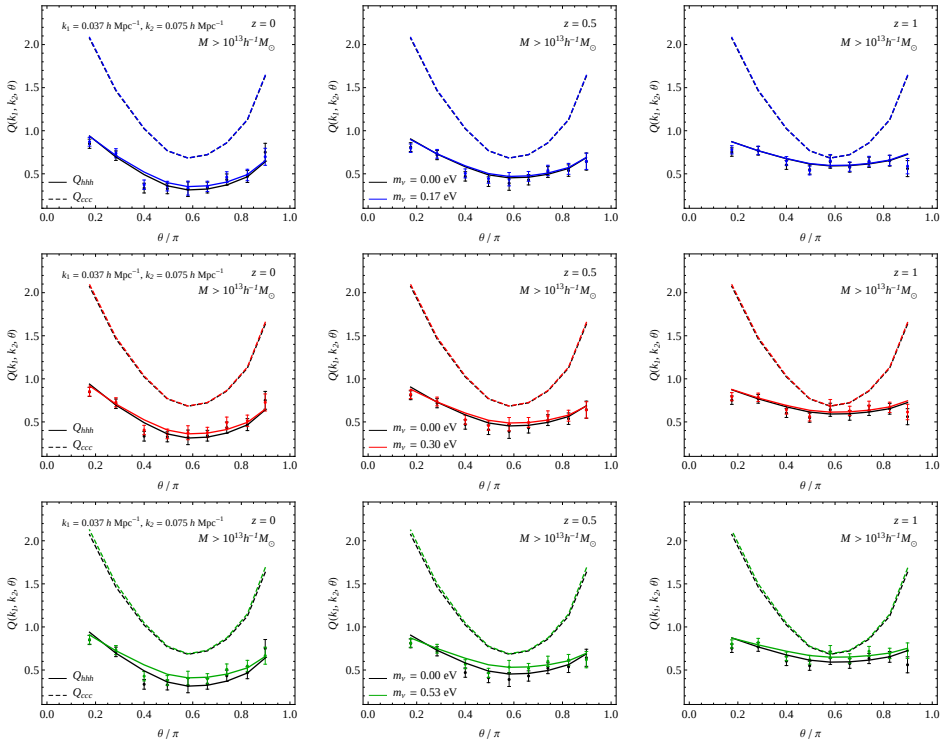

Figure 4.8: Halo reduce bispectrum for a folded configuration with $k_1 = 2k_2$ and $k_1 = 0.075\,h^{-1}\,\mathrm{Mpc}$ with and without massive neutrinos.

second panel we compare the best linear bias between the different models. Only including non local bias γ_2 one recovers the same linear bias as in a power spectrum analysis (in black). Then, as shown in the third panels, it follows that the inferred value of quadratic bias is the same, whether we fix or not the value of b_1 from the power spectrum, only in the non local model. Finally the bottom panel shows the best fit value of non local bias γ_2 and it should be noted that the best fit value is always systematically lower than the PT prediction, dashed line (we will come back to this shortly). The same analysis can be carried out at another redshift, see Figure 4.6, or using another population of halos, not shown for brevity of the analysis.

Now we are in the position to compare the measurements of the halo bispectrum with the fit, for which we assume that b_1 is fixed from the power spectrum and b_2 and γ_2 from the bispectrum, since it is the consistent model yielding smaller errorbars. We have to choose the value of the best

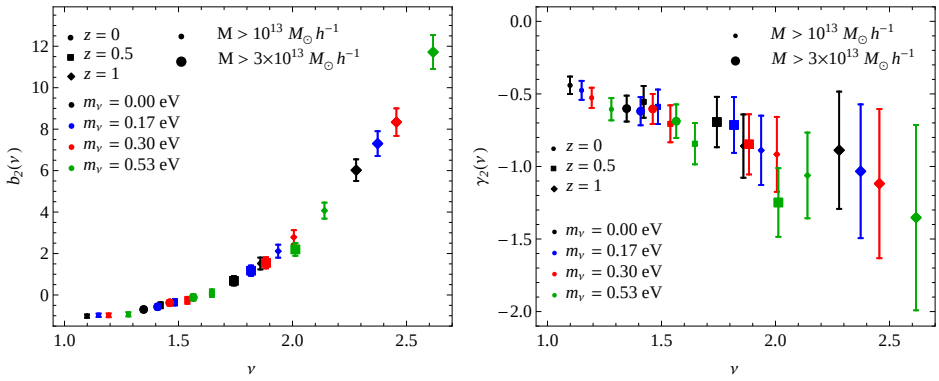

Figure 4.9: Universality of quadratic and non local bias as a function of peak height ν.

fit parameters at a given k_{max} and by inspection of the χ^2 we found that $k_{max} = 0.065\,h^{-1}\,\mathrm{Mpc}$ is the smallest scale up to which the reduced χ^2 remains constant.

For equilateral configuration the comparison is done in Figure 4.7. The left column shows the measurements with the best fit for low mass halos, $M > 3 \times 10^{13} M_\odot$, at $z = 0$ (bottom panel) and $z = 1$ (upper panel), while the right one the same measurements but for more massive halos, $M > 3 \times 10^{13} M_\odot$. Those configurations are quite sensitive to the presence of non local bias since in this case $\mu_{12}^2 = 0.25$. We see that the fit is good on a wide range of scale, and both in redshift and halo populations.

Next we discuss the halo bispectrum for the same folded configuration presented for the matter bispectrum in Section 4.1, in Figure 4.8. In this case to highlight difference in the bias between different cosmologies and redshift we plot the reduced bispectrum. The first thing worth noticing is that the dependence on the angle is suppressed in halos with respect to matter, a direct consequences of the presence of linear bias in the denominator of Eq. (4.6). For massive neutrinos cosmologies since linear bias at fixed mass threshold is higher than the ΛCDM case the suppression is even larger, and this is particularly evident for $m_\nu = 0.53$ eV. As before the agreement between the theory and the measurements is good, but it remains the same regardless of the presence of massive neutrinos.

A final remark about the analysis discussed in this section. We would like to stress again that this is a preliminary test, in fact all the results we have presented are known in ΛCDM cosmologies and we have just shown

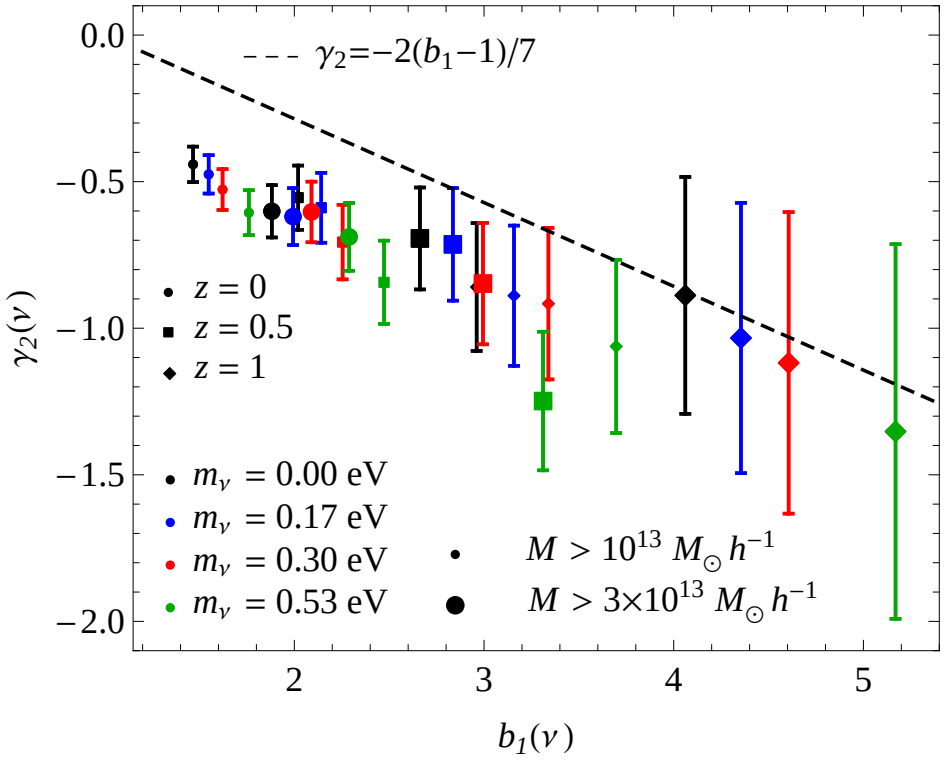

Figure 4.10: Non local bias as a function of linear bias for all cosmologies, redshifts and halo populations.

how to straightforwardly extend them to massive neutrino Universes arriving to the same conclusions. A more careful analysis, including the one loop bispectrum, scale dependent bias parameters as in [119], and a combined analysis of power spectrum and bispectrum as in [146], also including the halo filter is currently under investigation.

The last piece of information we want to add regards the universality of quadratic bias and non local bias. We produced the same plot as in Figure 3.13 but this time for b_2 and γ_2 and the result is shown in Figure 4.9. As expected we find that when expressed in terms of CDM only fluctuations bias coefficients are universal functions in both redshift and cosmologies.

Finally in Figure 4.10 we confirm previous findings in ΛCDM cosmologies [120; 121; 146] for non local bias , the best fit value of γ_2 is systematically lower that the PT prediction, going in the direction of a contribution to non

local bias also at the lagrangian level as proposed by [154; 155].

Chapter 5

Conclusions and Outlook

We have investigated the effects of massive neutrinos on several observables in Large Scale Structures. In Section 2 we presented measurements of the power spectrum of each individual component of the total matter density, that is the cold dark matter and baryons (here treated on the same footing and called CDM) and the neutrinos, along with their cross-power spectrum and the total matter power spectrum, given by the weighted sum of the three. The analysis in terms of distinct components allows to test early hypothesis regarding the possibility of neglecting the nonlinear evolution of neutrino perturbations in analytical predictions [61]. In this respect we point-out, with direct reference to our measurements, that the neutrino power spectrum, as well as the cross-power spectrum provide a significant contribution to the total matter power spectrum, Eq. (8), only at large-scales, where the linear approximation is sufficient. Since the total matter power spectrum, $P_{mm}(k)$, and the cold matter power spectrum, $P_{cc}(k)$, are the only quantities directly related to actual observables, a 1% accuracy appears to be achievable even neglecting the nonlinear evolution of neutrino perturbations. With this in mind, we focused on the accurate description of nonlinearity of the cold matter component *alone*, considering various predictions in perturbation theory, and using, as input quantity, the simple cold matter linear power spectrum. While this is clearly an effective, not rigorous, approach, we have shown that the accuracy provided by PT techniques, and their limits of validity on the matter power spectrum in ΛCDM cosmologies, can be achieved as well for massive neutrino models in a rather simple way. In a completely similar fashion, fitting formulae obtained from ΛCDM simulations, and used beyond the perturbative regime like HALOFIT, can be safely applied to predictions of the nonlinear cold matter power spectrum, and simply

extended, with the addition of the linear contributions from the neutrino auto- and CDM-neutrino cross-spectra, to the total matter power spectrum, retaining the same accuracy in presence of massive neutrinos as in a standard massless cosmology, without resorting to additional fitting parameters.

We have shown evidence in Section 3.1 that the halo mass function for models with massive neutrinos can be reproduced by existing fitting formulae derived from simulations of standard ΛCDM cosmologies only if evaluated in terms of the variance of small-scale cold dark matter perturbations. Previous studies commonly assumed, however, a dependence on the total matter density variance, leading to large and ultimately artificial departures from universality as the total neutrino mass is varied. Our results are based on halo catalogs determined by means of a FoF and spherical halo finders accounting for CDM particles only. Lacking a proper definition of a halo finder for neutrino particles we tested our results by considering as well catalogs obtained including all particles, finding percent-level differences in the mass function for low masses. Such differences are expected to be even smaller once unbound neutrino particles with large thermal velocities are removed from the halo by a suitable algorithm. The emerging picture shows neutrinos with masses in the currently viable range playing a minor role in the nonlinear collapse of cold DM structures: even though a fraction of them do cluster inside CDM halos, their contribution to the total mass of a halo is negligible [156; 157; 45; 158; 49].

We studied in detail the halo abundance as a function of the variable $\nu = \delta_{cr}/\sigma$, showing that while universality is recovered to a large extent by setting $\sigma = \sigma_{cc}$, minor departures with respect to neutrino masses are detectable and comparable to those already seen in standard ΛCDM models for instance as a function of redshift [92; 93]. Neutrino masses are therefore primarily degenerate with the amplitude of the fluctuations in the CDM field $\sigma_{8,cc}$, and, to a lesser extent, to the slope of the spectral index on the scale where $\sigma_{8,cc} = \delta_{cr}$.

The impact of these findings on cosmological analyses from galaxy clusters abundances can be significant. An estimate of the systematic error induced by the wrong assumption for the mass function dependence on the linear power spectrum is done in section 3.1.3 and an application to recent data-sets is the subject of [111].

We studied halo clustering in Section 3.2, identifying a definition of halo bias in terms of cold dark matter perturbations as the only one able to recover the expected constant bias parameters at large scales. This is, to a large extent, a natural consequence of the results on the mass function. We notice some small, residual scale-dependence for large bias values possibly due to

nonlinear effects. However, bias coefficients computed from the total dark matter power spectrum are significantly scale-dependent. A comparison of bias measurements as a function of $\nu = \delta_{cr}/\sigma_{cc}$ shows remarkable universality, in stark contrast with the total matter description with variable $\nu = \delta_{cr}/\sigma_{mm}$.

Our results on bias have, as well, important implications for the analysis of galaxy clustering aiming at constraining neutrino masses. In previous works, bias parameters defined in terms of total matter perturbations are assumed as constant and marginalized over, introducing a non-negligible systematic error in the results. Ambiguity in the definition of halo (and galaxy) bias, motivated a preliminary test of the Kaiser formula for redshift-space distortions [123], where linear bias is a relevant parameter. We found, despite the yet large statistical uncertainty, some indications of the expected scale-dependence of the growth rate of matter perturbation, characteristic of massive neutrino cosmologies. If such indications are correct, then we have shown that defining the galaxy bias w.r.t. the cold matter component is necessary to avoid a systematic error on the determination of the growth rate $f(k)$ at the few percent level. Indeed as discussed in [159] theoretical uncertainties on the halo mass function and halo bias could have a large impact on the constraining power of next generation surveys, and they needed to be understood at the % level. That is exactly the level at which neutrino mass effects become important.

Finally we have presented preliminary results for the matter and halo bispectrum in cosmologies with massive neutrinos in Section 4. We confirm all the results for both density and halo fields we have seen for the power spectrum also at the bispectrum level. In analogy with the ΛCDM case, a non local bias model is the only one able to consistently describe the bispectrum of halos, and we find, in agreement with other studies, a value of non local bias lower that PT prediction.

A lot of work has still to be done. The analysis we presented for the bispectrum has to be improved towards more realistic modeling of both clustering and bias, and the same higher order bias model should then be applied to the halo power spectrum. RSD beyond Kaiser approximation are on top of the list, for both halos and matter distribution.

With a good handle on halo statistics one should then populate those halos with galaxies and build up realistic galaxy catalogs. Only at this stage we will be able to check whether or not our theoretical models of structure formation are able to recover the the input value of neutrino masses and other parameters in the simulations.

All previous analysis should be carried out in configuration space as well. Very little has been done in this respect, [100; 49; 68]. For instance the study

of the BAO peak in cosmologies with massive neutrinos has been recently discussed in [68], and it could be extended to the full shape of the two-point correlation function.

This list could go on a few pages more, but we hope it is clear from the discussion in this work that *any* observables has to be studied in cosmologies with massive neutrinos. Not only to see which probes are the best in constraining neutrino masses but also to avoid possible systematics effect in the determination of other cosmological parameters introduce by our poor knowledge of physical effect induced by massive neutrinos.

Bibliography

[1] Y. Fukuda, T. Hayakawa, E. Ichihara, K. Inoue, K. Ishihara, H. Ishino, Y. Itow, T. Kajita, J. Kameda, S. Kasuga, K. Kobayashi, Y. Kobayashi, Y. Koshio, M. Miura, M. Nakahata, S. Nakayama, A. Okada, K. Okumura, N. Sakurai, M. Shiozawa, Y. Suzuki, Y. Takeuchi, Y. Totsuka, S. Yamada, M. Earl, A. Habig, E. Kearns, M. D. Messier, K. Scholberg, J. L. Stone, L. R. Sulak, C. W. Walter, M. Goldhaber, T. Barszczxak, D. Casper, W. Gajewski, P. G. Halverson, J. Hsu, W. R. Kropp, L. R. Price, F. Reines, M. Smy, H. W. Sobel, M. R. Vagins, K. S. Ganezer, W. E. Keig, R. W. Ellsworth, S. Tasaka, J. W. Flanagan, A. Kibayashi, J. G. Learned, S. Matsuno, V. J. Stenger, D. Takemori, T. Ishii, J. Kanzaki, T. Kobayashi, S. Mine, K. Nakamura, K. Nishikawa, Y. Oyama, A. Sakai, M. Sakuda, O. Sasaki, S. Echigo, M. Kohama, A. T. Suzuki, T. J. Haines, E. Blaufuss, B. K. Kim, R. Sanford, R. Svoboda, M. L. Chen, Z. Conner, J. A. Goodman, G. W. Sullivan, J. Hill, C. K. Jung, K. Martens, C. Mauger, C. McGrew, E. Sharkey, B. Viren, C. Yanagisawa, W. Doki, K. Miyano, H. Okazawa, C. Saji, M. Takahata, Y. Nagashima, M. Takita, T. Yamaguchi, M. Yoshida, S. B. Kim, M. Etoh, K. Fujita, A. Hasegawa, T. Hasegawa, S. Hatakeyama, T. Iwamoto, M. Koga, T. Maruyama, H. Ogawa, J. Shirai, A. Suzuki, F. Tsushima, M. Koshiba, M. Nemoto, K. Nishijima, T. Futagami, Y. Hayato, Y. Kanaya, K. Kaneyuki, Y. Watanabe, D. Kielczewska, R. A. Doyle, J. S. George, A. L. Stachyra, L. L. Wai, R. J. Wilkes, and K. K. Young, "Evidence for Oscillation of Atmospheric Neutrinos," *Physical Review Letters* **81** (Aug., 1998) 1562–1567, `hep-ex/9807003`.

[2] G. L. Fogli, E. Lisi, A. Marrone, D. Montanino, A. Palazzo, and A. M. Rotunno, "Global analysis of neutrino masses, mixings, and phases: Entering the era of leptonic CP violation searches," *Phys. Rev. D* **86**

no. 1, (July, 2012) 013012, arXiv:1205.5254 [hep-ph].

[3] D. V. Forero, M. Tórtola, and J. W. F. Valle, "Global status of neutrino oscillation parameters after Neutrino-2012," *Phys. Rev. D* **86** no. 7, (Oct., 2012) 073012, arXiv:1205.4018 [hep-ph].

[4] **Particle Data Group** Collaboration, K. A. Olive *et al.*, "Review of Particle Physics," *Chin. Phys.* **C38** .

[5] **Hyper-Kamiokande Proto-Collaboration** Collaboration, K. Abe *et al.*, "Physics potential of a long-baseline neutrino oscillation experiment using a J-PARC neutrino beam and Hyper-Kamiokande," *PTEP* **2015** no. 5, (2015) 053C02, arXiv:1502.05199 [hep-ex].

[6] J. Lesgourgues and S. Pastor, "Massive neutrinos and cosmology," Phys. Rep. **429** (July, 2006) 307–379, arXiv:astro-ph/0603494.

[7] J. Lesgourgues, G. Mangano, G. Miele, and S. Pastor, *Neutrino Cosmology*. Cambridge, UK: Cambridge University Press, Feb., 2013.

[8] S. Hannestad, "Neutrino masses and the number of neutrino species from WMAP and 2dFGRS," *Journal of Cosmology and Astro-Particle Physics* **5** (May, 2003) 4, astro-ph/0303076.

[9] B. A. Reid, L. Verde, R. Jimenez, and O. Mena, "Robust neutrino constraints by combining low redshift observations with the CMB," *Journal of Cosmology and Astro-Particle Physics* **1** (Jan., 2010) 3, arXiv:0910.0008 [astro-ph.CO].

[10] S. A. Thomas, F. B. Abdalla, and O. Lahav, "Upper Bound of 0.28 eV on Neutrino Masses from the Largest Photometric Redshift Survey," *Physical Review Letters* **105** no. 3, (July, 2010) 031301, arXiv:0911.5291 [astro-ph.CO].

[11] M. E. C. Swanson, W. J. Percival, and O. Lahav, "Neutrino masses from clustering of red and blue galaxies: a test of astrophysical uncertainties," *Mon. Not. R. Astron. Soc.* **409** (Dec., 2010) 1100–1112, arXiv:1006.2825 [astro-ph.CO].

[12] S. Saito, M. Takada, and A. Taruya, "Neutrino mass constraint from the Sloan Digital Sky Survey power spectrum of luminous red galaxies and perturbation theory," *Phys. Rev. D* **83** no. 4, (Feb., 2011) 043529, arXiv:1006.4845 [astro-ph.CO].

[13] C. Carbone, L. Verde, Y. Wang, and A. Cimatti, "Neutrino constraints from future nearly all-sky spectroscopic galaxy surveys," *Journal of Cosmology and Astro-Particle Physics* **3** (Mar., 2011) 30, arXiv:1012.2868.

[14] R. de Putter, O. Mena, E. Giusarma, S. Ho, A. Cuesta, H.-J. Seo, A. J. Ross, M. White, D. Bizyaev, H. Brewington, D. Kirkby, E. Malanushenko, V. Malanushenko, D. Oravetz, K. Pan, W. J. Percival, N. P. Ross, D. P. Schneider, A. Shelden, A. Simmons, and S. Snedden, "New Neutrino Mass Bounds from SDSS-III Data Release 8 Photometric Luminous Galaxies," *Astrophys. J.* **761** (Dec., 2012) 12, arXiv:1201.1909 [astro-ph.CO].

[15] J.-Q. Xia, B. R. Granett, M. Viel, S. Bird, L. Guzzo, M. G. Haehnelt, J. Coupon, H. J. McCracken, and Y. Mellier, "Constraints on massive neutrinos from the CFHTLS angular power spectrum," *Journal of Cosmology and Astro-Particle Physics* **6** (June, 2012) 10, arXiv:1203.5105 [astro-ph.CO].

[16] S. Riemer-Sørensen, C. Blake, D. Parkinson, T. M. Davis, S. Brough, M. Colless, C. Contreras, W. Couch, S. Croom, D. Croton, M. J. Drinkwater, K. Forster, D. Gilbank, M. Gladders, K. Glazebrook, B. Jelliffe, R. J. Jurek, I.-h. Li, B. Madore, D. C. Martin, K. Pimbblet, G. B. Poole, M. Pracy, R. Sharp, E. Wisnioski, D. Woods, T. K. Wyder, and H. K. C. Yee, "WiggleZ Dark Energy Survey: Cosmological neutrino mass constraint from blue high-redshift galaxies," *Phys. Rev. D* **85** no. 8, (Apr., 2012) 081101, arXiv:1112.4940 [astro-ph.CO].

[17] G.-B. Zhao, S. Saito, W. J. Percival, A. J. Ross, F. Montesano, M. Viel, D. P. Schneider, M. Manera, J. Miralda-Escudé, N. Palanque-Delabrouille, N. P. Ross, L. Samushia, A. G. Sánchez, M. E. C. Swanson, D. Thomas, R. Tojeiro, C. Yèche, and D. G. York, "The clustering of galaxies in the SDSS-III Baryon Oscillation Spectroscopic Survey: weighing the neutrino mass using the galaxy power spectrum of the CMASS sample," *Mon. Not. R. Astron. Soc.* (Oct., 2013) , arXiv:1211.3741 [astro-ph.CO].

[18] S. More, F. C. van den Bosch, M. Cacciato, A. More, H. Mo, and X. Yang, "Cosmological constraints from a combination of galaxy clustering and lensing - II. Fisher matrix analysis," *Mon. Not. R.*

Astron. Soc. **430** (Apr., 2013) 747–766, arXiv:1207.0004 [astro-ph.CO].

[19] E. Giusarma, R. de Putter, S. Ho, and O. Mena, "Constraints on neutrino masses from Planck and Galaxy clustering data," *Phys. Rev. D* **88** no. 6, (Sept., 2013) 063515, arXiv:1306.5544 [astro-ph.CO].

[20] M. Wyman, D. H. Rudd, R. A. Vanderveld, and W. Hu, "nu-LCDM: Neutrinos reconcile Planck with the Local Universe," *ArXiv e-prints* (July, 2013) , arXiv:1307.7715 [astro-ph.CO].

[21] R. A. Battye and A. Moss, "Evidence for Massive Neutrinos from Cosmic Microwave Background and Lensing Observations," *Physical Review Letters* **112** no. 5, (Feb., 2014) 051303, arXiv:1308.5870 [astro-ph.CO].

[22] S. Riemer-Sørensen, D. Parkinson, and T. M. Davis, "Combining Planck data with large scale structure information gives a strong neutrino mass constraint," *Phys. Rev. D* **89** no. 10, (May, 2014) 103505, arXiv:1306.4153 [astro-ph.CO].

[23] F. Beutler, S. Saito, J. R. Brownstein, C.-H. Chuang, A. J. Cuesta, W. J. Percival, A. J. Ross, N. P. Ross, D. P. Schneider, L. Samushia, A. G. Sánchez, H.-J. Seo, J. L. Tinker, C. Wagner, and B. A. Weaver, "The clustering of galaxies in the SDSS-III Baryon Oscillation Spectroscopic Survey: signs of neutrino mass in current cosmological data sets," *Mon. Not. R. Astron. Soc.* **444** (Nov., 2014) 3501–3516, arXiv:1403.4599.

[24] K. N. Abazajian, K. Arnold, J. Austermann, B. A. Benson, C. Bischoff, J. Bock, J. R. Bond, J. Borrill, E. Calabrese, J. E. Carlstrom, C. S. Carvalho, C. L. Chang, H. C. Chiang, S. Church, A. Cooray, T. M. Crawford, K. S. Dawson, S. Das, M. J. Devlin, M. Dobbs, S. Dodelson, O. Doré, J. Dunkley, J. Errard, A. Fraisse, J. Gallicchio, N. W. Halverson, S. Hanany, S. R. Hildebrandt, A. Hincks, R. Hlozek, G. Holder, W. L. Holzapfel, K. Honscheid, W. Hu, J. Hubmayr, K. Irwin, W. C. Jones, M. Kamionkowski, B. Keating, R. Keisler, L. Knox, E. Komatsu, J. Kovac, C.-L. Kuo, C. Lawrence, A. T. Lee, E. Leitch, E. Linder, P. Lubin, J. McMahon, A. Miller, L. Newburgh, M. D. Niemack, H. Nguyen, H. T. Nguyen, L. Page, C. Pryke, C. L. Reichardt, J. E. Ruhl, N. Sehgal, U. Seljak, J. Sievers, E. Silverstein, A. Slosar, K. M. Smith, D. Spergel, S. T.

Staggs, A. Stark, R. Stompor, A. G. Vieregg, G. Wang, S. Watson, E. J. Wollack, W. L. K. Wu, K. W. Yoon, and O. Zahn, "Neutrino physics from the cosmic microwave background and large scale structure," *Astroparticle Physics* **63** (Mar., 2015) 66–80.

[25] H. Böhringer and G. Chon, "The extended ROSAT-ESO Flux-Limited X-ray Galaxy Cluster Survey (REFLEX II). VI. Effect of massive neutrinos on the cosmological constraints from clusters," *Astron. Astrophys.* **574** (Feb., 2015) L8, arXiv:1501.04953.

[26] R. Laureijs, J. Amiaux, S. Arduini, J. . Augueres, J. Brinchmann, R. Cole, M. Cropper, C. Dabin, L. Duvet, A. Ealet, and et al., "Euclid Definition Study Report," *ArXiv e-prints* (Oct., 2011) , arXiv:1110.3193 [astro-ph.CO].

[27] A. Font-Ribera, P. McDonald, N. Mostek, B. A. Reid, H.-J. Seo, and A. Slosar, "DESI and other Dark Energy experiments in the era of neutrino mass measurements," *Journal of Cosmology and Astro-Particle Physics* **5** (May, 2014) 23, arXiv:1308.4164.

[28] B. Audren, J. Lesgourgues, S. Bird, M. G. Haehnelt, and M. Viel, "Neutrino masses and cosmological parameters from a Euclid-like survey: Markov Chain Monte Carlo forecasts including theoretical errors," *Journal of Cosmology and Astro-Particle Physics* **1** (Jan., 2013) 26, arXiv:1210.2194 [astro-ph.CO].

[29] J. Lesgourgues, G. Mangano, G. Miele, and S. Pastor, *Neutrino Cosmology*. Cambridge University Press, Feb., 2013.

[30] J. R. Bond, G. P. Efstathiou, and J. Silk, "Massive neutrinos and the large-scale structure of the universe," *Physical Review Letters* **45** (Dec., 1980) 1980–1984.

[31] A. Lewis, A. Challinor, and A. Lasenby, "Efficient computation of cosmic microwave background anisotropies in closed friedmann-robertson-walker models," *Astrophys. J.* **538** (Aug., 2000) 473–476, astro-ph/9911177.

[32] D. Blas, J. Lesgourgues, and T. Tram, "The Cosmic Linear Anisotropy Solving System (CLASS). Part II: Approximation schemes," *Journal of Cosmology and Astro-Particle Physics* **7** (July, 2011) 34, arXiv:1104.2933 [astro-ph.CO].

[33] M. Shoji and E. Komatsu, "Massive neutrinos in cosmology: Analytic solutions and fluid approximation," *Phys. Rev. D* **81** no. 12, (June, 2010) 123516.

[34] J. Lesgourgues and T. Tram, "The Cosmic Linear Anisotropy Solving System (CLASS) IV: efficient implementation of non-cold relics," *Journal of Cosmology and Astro-Particle Physics* **9** (Sept., 2011) 32, arXiv:1104.2935 [astro-ph.CO].

[35] P. A. R. Ade, N. Aghanim, C. Armitage-Caplan, M. Arnaud, M. Ashdown, F. Atrio-Barandela, J. Aumont, C. Baccigalupi, A. J. Banday, and et al., "Planck 2013 results. XVI. Cosmological parameters," *ArXiv e-prints* (Mar., 2013) , arXiv:1303.5076 [astro-ph.CO].

[36] W. Hu, D. J. Eisenstein, and M. Tegmark, "Weighing Neutrinos with Galaxy Surveys," *Physical Review Letters* **80** (June, 1998) 5255–5258, astro-ph/9712057.

[37] Planck Collaboration, P. A. R. Ade, N. Aghanim, M. Arnaud, M. Ashdown, J. Aumont, C. Baccigalupi, A. J. Banday, R. B. Barreiro, J. G. Bartlett, and et al., "Planck 2015 results. XIII. Cosmological parameters," *ArXiv e-prints* (Feb., 2015) , arXiv:1502.01589.

[38] N. Palanque-Delabrouille *et al.*, "Cosmology with Lyman-alpha forest power spectrum," arXiv:1506.05976 [astro-ph.CO].

[39] **BOSS** Collaboration, L. Anderson *et al.*, "The clustering of galaxies in the SDSS-III Baryon Oscillation Spectroscopic Survey: baryon acoustic oscillations in the Data Releases 10 and 11 Galaxy samples," *Mon. Not. Roy. Astron. Soc.* **441** no. 1, (2014) 24–62, arXiv:1312.4877 [astro-ph.CO].

[40] A. G. Sanchez *et al.*, "The clustering of galaxies in the SDSS-III Baryon Oscillation Spectroscopic Survey: cosmological implications of the full shape of the clustering wedges in the data release 10 and 11 galaxy samples," *Mon. Not. Roy. Astron. Soc.* **440** no. 3, (2014) 2692–2713, arXiv:1312.4854 [astro-ph.CO].

[41] Planck Collaboration, P. A. R. Ade, N. Aghanim, C. Armitage-Caplan, M. Arnaud, M. Ashdown, F. Atrio-Barandela, J. Aumont, C. Baccigalupi, A. J. Banday, and et al., "Planck 2013

results. XX. Cosmology from Sunyaev-Zeldovich cluster counts," *ArXiv e-prints* (Mar., 2013) , arXiv:1303.5080 [astro-ph.CO].

[42] M. Costanzi, B. Sartoris, M. Viel, and S. Borgani, "Neutrino constraints: what large-scale structure and CMB data are telling us?," *Journal of Cosmology and Astro-Particle Physics* **10** (Oct., 2014) 81, arXiv:1407.8338.

[43] J. Brandbyge and S. Hannestad, "Grid Based Linear Neutrino Perturbations in Cosmological N-body Simulations," *JCAP* **0905** (2009) 002, arXiv:0812.3149 [astro-ph].

[44] M. Viel, M. G. Haehnelt, and V. Springel, "The effect of neutrinos on the matter distribution as probed by the intergalactic medium," *Journal of Cosmology and Astro-Particle Physics* **6** (June, 2010) 15, arXiv:1003.2422 [astro-ph.CO].

[45] J. Brandbyge, S. Hannestad, T. Haugbølle, and Y. Y. Y. Wong, "Neutrinos in non-linear structure formation - the effect on halo properties," *Journal of Cosmology and Astro-Particle Physics* **9** (Sept., 2010) 14, arXiv:1004.4105 [astro-ph.CO].

[46] F. Villaescusa-Navarro, S. Bird, C. Peña-Garay, and M. Viel, "Non-linear evolution of the cosmic neutrino background," *Journal of Cosmology and Astro-Particle Physics* **3** (Mar., 2013) 19, arXiv:1212.4855 [astro-ph.CO].

[47] V. Springel, "The cosmological simulation code GADGET-2," *Mon. Not. R. Astron. Soc.* **364** (Dec., 2005) 1105–1134, arXiv::astro-ph/0505010.

[48] S. Bird, M. Viel, and M. G. Haehnelt, "Massive neutrinos and the non-linear matter power spectrum," *Mon. Not. R. Astron. Soc.* **420** (Mar., 2012) 2551–2561, arXiv:1109.4416 [astro-ph.CO].

[49] F. Villaescusa-Navarro, F. Marulli, M. Viel, E. Branchini, E. Castorina, E. Sefusatti, and S. Saito, "Cosmology with massive neutrinos I: towards a realistic modeling of the relation between matter, haloes and galaxies," *Journal of Cosmology and Astro-Particle Physics* **3** (Mar., 2014) 11, arXiv:1311.0866 [astro-ph.CO].

[50] E. Castorina, E. Sefusatti, R. K. Sheth, F. Villaescusa-Navarro, and M. Viel, "Cosmology with massive neutrinos II: on the universality of

the halo mass function and bias," *Journal of Cosmology and Astro-Particle Physics* **2** (Feb., 2014) 49, arXiv:1311.1212 [astro-ph.CO].

[51] M. Costanzi Alunno Cerbolini, B. Sartoris, J.-Q. Xia, A. Biviano, S. Borgani, and M. Viel, "Constraining neutrino properties with a Euclid-like galaxy cluster survey," *ArXiv e-prints* (Mar., 2013) , arXiv:1303.4550 [astro-ph.CO].

[52] E. Castorina, C. Carbone, J. Bel, E. Sefusatti, and K. Dolag, "DEMNUni: The clustering of large-scale structures in the presence of massive neutrinos," arXiv:1505.07148 [astro-ph.CO].

[53] R. E. Smith, J. A. Peacock, A. Jenkins, S. D. M. White, C. S. Frenk, F. R. Pearce, P. A. Thomas, G. Efstathiou, and H. M. P. Couchman, "Stable clustering, the halo model and non-linear cosmological power spectra," *Mon. Not. R. Astron. Soc.* **341** (June, 2003) 1311–1332, astro-ph/0207664.

[54] R. Takahashi, M. Sato, T. Nishimichi, A. Taruya, and M. Oguri, "Revising the Halofit Model for the Nonlinear Matter Power Spectrum," *Astrophys. J.* **761** (Dec., 2012) 152, arXiv:1208.2701 [astro-ph.CO].

[55] D. H. Rudd, A. R. Zentner, and A. V. Kravtsov, "Effects of Baryons and Dissipation on the Matter Power Spectrum," *Astrophys. J.* **672** (Jan., 2008) 19–32, arXiv:astro-ph/0703741.

[56] T. Guillet, R. Teyssier, and S. Colombi, "The effect of baryons on the variance and the skewness of the mass distribution in the Universe at small scales," *Mon. Not. R. Astron. Soc.* **405** (June, 2010) 525–534, arXiv:0905.2615 [astro-ph.CO].

[57] L. Casarini, A. V. Macciò, S. A. Bonometto, and G. S. Stinson, "High-accuracy power spectra including baryonic physics in dynamical Dark Energy models," *Mon. Not. R. Astron. Soc.* **412** (Apr., 2011) 911–920, arXiv:1005.4683 [astro-ph.CO].

[58] M. P. van Daalen, J. Schaye, C. M. Booth, and C. Dalla Vecchia, "The effects of galaxy formation on the matter power spectrum: a challenge for precision cosmology," *Mon. Not. R. Astron. Soc.* **415** (Aug., 2011) 3649–3665, arXiv:1104.1174 [astro-ph.CO].

[59] M. P. van Daalen, J. Schaye, I. G. McCarthy, C. M. Booth, and C. Dalla Vecchia, "The impact of baryonic processes on the two-point correlation functions of galaxies, subhaloes and matter," *ArXiv e-prints* (Oct., 2013) , arXiv:1310.7571 [astro-ph.CO].

[60] J. Bel, M. Zennaro, F. Villaescusa-Navarro, E. Sefusatti, and C. Carbone in preparation.

[61] S. Saito, M. Takada, and A. Taruya, "Impact of Massive Neutrinos on the Nonlinear Matter Power Spectrum," *Physical Review Letters* **100** no. 19, (May, 2008) 191301, arXiv:0801.0607.

[62] Y. Y. Y. Wong, "Higher order corrections to the large scale matter power spectrum in the presence of massive neutrinos," *Journal of Cosmology and Astro-Particle Physics* **10** (Oct., 2008) 35, arXiv:0809.0693.

[63] S. Saito, M. Takada, and A. Taruya, "Nonlinear power spectrum in the presence of massive neutrinos: Perturbation theory approach, galaxy bias, and parameter forecasts," *Phys. Rev. D* **80** no. 8, (Oct., 2009) 083528, arXiv:0907.2922 [astro-ph.CO].

[64] J. Lesgourgues, S. Matarrese, M. Pietroni, and A. Riotto, "Non-linear power spectrum including massive neutrinos: the time-rg flow approach," *Journal of Cosmology and Astro-Particle Physics* **6** (June, 2009) 17, arXiv:arXiv: 0901.4550 [astro-ph.CO] [astro-ph.CO].

[65] M. Shoji and E. Komatsu, "Third-order perturbation theory with nonlinear pressure," *Astrophys. J.* **700** (July, 2009) 705–719, arXiv:0903.2669 [astro-ph.CO].

[66] F. Führer and Y. Y. Y. Wong, "Higher-order massive neutrino perturbations in large-scale structure," *Journal of Cosmology and Astro-Particle Physics* **3** (Mar., 2015) 46, arXiv:1412.2764.

[67] D. Blas, M. Garny, T. Konstandin, and J. Lesgourgues, "Structure formation with massive neutrinos: going beyond linear theory," *Journal of Cosmology and Astro-Particle Physics* **11** (Nov., 2014) 39, arXiv:1408.2995.

[68] M. Peloso, M. Pietroni, M. Viel, and F. Villaescusa-Navarro, "The effect of massive neutrinos on the BAO peak," *JCAP* **1507** no. 07, (2015) 001, arXiv:1505.07477 [astro-ph.CO].

[69] H. Dupuy and F. Bernardeau, "Describing massive neutrinos in cosmology as a collection of independent flows," *Journal of Cosmology and Astro-Particle Physics* **1** (Jan., 2014) 30, arXiv:1311.5487 [astro-ph.CO].

[70] H. Dupuy and F. Bernardeau, "On the importance of nonlinear couplings in large-scale neutrino streams," *ArXiv e-prints* (Mar., 2015) , arXiv:1503.05707.

[71] F. Bernardeau, M. Crocce, and R. Scoccimarro, "Multipoint propagators in cosmological gravitational instability," *Phys. Rev. D* **78** no. 10, (Nov., 2008) 103521, arXiv:0806.2334.

[72] A. Taruya, F. Bernardeau, T. Nishimichi, and S. Codis, "Direct and fast calculation of regularized cosmological power spectrum at two-loop order," *Phys. Rev. D* **86** no. 10, (Nov., 2012) 103528, arXiv:1208.1191 [astro-ph.CO].

[73] A. Schneider, R. Teyssier, D. Potter, J. Stadel, J. Onions, D. S. Reed, R. E. Smith, V. Springel, and F. R. Pearce, "Matter power spectrum and the challenge of percent accuracy," *ArXiv e-prints* (Mar., 2015) , arXiv:1503.05920.

[74] D. Blas, M. Garny, and T. Konstandin, "Cosmological perturbation theory at three-loop order," *Journal of Cosmology and Astro-Particle Physics* **1** (Jan., 2014) 10, arXiv:1309.3308 [astro-ph.CO].

[75] J. Carlson, M. White, and N. Padmanabhan, "Critical look at cosmological perturbation theory techniques," *Phys. Rev. D* **80** no. 4, (Aug., 2009) 043531, arXiv:arXiv: 0905.0479 [astro-ph.CO] [astro-ph.CO].

[76] P. Fosalba, M. Crocce, E. Gaztañaga, and F. J. Castander, "The MICE Grand Challenge Lightcone Simulation I: Dark matter clustering," *ArXiv e-prints* (Dec., 2013) , arXiv:1312.1707 [astro-ph.CO].

[77] A. Upadhye, R. Biswas, A. Pope, K. Heitmann, S. Habib, H. Finkel, and N. Frontiere, "Large-scale structure formation with massive neutrinos and dynamical dark energy," *Phys. Rev. D* **89** no. 10, (May, 2014) 103515, arXiv:1309.5872.

[78] M. Pietroni, "Flowing with time: a new approach to non-linear cosmological perturbations," *Journal of Cosmology and Astro-Particle Physics* **10** (Oct., 2008) 36, arXiv:0806.0971.

[79] A. J. S. Hamilton, P. Kumar, E. Lu, and A. Matthews, "Reconstructing the primordial spectrum of fluctuations of the universe from the observed nonlinear clustering of galaxies," *Astrophys. J. Lett.* **374** (June, 1991) L1–L4.

[80] J. A. Peacock and S. J. Dodds, "Reconstructing the Linear Power Spectrum of Cosmological Mass Fluctuations," *Mon. Not. R. Astron. Soc.* **267** (Apr., 1994) 1020, arXiv::astro-ph/9311057.

[81] J. Lesgourgues, "The Cosmic Linear Anisotropy Solving System (CLASS) I: Overview," *ArXiv e-prints* (Apr., 2011) , arXiv:1104.2932 [astro-ph.IM].

[82] E. Massara, F. Villaescusa-Navarro, and M. Viel, "The halo model in a massive neutrino cosmology," *Journal of Cosmology and Astro-Particle Physics* **12** (Dec., 2014) 53, arXiv:1410.6813.

[83] S. Borgani, "Cosmology with Clusters of Galaxies," in *A Pan-Chromatic View of Clusters of Galaxies and the Large-Scale Structure*, M. Plionis, O. López-Cruz, and D. Hughes, eds., vol. 740 of *Lecture Notes in Physics, Berlin Springer Verlag*, p. 287. 2008. astro-ph/0605575.

[84] E. Rozo, E. S. Rykoff, J. G. Bartlett, and A. E. Evrard, "Cluster Cosmology at a Crossroads: Neutrino Masses," *ArXiv e-prints* (Feb., 2013) , arXiv:1302.5086 [astro-ph.CO].

[85] N. Mehrtens, A. K. Romer, M. Hilton, E. J. Lloyd-Davies, C. J. Miller, S. A. Stanford, M. Hosmer, B. Hoyle, C. A. Collins, A. R. Liddle, P. T. P. Viana, R. C. Nichol, J. P. Stott, E. N. Dubois, S. T. Kay, M. Sahlén, O. Young, C. J. Short, L. Christodoulou, W. A. Watson, M. Davidson, C. D. Harrison, L. Baruah, M. Smith, C. Burke, J. A. Mayers, P.-J. Deadman, P. J. Rooney, E. M. Edmondson, M. West, H. C. Campbell, A. C. Edge, R. G. Mann, K. Sabirli, D. Wake, C. Benoist, L. da Costa, M. A. G. Maia, and R. Ogando, "The XMM Cluster Survey: optical analysis methodology and the first data release," *Mon. Not. R. Astron. Soc.* **423** (June, 2012) 1024–1052, arXiv:1106.3056 [astro-ph.CO].

[86] J. P. Willis, N. Clerc, M. N. Bremer, M. Pierre, C. Adami, O. Ilbert, B. Maughan, S. Maurogordato, F. Pacaud, I. Valtchanov, L. Chiappetti, K. Thanjavur, S. Gwyn, E. R. Stanway, and C. Winkworth, "Distant galaxy clusters in the XMM Large Scale Structure survey," *Mon. Not. R. Astron. Soc.* **430** (Mar., 2013) 134–156, arXiv:1212.4185 [astro-ph.CO].

[87] M. Hasselfield, M. Hilton, T. A. Marriage, G. E. Addison, L. F. Barrientos, N. Battaglia, E. S. Battistelli, J. R. Bond, D. Crichton, S. Das, M. J. Devlin, S. R. Dicker, J. Dunkley, R. Dünner, J. W. Fowler, M. B. Gralla, A. Hajian, M. Halpern, A. D. Hincks, R. Hlozek, J. P. Hughes, L. Infante, K. D. Irwin, A. Kosowsky, D. Marsden, F. Menanteau, K. Moodley, M. D. Niemack, M. R. Nolta, L. A. Page, B. Partridge, E. D. Reese, B. L. Schmitt, N. Sehgal, B. D. Sherwin, J. Sievers, C. Sifón, D. N. Spergel, S. T. Staggs, D. S. Swetz, E. R. Switzer, R. Thornton, H. Trac, and E. J. Wollack, "The Atacama Cosmology Telescope: Sunyaev-Zel'dovich selected galaxy clusters at 148 GHz from three seasons of data," *Journal of Cosmology and Astro-Particle Physics* **7** (July, 2013) 8, arXiv:1301.0816 [astro-ph.CO].

[88] C. L. Reichardt, B. Stalder, L. E. Bleem, T. E. Montroy, K. A. Aird, K. Andersson, R. Armstrong, M. L. N. Ashby, M. Bautz, M. Bayliss, G. Bazin, B. A. Benson, M. Brodwin, J. E. Carlstrom, C. L. Chang, H. M. Cho, A. Clocchiatti, T. M. Crawford, A. T. Crites, T. de Haan, S. Desai, M. A. Dobbs, J. P. Dudley, R. J. Foley, W. R. Forman, E. M. George, M. D. Gladders, A. H. Gonzalez, N. W. Halverson, N. L. Harrington, F. W. High, G. P. Holder, W. L. Holzapfel, S. Hoover, J. D. Hrubes, C. Jones, M. Joy, R. Keisler, L. Knox, A. T. Lee, E. M. Leitch, J. Liu, M. Lueker, D. Luong-Van, A. Mantz, D. P. Marrone, M. McDonald, J. J. McMahon, J. Mehl, S. S. Meyer, L. Mocanu, J. J. Mohr, S. S. Murray, T. Natoli, S. Padin, T. Plagge, C. Pryke, A. Rest, J. Ruel, J. E. Ruhl, B. R. Saliwanchik, A. Saro, J. T. Sayre, K. K. Schaffer, L. Shaw, E. Shirokoff, J. Song, H. G. Spieler, Z. Staniszewski, A. A. Stark, K. Story, C. W. Stubbs, R. Šuhada, A. van Engelen, K. Vanderlinde, J. D. Vieira, A. Vikhlinin, R. Williamson, O. Zahn, and A. Zenteno, "Galaxy Clusters Discovered via the Sunyaev-Zel'dovich Effect in the First 720 Square Degrees of the South Pole Telescope Survey," *Astrophys. J.* **763** (Feb., 2013) 127, arXiv:1203.5775 [astro-ph.CO].

[89] W. H. Press and P. Schechter, "Formation of Galaxies and Clusters of Galaxies by Self-Similar Gravitational Condensation," *Astrophys. J.* **187** (Feb., 1974) 425–438.

[90] R. K. Sheth and G. Tormen, "Large-scale bias and the peak background split," *Mon. Not. R. Astron. Soc.* **308** (Sept., 1999) 119–126, astro-ph/9901122.

[91] A. Paranjape, E. Sefusatti, K. C. Chan, V. Desjacques, P. Monaco, and R. K. Sheth, "Bias deconstructed: unravelling the scale dependence of halo bias using real-space measurements," *Mon. Not. R. Astron. Soc.* **436** (Nov., 2013) 449–459, arXiv:1305.5830 [astro-ph.CO].

[92] J. Tinker, A. V. Kravtsov, A. A. Klypin, K. Abazajian, M. S. Warren, G. Yepes, S. Gottlöber, and D. E. Holz, "Toward a Halo Mass Function for Precision Cosmology: The Limits of Universality," *Astrophys. J.* **688** (Dec., 2008) 709–728, arXiv:0803.2706.

[93] M. Crocce, P. Fosalba, F. J. Castander, and E. Gaztañaga, "Simulating the Universe with MICE: the abundance of massive clusters," *Mon. Not. R. Astron. Soc.* **403** (Apr., 2010) 1353–1367, arXiv:0907.0019 [astro-ph.CO].

[94] Planck Collaboration, P. A. R. Ade, N. Aghanim, M. Arnaud, M. Ashdown, J. Aumont, C. Baccigalupi, A. J. Banday, R. B. Barreiro, J. G. Bartlett, and et al., "Planck 2015 results. XXIV. Cosmology from Sunyaev-Zeldovich cluster counts," *ArXiv e-prints* (Feb., 2015) , arXiv:1502.01597.

[95] L. Anderson, E. Aubourg, S. Bailey, D. Bizyaev, M. Blanton, A. S. Bolton, J. Brinkmann, J. R. Brownstein, A. Burden, A. J. Cuesta, L. A. N. da Costa, K. S. Dawson, R. de Putter, D. J. Eisenstein, J. E. Gunn, H. Guo, J.-C. Hamilton, P. Harding, S. Ho, K. Honscheid, E. Kazin, D. Kirkby, J.-P. Kneib, A. Labatie, C. Loomis, R. H. Lupton, E. Malanushenko, V. Malanushenko, R. Mandelbaum, M. Manera, C. Maraston, C. K. McBride, K. T. Mehta, O. Mena, F. Montesano, D. Muna, R. C. Nichol, S. E. Nuza, M. D. Olmstead, D. Oravetz, N. Padmanabhan, N. Palanque-Delabrouille, K. Pan, J. Parejko, I. Pâris, W. J. Percival, P. Petitjean, F. Prada, B. Reid, N. A. Roe, A. J. Ross, N. P. Ross, L. Samushia, A. G. Sánchez, D. J. Schlegel, D. P. Schneider, C. G. Scóccola, H.-J. Seo, E. S. Sheldon,

A. Simmons, R. A. Skibba, M. A. Strauss, M. E. C. Swanson, D. Thomas, J. L. Tinker, R. Tojeiro, M. V. Magaña, L. Verde, C. Wagner, D. A. Wake, B. A. Weaver, D. H. Weinberg, M. White, X. Xu, C. Yèche, I. Zehavi, and G.-B. Zhao, "The clustering of galaxies in the SDSS-III Baryon Oscillation Spectroscopic Survey: baryon acoustic oscillations in the Data Release 9 spectroscopic galaxy sample," *Mon. Not. R. Astron. Soc.* **427** (Dec., 2012) 3435–3467, arXiv:1203.6594 [astro-ph.CO].

[96] A. G. Sánchez, C. G. Scóccola, A. J. Ross, W. Percival, M. Manera, F. Montesano, X. Mazzalay, A. J. Cuesta, D. J. Eisenstein, E. Kazin, C. K. McBride, K. Mehta, A. D. Montero-Dorta, N. Padmanabhan, F. Prada, J. A. Rubiño-Martín, R. Tojeiro, X. Xu, M. V. Magaña, E. Aubourg, N. A. Bahcall, S. Bailey, D. Bizyaev, A. S. Bolton, H. Brewington, J. Brinkmann, J. R. Brownstein, J. R. Gott, J. C. Hamilton, S. Ho, K. Honscheid, A. Labatie, E. Malanushenko, V. Malanushenko, C. Maraston, D. Muna, R. C. Nichol, D. Oravetz, K. Pan, N. P. Ross, N. A. Roe, B. A. Reid, D. J. Schlegel, A. Shelden, D. P. Schneider, A. Simmons, R. Skibba, S. Snedden, D. Thomas, J. Tinker, D. A. Wake, B. A. Weaver, D. H. Weinberg, M. White, I. Zehavi, and G. Zhao, "The clustering of galaxies in the SDSS-III Baryon Oscillation Spectroscopic Survey: cosmological implications of the large-scale two-point correlation function," *Mon. Not. R. Astron. Soc.* **425** (Sept., 2012) 415–437, arXiv:1203.6616 [astro-ph.CO].

[97] A. Cooray and R. K. Sheth, "Halo models of large scale structure," Phys. Rep. **372** (Dec., 2002) 1–129, astro-ph/0206508.

[98] M. Davis, G. P. Efstathiou, C. S. Frenk, and S. D. M. White, "The evolution of large-scale structure in a universe dominated by cold dark matter," *Astrophys. J.* **292** (May, 1985) 371–394.

[99] M. S. Warren, K. Abazajian, D. E. Holz, and L. Teodoro, "Precision Determination of the Mass Function of Dark Matter Halos," *Astrophys. J.* **646** (Aug., 2006) 881–885, astro-ph/0506395.

[100] F. Marulli, C. Carbone, M. Viel, L. Moscardini, and A. Cimatti, "Effects of massive neutrinos on the large-scale structure of the Universe," *Mon. Not. R. Astron. Soc.* **418** (Nov., 2011) 346–356, arXiv:1103.0278 [astro-ph.CO].

[101] K. Ichiki and M. Takada, "Impact of massive neutrinos on the abundance of massive clusters," *Phys. Rev. D* **85** no. 6, (Mar., 2012) 063521, arXiv:1108.4688 [astro-ph.CO].

[102] J. R. Bond, S. Cole, G. Efstathiou, and N. Kaiser, "Excursion set mass functions for hierarchical gaussian fluctuations," *Astrophys. J.* **379** (Oct., 1991) 440–460.

[103] T. Kitayama and Y. Suto, "Semianalytic predictions for statistical properties of x-ray clusters of galaxies in cold dark matter universes," *Astrophys. J.* **469** (Oct., 1996) 480, astro-ph/9604141.

[104] M. LoVerde and M. Zaldarriaga, "Neutrino clustering around spherical dark matter halos," *Phys. Rev. D* **89** no. 6, (Mar., 2014) 063502, arXiv:1310.6459.

[105] M. LoVerde, "Spherical collapse in $\nu\Lambda$CDM," *Phys. Rev. D* **90** no. 8, (Oct., 2014) 083518, arXiv:1405.4858.

[106] E. Castorina and R. K. Sheth, "Stochastic bias in multidimensional excursion set approaches," *Mon. Not. R. Astron. Soc.* **433** (Aug., 2013) 1529–1536, arXiv:1301.5128 [astro-ph.CO].

[107] D. S. Reed, R. Bower, C. S. Frenk, A. Jenkins, and T. Theuns, "The halo mass function from the dark ages through the present day," *Mon. Not. R. Astron. Soc.* **374** (Jan., 2007) 2–15, arXiv:astro-ph/0607150.

[108] W. A. Watson, I. T. Iliev, A. D'Aloisio, A. Knebe, P. R. Shapiro, and G. Yepes, "The halo mass function through the cosmic ages," *Mon. Not. R. Astron. Soc.* (June, 2013) , arXiv:1212.0095 [astro-ph.CO].

[109] V. Springel, N. Yoshida, and S. D. M. White, "GADGET: a code for collisionless and gasdynamical cosmological simulations," *New Astronomy* **6** (Apr., 2001) 79–117, astro-ph/0003162.

[110] K. Dolag, S. Borgani, G. Murante, and V. Springel, "Substructures in hydrodynamical cluster simulations," *Mon. Not. R. Astron. Soc.* **399** (Oct., 2009) 497–514, arXiv:0808.3401.

[111] M. Costanzi, F. Villaescusa-Navarro, M. Viel, J.-Q. Xia, S. Borgani, E. Castorina, and E. Sefusatti, "Cosmology with massive neutrinos III:

the halo mass function and an application to galaxy clusters," *Journal of Cosmology and Astro-Particle Physics* **12** (Dec., 2013) 12, arXiv:1311.1514 [astro-ph.CO].

[112] M. Lima and W. Hu, "Self-calibration of cluster dark energy studies: Observable-mass distribution," *Phys. Rev. D* **72** no. 4, (Aug., 2005) 043006–+, arXiv:astro-ph/0503363.

[113] W. Hu and A. V. Kravtsov, "Sample variance considerations for cluster surveys," *Astrophys. J.* **584** (Feb., 2003) 702–715, arXiv:astro-ph/0203169.

[114] F. Bernardeau, S. Colombi, E. Gaztañaga, and R. Scoccimarro, "Large-scale structure of the universe and cosmological perturbation theory," Phys. Rep. **367** (Sept., 2002) 1–3, astro-ph/0112551.

[115] N. Kaiser, "On the spatial correlations of abell clusters," *Astrophys. J. Lett.* **284** (Sept., 1984) L9–L12.

[116] J. N. Fry and E. Gaztañaga, "Biasing and hierarchical statistics in large-scale structure," *Astrophys. J.* **413** (Aug., 1993) 447–452, astro-ph/9302009.

[117] M. Manera, R. K. Sheth, and R. Scoccimarro, "Large-scale bias and the inaccuracy of the peak-background split," *Mon. Not. R. Astron. Soc.* **402** (Feb., 2010) 589–602, arXiv:0906.1314 [astro-ph.CO].

[118] J. E. Pollack, R. E. Smith, and C. Porciani, "A new method to measure galaxy bias," *ArXiv e-prints* (Sept., 2013) , arXiv:1309.0504 [astro-ph.CO].

[119] M. Biagetti, V. Desjacques, A. Kehagias, and A. Riotto, "Non-local halo bias with and without massive neutrinos," *ArXiv e-prints* (May, 2014) , arXiv:1405.1435.

[120] K. C. Chan, R. Scoccimarro, and R. K. Sheth, "Gravity and large-scale nonlocal bias," *Phys. Rev. D* **85** no. 8, (Apr., 2012) 083509, arXiv:1201.3614 [astro-ph.CO].

[121] T. Baldauf, U. Seljak, V. Desjacques, and P. McDonald, "Evidence for quadratic tidal tensor bias from the halo bispectrum," *Phys. Rev. D* **86** no. 8, (Oct., 2012) 083540, arXiv:1201.4827 [astro-ph.CO].

[122] J. L. Tinker, B. E. Robertson, A. V. Kravtsov, A. Klypin, M. S. Warren, G. Yepes, and S. Gottlöber, "The Large-scale Bias of Dark Matter Halos: Numerical Calibration and Model Tests," *Astrophys. J.* **724** (Dec., 2010) 878–886, arXiv:1001.3162 [astro-ph.CO].

[123] N. Kaiser, "Clustering in real space and in redshift space," *Mon. Not. R. Astron. Soc.* **227** (July, 1987) 1–21.

[124] R. Scoccimarro, "Redshift-space distortions, pairwise velocities, and nonlinearities," *Phys. Rev. D* **70** no. 8, (Oct., 2004) 083007–+, arXiv:astro-ph/0407214.

[125] B. A. Reid and M. White, "Towards an accurate model of the redshift-space clustering of haloes in the quasi-linear regime," *Mon. Not. R. Astron. Soc.* **417** (Nov., 2011) 1913–1927, arXiv:1105.4165 [astro-ph.CO].

[126] D. Bianchi, M. Chiesa, and L. Guzzo, "Improving the modelling of redshift-space distortions - I. A bivariate Gaussian description for the galaxy pairwise velocity distributions," *Mon. Not. R. Astron. Soc.* **446** (Jan., 2015) 75–84, arXiv:1407.4753.

[127] L. Guzzo, M. Pierleoni, B. Meneux, E. Branchini, O. Le Fèvre, C. Marinoni, B. Garilli, J. Blaizot, G. De Lucia, A. Pollo, H. J. McCracken, D. Bottini, V. Le Brun, D. Maccagni, J. P. Picat, R. Scaramella, M. Scodeggio, L. Tresse, G. Vettolani, A. Zanichelli, C. Adami, S. Arnouts, S. Bardelli, M. Bolzonella, A. Bongiorno, A. Cappi, S. Charlot, P. Ciliegi, T. Contini, O. Cucciati, S. de la Torre, K. Dolag, S. Foucaud, P. Franzetti, I. Gavignaud, O. Ilbert, A. Iovino, F. Lamareille, B. Marano, A. Mazure, P. Memeo, R. Merighi, L. Moscardini, S. Paltani, R. Pellò, E. Perez-Montero, L. Pozzetti, M. Radovich, D. Vergani, G. Zamorani, and E. Zucca, "A test of the nature of cosmic acceleration using galaxy redshift distortions," *Nature* **451** (Jan., 2008) 541–544, arXiv:0802.1944.

[128] S. de la Torre, L. Guzzo, J. A. Peacock, E. Branchini, A. Iovino, B. R. Granett, U. Abbas, C. Adami, S. Arnouts, J. Bel, M. Bolzonella, D. Bottini, A. Cappi, J. Coupon, O. Cucciati, I. Davidzon, G. De Lucia, A. Fritz, P. Franzetti, M. Fumana, B. Garilli, O. Ilbert, J. Krywult, V. Le Brun, O. Le Fevre, D. Maccagni, K. Malek, F. Marulli, H. J. McCracken, L. Moscardini, L. Paioro, W. J. Percival, M. Polletta, A. Pollo, H. Schlagenhaufer, M. Scodeggio, L. A. M.

Tasca, R. Tojeiro, D. Vergani, A. Zanichelli, A. Burden, C. Di Porto, A. Marchetti, C. Marinoni, Y. Mellier, P. Monaco, R. C. Nichol, S. Phleps, M. Wolk, and G. Zamorani, "The VIMOS Public Extragalactic Redshift Survey (VIPERS). Galaxy clustering and redshift-space distortions at z=0.8 in the first data release," *ArXiv e-prints* (Mar., 2013) , arXiv:1303.2622 [astro-ph.CO].

[129] C. Contreras, C. Blake, G. B. Poole, F. Marin, S. Brough, M. Colless, W. Couch, S. Croom, D. Croton, T. M. Davis, M. J. Drinkwater, K. Forster, D. Gilbank, M. Gladders, K. Glazebrook, B. Jelliffe, R. J. Jurek, I.-h. Li, B. Madore, D. C. Martin, K. Pimbblet, M. Pracy, R. Sharp, E. Wisnioski, D. Woods, T. K. Wyder, and H. K. C. Yee, "The WiggleZ Dark Energy Survey: measuring the cosmic growth rate with the two-point galaxy correlation function," *Mon. Not. R. Astron. Soc.* **430** (Apr., 2013) 924–933, arXiv:1302.5178 [astro-ph.CO].

[130] F. Beutler, S. Saito, H.-J. Seo, J. Brinkmann, K. S. Dawson, D. J. Eisenstein, A. Font-Ribera, S. Ho, C. K. McBride, F. Montesano, W. J. Percival, A. J. Ross, N. P. Ross, L. Samushia, D. J. Schlegel, A. G. Sánchez, J. L. Tinker, and B. A. Weaver, "The clustering of galaxies in the SDSS-III Baryon Oscillation Spectroscopic Survey: testing gravity with redshift space distortions using the power spectrum multipoles," *Mon. Not. R. Astron. Soc.* **443** (Sept., 2014) 1065–1089, arXiv:1312.4611.

[131] R. Scoccimarro, S. Colombi, J. N. Fry, J. A. Frieman, E. Hivon, and A. Melott, "Nonlinear evolution of the bispectrum of cosmological perturbations," *Astrophys. J.* **496** (Mar., 1998) 586, astro-ph/9704075.

[132] L. Verde, A. F. Heavens, S. Matarrese, and L. Moscardini, "Large-scale bias in the universe - ii. redshift-space bispectrum," *Mon. Not. R. Astron. Soc.* **300** (Nov., 1998) 747–756, arXiv:astro-ph/9806028.

[133] R. Scoccimarro, "The bispectrum: From theory to observations," *Astrophys. J.* **544** (Dec., 2000) 597–615, astro-ph/0004086.

[134] R. Scoccimarro and H. M. P. Couchman, "A fitting formula for the non-linear evolution of the bispectrum," *Mon. Not. R. Astron. Soc.* **325** (Aug., 2001) 1312–1316, arXiv:astro-ph/0009427.

[135] H. Gil-Marín, C. Wagner, F. Fragkoudi, R. Jimenez, and L. Verde, "An improved fitting formula for the dark matter bispectrum," *Journal of Cosmology and Astro-Particle Physics* **2** (Feb., 2012) 47, arXiv:1111.4477 [astro-ph.CO].

[136] T. Baldauf, L. Mercolli, M. Mirbabayi, and E. Pajer, "The Bispectrum in the Effective Field Theory of Large Scale Structure," *ArXiv e-prints* (June, 2014) , arXiv:1406.4135.

[137] R. E. Smith, R. K. Sheth, and R. Scoccimarro, "Analytic model for the bispectrum of galaxies in redshift space," *Phys. Rev. D* **78** no. 2, (July, 2008) 023523–+, arXiv:0712.0017.

[138] T. Nishimichi, I. Kayo, C. Hikage, K. Yahata, A. Taruya, Y. P. Jing, R. K. Sheth, and Y. Suto, "Bispectrum and nonlinear biasing of galaxies: Perturbation analysis, numerical simulation, and sdss galaxy clustering," *Publ. Astron. Soc. Japan* **59** (Feb., 2007) 93–106, arXiv:astro-ph/0609740.

[139] N. McCullagh, D. Jeong, and A. S. Szalay, "Toward Accurate Modeling of the Nonlinear Matter Bispectrum: Standard Perturbation Theory and Transients from Initial Conditions," *ArXiv e-prints* (July, 2015) , arXiv:1507.07824.

[140] R. E. Angulo, S. Foreman, M. Schmittfull, and L. Senatore, "The One-Loop Matter Bispectrum in the Effective Field Theory of Large Scale Structures," *ArXiv e-prints* (June, 2014) , arXiv:1406.4143.

[141] E. Sefusatti and R. Scoccimarro, "Galaxy bias and halo-occupation numbers from large-scale clustering," *Phys. Rev. D* **71** no. 6, (Mar., 2005) 063001, astro-ph/0412626.

[142] E. Sefusatti and E. Komatsu, "Bispectrum of galaxies from high-redshift galaxy surveys: Primordial non-gaussianity and nonlinear galaxy bias," *Phys. Rev. D* **76** no. 8, (Oct., 2007) 083004, arXiv:0705.0343.

[143] E. Sefusatti, M. Crocce, S. Pueblas, and R. Scoccimarro, "Cosmology and the bispectrum," *Phys. Rev. D* **74** no. 2, (July, 2006) 023522, arXiv: astro-ph/0604505.

[144] M. Schmittfull, T. Baldauf, and U. Seljak, "Near optimal bispectrum estimators for large-scale structure," *Phys. Rev. D* **91** no. 4, (Feb., 2015) 043530, arXiv:1411.6595.

[145] J. E. Pollack, R. E. Smith, and C. Porciani, "Modelling large-scale halo bias using the bispectrum," *Mon. Not. R. Astron. Soc.* **420** (Mar., 2012) 3469–3489, arXiv:1109.3458 [astro-ph.CO].

[146] S. Saito, T. Baldauf, Z. Vlah, U. Seljak, T. Okumura, and P. McDonald, "Understanding higher-order nonlocal halo bias at large scales by combining the power spectrum with the bispectrum," *Phys. Rev. D* **90** no. 12, (Dec., 2014) 123522, arXiv:1405.1447.

[147] L. Verde, A. F. Heavens, W. J. Percival, S. Matarrese, C. M. Baugh, J. Bland-Hawthorn, T. Bridges, R. Cannon, S. Cole, M. Colless, C. Collins, W. Couch, G. Dalton, R. De Propris, S. P. Driver, G. Efstathiou, R. S. Ellis, C. S. Frenk, K. Glazebrook, C. Jackson, O. Lahav, I. Lewis, S. Lumsden, S. Maddox, D. Madgwick, P. Norberg, J. A. Peacock, B. A. Peterson, W. Sutherland, and K. Taylor, "The 2df galaxy redshift survey: the bias of galaxies and the density of the universe," *Mon. Not. R. Astron. Soc.* **335** (Sept., 2002) 432–440, astro-ph/0112161.

[148] Y.-S. Song, A. Taruya, and A. Oka, "Cosmology with anisotropic galaxy clustering from the combination of power spectrum and bispectrum," *ArXiv e-prints* (Feb., 2015) , arXiv:1502.03099.

[149] R. Scoccimarro, H. A. Feldman, J. N. Fry, and J. A. Frieman, "The bispectrum of iras redshift catalogs," *Astrophys. J.* **546** (Jan., 2001) 652–664, astro-ph/0004087.

[150] F. Marin, C. Blake, G. Poole, C. McBride, S. Brough, M. Colless, W. Couch, S. Croom, D. Croton, T. M. Davis, M. J. Drinkwater, K. Forster, D. Gilbank, M. Gladders, K. Glazebrook, B. Jelliffe, R. J. Jurek, I. Li, B. Madore, D. C. Martin, K. Pimbblet, M. Pracy, R. Sharp, E. Wisnioski, D. Woods, T. K. Wyder, and H. K. C. Yee, "The WiggleZ Dark Energy Survey: constraining galaxy bias and cosmic growth with 3-point correlation functions," *ArXiv e-prints* (Mar., 2013) , arXiv:1303.6644 [astro-ph.CO].

[151] H. Gil-Marín, J. Noreña, L. Verde, W. J. Percival, C. Wagner, M. Manera, and D. P. Schneider, "The power spectrum and bispectrum of SDSS DR11 BOSS galaxies I: bias and gravity," *ArXiv e-prints* (July, 2014) , arXiv:1407.5668.

[152] L. Verde, R. Jimenez, F. Simpson, L. Alvarez-Gaume, A. Heavens, and S. Matarrese, "The bias of weighted dark matter halos from peak theory," *ArXiv e-prints* (Apr., 2014) , arXiv:1404.2241.

[153] H. Gil-Marín, L. Verde, J. Noreña, A. J. Cuesta, L. Samushia, W. J. Percival, C. Wagner, M. Manera, and D. P. Schneider, "The power spectrum and bispectrum of SDSS DR11 BOSS galaxies II: cosmological interpretation," *ArXiv e-prints* (July, 2014) , arXiv:1408.0027.

[154] R. K. Sheth, K. C. Chan, and R. Scoccimarro, "Nonlocal Lagrangian bias," *Phys. Rev. D* **87** no. 8, (Apr., 2013) 083002, arXiv:1207.7117 [astro-ph.CO].

[155] M. Biagetti, K. Chuen Chan, V. Desjacques, and A. Paranjape, "Measuring nonlocal Lagrangian peak bias," *ArXiv e-prints* (Oct., 2013) , arXiv:1310.1401 [astro-ph.CO].

[156] S. Singh and C.-P. Ma, "Neutrino clustering in cold dark matter halos: Implications for ultrahigh energy cosmic rays," *Phys. Rev. D* **67** no. 2, (Jan., 2003) 023506, astro-ph/0208419.

[157] A. Ringwald and Y. Y. Y. Wong, "Gravitational clustering of relic neutrinos and implications for their detection," *Journal of Cosmology and Astro-Particle Physics* **12** (Dec., 2004) 5, hep-ph/0408241.

[158] F. Villaescusa-Navarro, J. Miralda-Escudé, C. Peña-Garay, and V. Quilis, "Neutrino halos in clusters of galaxies and their weak lensing signature," *Journal of Cosmology and Astro-Particle Physics* **6** (June, 2011) 27, arXiv:1104.4770 [astro-ph.CO].

[159] H.-Y. Wu, A. R. Zentner, and R. H. Wechsler, "The Impact of Theoretical Uncertainties in the Halo Mass Function and Halo Bias on Precision Cosmology," *Astrophys. J.* **713** (Apr., 2010) 856–864, arXiv:0910.3668 [astro-ph.CO].